# PERFORMANCE OF SUPERPLASTIC TIN - LEAD

# MATERIAL AS ENERGY ABSORBING SYSTEM

### By

### Riyad Mohammad Abu-Mallouh

### Supervisor

### Professor Sa'd M. Habbali

### Co-Supervisor

### Professor Adnan I. O. Zaid Kilani

### Submitted in Partial Fulfillment of the Requirements for the Degree of

### Doctor of Philosophy in Mechanical Engineering

### Faculty of Graduate Studies

### University of Jordan

### January 2003

# This these was successfully defended and approved on

# January 16$^{th}$, 2003

<u>**Examination Committee**</u>　　　　　　　　　<u>**Signature**</u>

Dr. Sa'd Mohammad Habbali

Prof. of Mechanical Engineering

Mech. Eng. Dept, Univ. of Jordan.


Dr. Adnan I. O. Z. Kilani

Prof. of Industrial Engineering

Ind. Eng. Dept, Univ. of Jordan.


Dr. Mazen I. Al-Kaisi
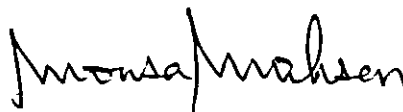
Prof. of Mechanical Engineering

Mech. Eng. Dept, Univ. of Jordan.


Dr. Mousa S. Mohsen
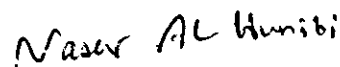
Assoc. Prof. of Mechanical Engineering

Mech. Eng. Dept, The Hashemite Univ.


Dr. Naser S. Al-Hunaiti

Assoc. Prof. of Mechanical Engineering

Mech. Eng. Dept, Univ. of Jordan.

# DEDICATION

TO MY FATHER

    MY MOTHER

        MY WIFE

            MY CHILDREN

                MOHAMMAD

                    MO'ATASEM

                        AND MOAYYAD

# PERFORMANCE OF SUPERPLASTIC TIN - LEAD MATERIAL AS ENERGY ABSORBING SYSTEM

By

## Riyad Mohammad Abu-Mallouh

Supervisor

## Professor Sa'd M. Habbali

Co-Supervisor

## Professor Adnan I. O. Z. Kilani

## ABSTRACT

Different systems and materials have been used to protect occupants during car accidents. Most of the reported work is directed towards the use of structural members made of engineering materials subjected to quasi-static loading conditions. It is well established that the behavior of materials under dynamic loading conditions is somewhat different from their behavior under quasi-static loading.

In this work, a superplastic Tin- Lead alloy which is sensitive to strain rate in the quasi-static range from $10^{-2}$ /s to $10^{0}$ /s was used to simulate the behavior of ordinary engineering materials. These materials are only sensitive to strain rate in the range of 1

to $10^4$ /s which is not possible to obtain on available testing machines and needs special design of equipment.

Furthermore, other systems based on utilizing the plastic energy consumed in deforming the material as means for protection of occupants in the car collision were investigated.

Two different methods were investigated. One utilizing the extrusion process to a high extrusion ratio by extruding a cylindrical pellet of 26 mm diameter into 21 cylinders of 3 mm diameter each. The other method utilized the plastic work consumed in the inversion of a hollow cylinder around a die profile radius. Both methods were investigated on the superplastic Tin- Lead alloy at three different strain rates. The first in the rate sensitive region, the second below it and the third exceeds it, namely at $3 \times 10^{-4}$, $5 \times 10^{-3}$ and $1 \times 10^{-1}$ respectively.

It was found that the use of superplastic Tin- Lead alloy in the quasi-static loading condition is very successful to simulate the behavior of engineering materials when subjected to dynamic loading. It was also found that the utilization of the concept of plastic work consumed in deformation represented by extrusion and tube inversion is a successful method to be used against any collision problems in general and automobile accidents in particular to protect the car and occupants.

Finally, it was found that during the rate sensitive region, the effectiveness of the system based on extrusion was 2.3 times that in the region below that region whereas the effectiveness was 6.07 times in the case of the tube inversion method, in the same strain rate region.

# 1. INTRODUCTION

There are different situations for kinetic energy dissipation in use that utilize metallic or non- metallic materials. Among these is the utilization of the work consumed in plastic deformation. This applies particularly to the treatment of problems of plastic deformation in structures whose function is to collapse in an envisaged manner, when subjected to an external load, which may be encountered in the exceptional circumstance of an unintentional collision. In this chapter, an introduction about processes, materials, occupant protection during accidents and the objectives of this thesis is given.

## 1.1 METAL FORMING

Metal forming produces metallic parts from one shape to another in the plastic region at constant volume (Kalpakjian, 1991). It can be classified to primary processes like forging, extrusion rolling and rod drawing, and secondary processes like bending, blanking and deep drawing.

In these processes, force or mechanical energy is needed to overcome the mechanical strength of the material in the plastic region of deformation. The main parameters that affect the mechanical behavior of the material are temperature and strain rate as shown in Fig. (1-1) and Fig. (1-2) respectively.

It can be seen from Fig. (1-1) that increasing the temperature causes a decrease in the yield stress, flow stress and fracture stress. Further more, it reduces the work hardening characteristics of the material.

However, Fig. (1-2), indicates that increasing strain rate will cause an increase in yield stress, flow stress and fracture stress and also increase of the work hardening of the material. (i.e. reduces ductility).
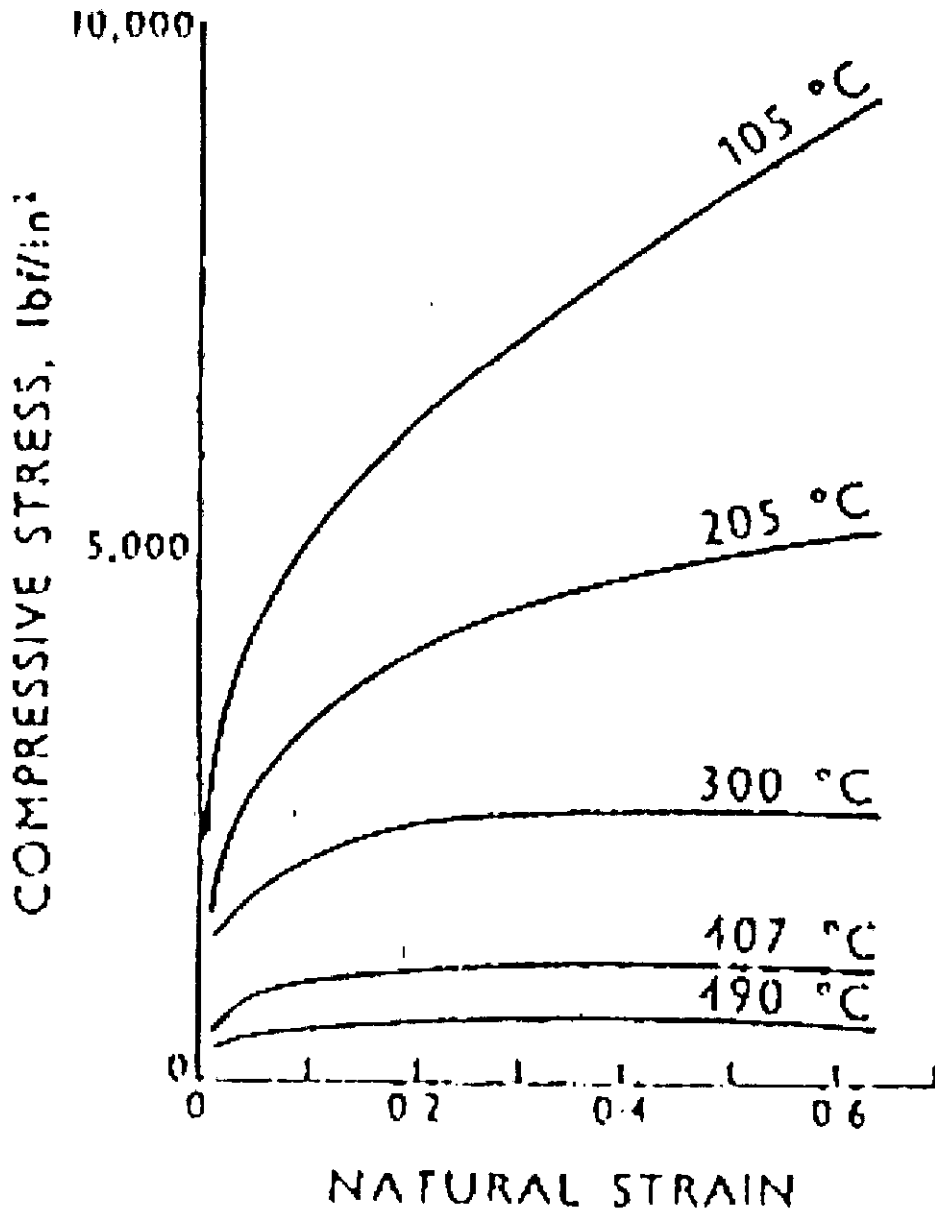
Fig. (1-1): Quasi – static compressive stress – strain curves at various temperatures for

super – pure aluminum ($\dot{\varepsilon} = 10^{-3}$ /s) ( Baraya *et al.*, 1965).
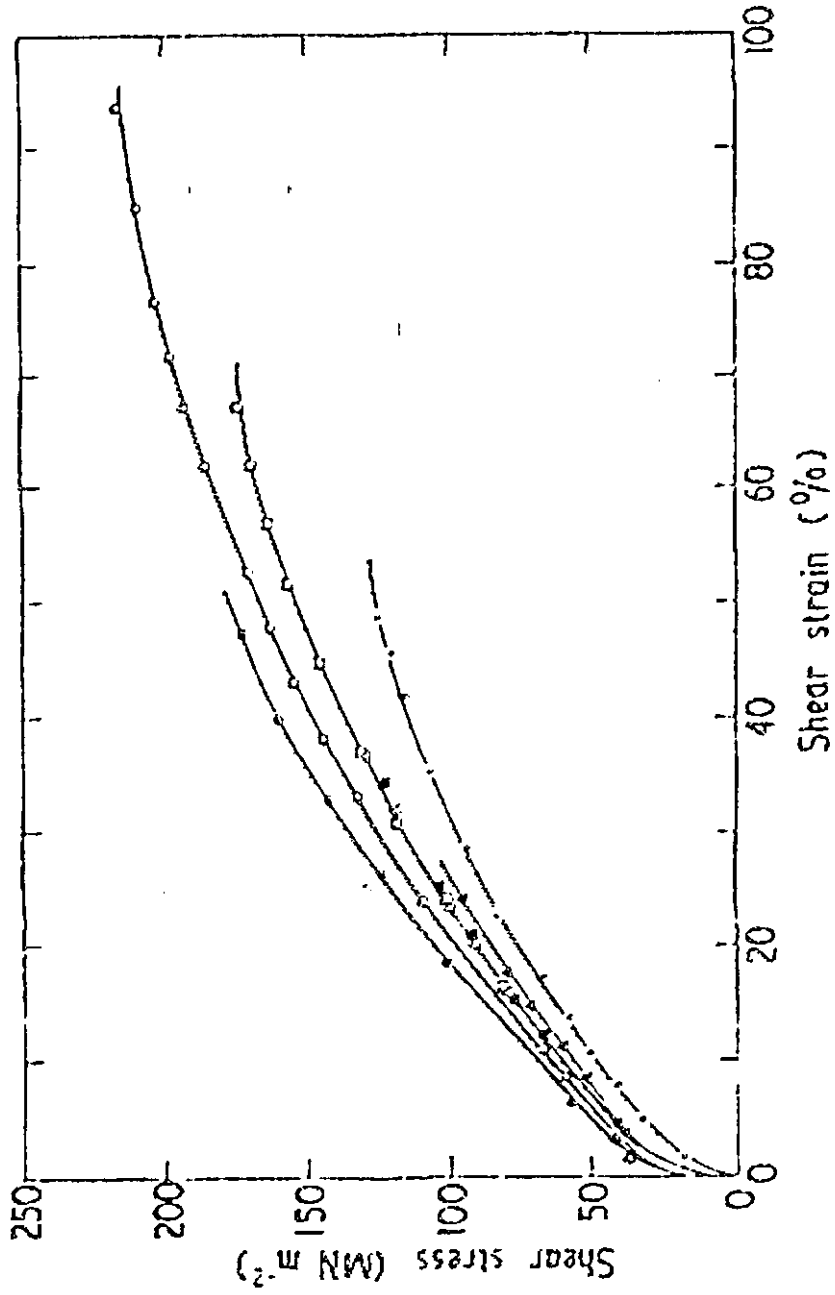
Fig. (1-2): Shear stress – strain curves for copper. Tests in short - base machine (rise time 25μs): • 2700 / s; ▪ 1900 / s. Tests in long - base machine (rise time 12μs): ○ 2500 / s; ▫ 1200 / s; ∆ 750 / s, +, test at 0.004/s in screw driven machine(Clynes and Campbell,1974).

Due to the importance of these two parameters, metal forming processes are classified accordingly as follows:

### 1.1.1 Classification of Metal Forming Processes With Respect to Temperature

Working processes are usually classified with respect to temperature to cold, worm or hot working processes depending on the homologous temperature, which is defined as:

$$Homologus\ temperature = \frac{Working\ temperature(K)}{Milting\ point(K)}$$

If (H.T) is less than 0.5, then we have a cold working process

If (H.T) is equal to 0.5, then we have a worm working process

If (H.T) is greater than 0.5, then we have a hot working process

For Tin $-$ Lead (pb $-$ sn) eutectic alloy with a melting point of 463K, worked at room temperature (295K) $\rightrightarrows$

$H.T. = 0.64 > 0.5 \Rightarrow Hot\ working\ process$

## 1.1.2 Classification of Metal Forming Processes With Respect to Strain Rate

Working processes are usually classified with respect to strain rate as follows:

### 1.1.2.1 Quasi Static Processes

$$\dot{\varepsilon} = 10^{-4}/s - 10^{0}/s$$

The forming time in these processes ranges from few seconds to few minutes. For example, metals formed by all types of presses whether mechanical or hydraulic. In this kind of processes, plastic work is converted into heat which is then dissipated to the surroundings because there is enough time for heat transfer. Accordingly these processes can be considered to be constant temperature processes, i.e. isothermal processes (Kalpakjian, 1991).

### 1.1.2.2 Intermediate Rate Processes

In these processes, the average strain rate ranges from $10^{0}$ to $10^{2}$ /s. The forming time in these processes is in the range of milliseconds. For example, forming on different types of hammers (Kalpakjian, 1991).

In this kind of processes, plastic work is also converted to heat, which does not have enough time to be dissipated to the surroundings. Hence these processes can be considered as adiabatic and a temperature rise occurs in the work piece.

### 1.1.2.3 Dynamic or High Strain Rate Processes

Dynamic or high strain rate processes are very often referred to as high energy rate forming processes (HERF). In these processes, the strain rate ranges from $10^{2}$ /s to $10^{4}$/s, and the forming time is in the range of microseconds. Examples on the high-energy rate forming processes (HERF) are explosive, electromagnetic, electro-hydraulic and gas forming processes. As the intermediate rate processes, the plastic work is converted to heat that is not dissipated to the surroundings because time is not

enough for heat transfer, hence it can be considered adiabatic and therefore a temperature rise occurs in the work piece.

### 1.1.2.4 Shock Loading

Where the strain rate is greater than $10^4$/s.

The effect of strain rate on the mechanical behavior of the material is usually indicated by the rate sensitivity of the material ($R.S.$), which is defined as the ratio of the dynamic flow stress, $\sigma_{F.D.}$ to the quasi – static flow stress, $\sigma_{F.S.}$, at the same strain, i.e.

$$Rate\ sensitivity(R.S) = \frac{Dynamic\ flow\ stress\,(\sigma_{F.D})}{Quazi-static\ flow\ stress\,(\sigma_{F.S})}$$

And usually its value ranges from 2 to 2.5 unless thermoplastic instability occurs (Kalpakjian, 1991).

### 1.2 MODEL MATERIALS:

Plasticine, although is a non-metallic material, has been repeatedly used to simulate the behavior of metals at high temperature (Aku *et al.*, 1967) and (Zaid and Al- Naib, 1980), since plasticine has almost the same behavior of steel at high temperature, as indicated in Fig. (1-3).

Whereas superplastic Tin – Lead has been used to simulate the behavior of metals at high strain rates, (Zaid and Abdullatif, 1984). It has the advantage of its sensitivity to strain rate at a rate of strain within the range $10^{-2} – 10^0$ /s, Fig. (1-4), which is available on all universal testing machines, (Quasi – static). Also being of low flow stress, it does not need high capacity machines.

It can be seen from the previous section that although strain rate increases the strength of the engineering material, it reduces its ductility. Therefor its liability to deform to high strain is reduced. Materials with high ductility at high strain rate will be

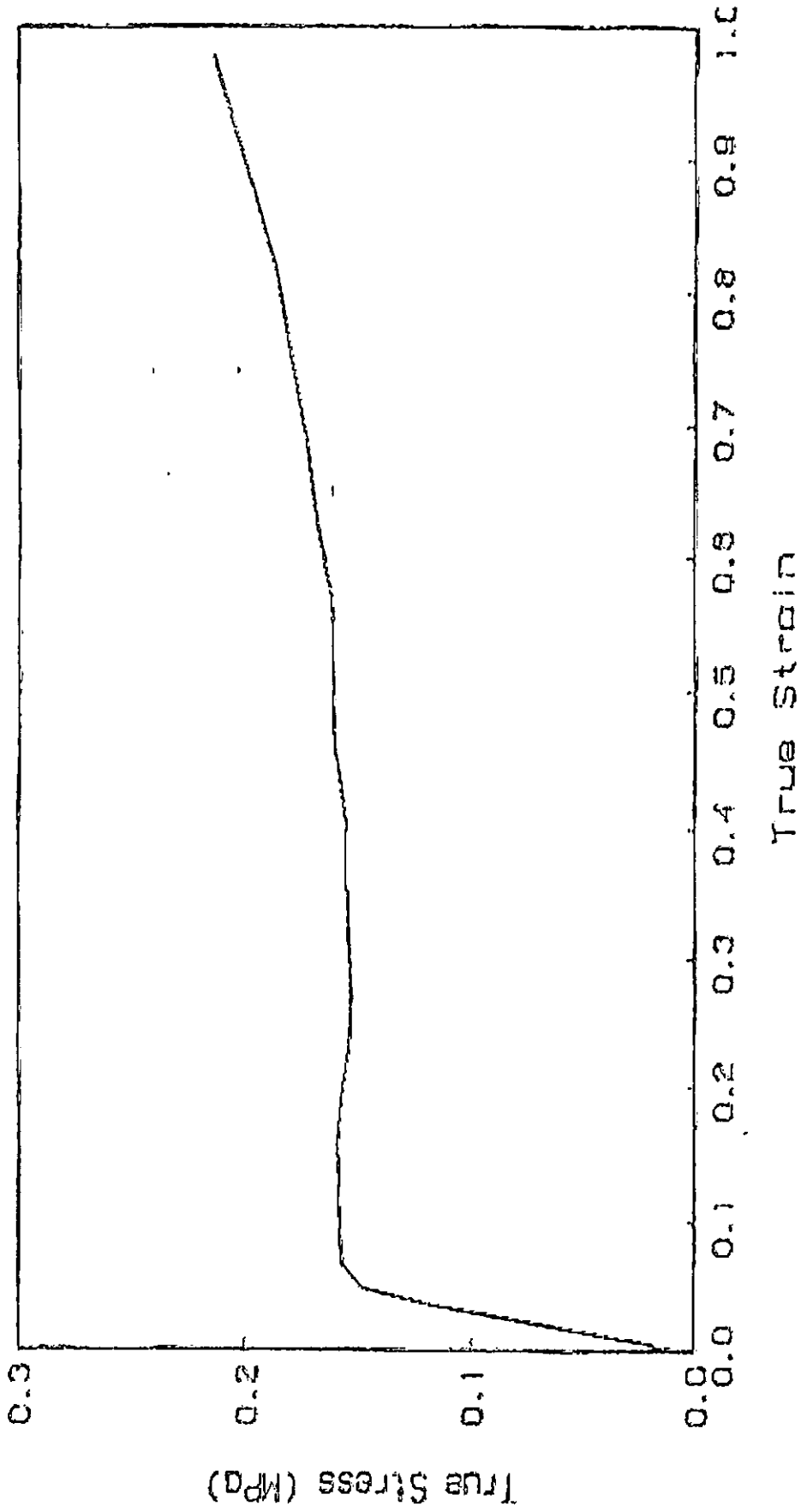Fig. (1-3): True stress – true strain for plasticine (Zaid and Al- Naib, 1980)
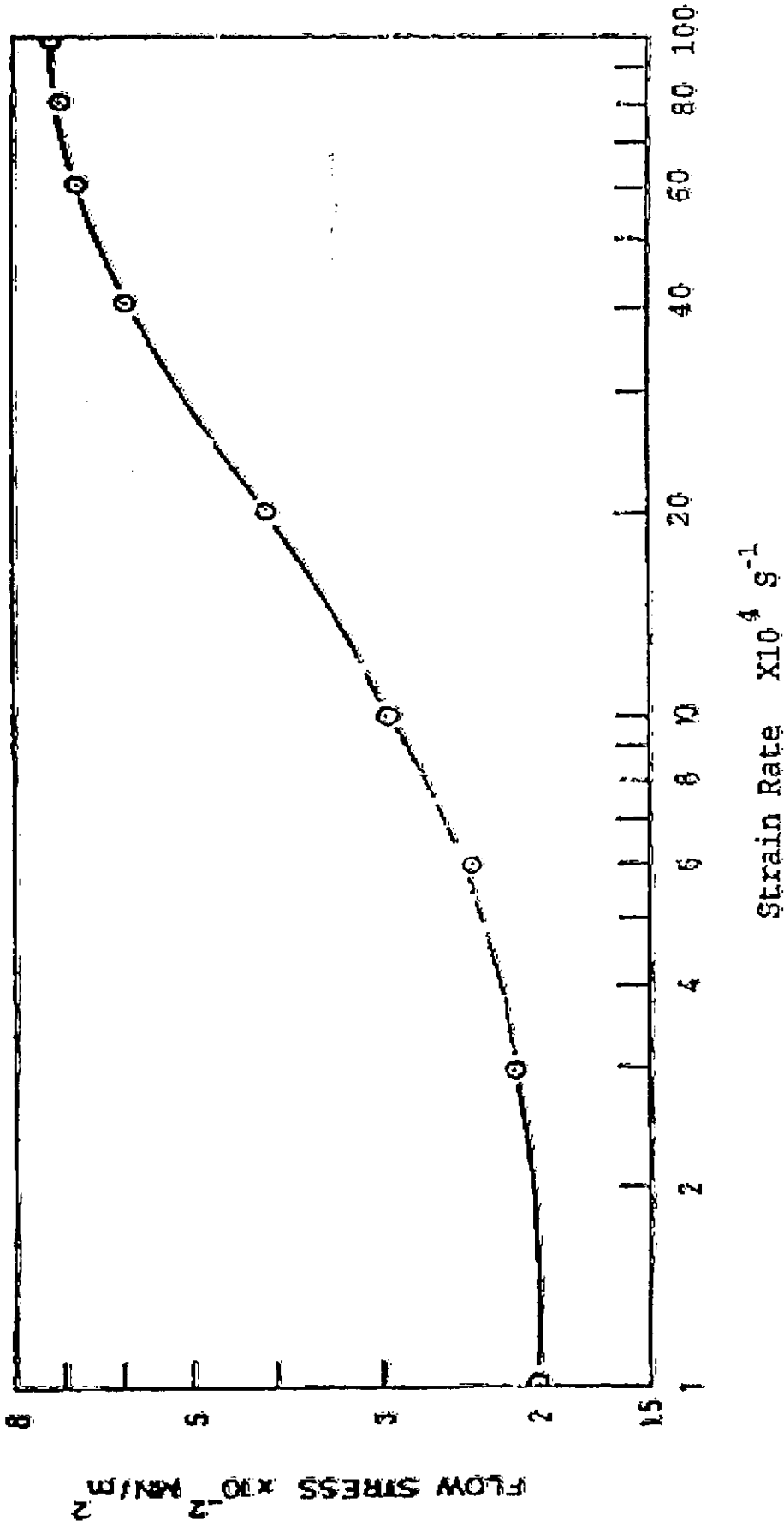
Fig. (1-4): Flow stress vs. strain – rate for extruded billets of superplastic lead – tin alloy in simple compression (Al- Naib And Zaid, 1984)

the answer for this problem. Such materials are the superplastic materials, which are very sensitive to strain rate and have an extra ordinary high ductility. For example, an elongation percentage of 1000 has been achieved.

## 1.3 SUPERPLASTIC MATERIALS

Superplasticity is the feature that allows the material to deform up to large strains (thousands of percents) with no need to high amounts of forces if the material is deformed under certain conditions. In other words, Superplasticity is the deformation process that produces essentially neck – free elongation of many hundreds of percent in metallic materials deformed in tension. This characteristic of material is invested in producing parts that need to generate bulk changes in shapes (macro forming). Superplastic materials require relatively low forces in their forming due to their low flow stresses, which results in energy savings. Superplastic lead – tin eutectic alloy is usually used for the laboratory investigations of superplasticity since it has low melting point, high ductility and very low strength (Kalpakjian, 1991).

Superplasticity can be induced both in materials possessing a stable, ultra fine grain size at the temperature of deformation ($\geq$ 0.4 $T_m$, where $T_m$ is the absolute melting point) and in those subjected to special environmental conditions, e.g. thermal cycling through a phase change). These two categories are best described as "structural" or "micrograin" superplasticity and "environmental" superplasticity, respectively (Kalpakjian, 1991).

Mechanical working, quenching or mechanically produced alloys may obtain the very fine grain structure of micrograin superplastic materials. The relation between the flow stress and strain rate of superplastic alloys can be expressed as:

$$\sigma = k \dot{\varepsilon}^{m}$$

Where:

*σ: flow stress*

*K: material constant*

*ε̇ : strain    rate*
*and*

*m: strain rate sensitivity index.*

Strain rate sensitivity index determines the rate at which necking proceeds after the initiation of localized plastic flow. When the elongation to failure increases to a maximum, the value of the strain rate sensitivity index, m, lies between 0.3 and 0.8.

## 1.4 DEFORMATION MECHANISMS:

Several theories have been suggested to explain the deformation mechanism of superplastic materials. Some of these theories are continuum; others are atomic, based on diffusional flow, dislocation and grain boundary sliding. Discussion of these theories was forwarded by (Todd, 2000). Summery of these theories will be given.

It has been suggested that deformation occur primarily by diffusion creep that causes the grains to elongate in the direction of the induced tensile or compressive stresses and to contract laterally. It was suggested that there is also a slip contribution to the overall strain, which reduces the value of index m from a maximum of one corresponding to Newtonian fluid viscosity to a lower value. One of the problems with this mechanism of superplastic deformation is that it does not account of the fact that grains remain equiaxed after deformation. An other theory attributes the high strain rate sensitivity of superplastic alloys to the rule of the grain boundary sliding. This sliding is accompanied by an other mechanism; either slip or diffusion to accommodate compatibility around triple points at the grain boundary intersection. Arieli and Mukharjee suggested that grain boundary sliding, as the dominant mechanism, cannot also be rate controlling at the same time and consequently accommodation is either

within the grains themselves or in the phase boundary. They maintain that this accommodation is due to dislocation motion.

In a micro indentation test of pure Pb and Pb – Sn eutectic alloy, the results established the role of grain boundaries in promoting high strain rate sensitivity and superplasticity. Also the results indicated that the increase of rate sensitivity in the presence of boundary is not due to grain boundary sliding.

Grain boundary sliding has been consistently observed during the testing of superplastic Pb – Sn eutectic alloy, but only in the initial stages of deformation. A core and mantle model was suggested to explain the deformation after grain boundary sliding stopping, in which the mantle or near boundary region of the grain was found to deform much faster than center or core region. By this mechanism, a small region of boundary material surrounding each grain took up most of the strain experienced by the deforming sample.

Environmental superplasticity has been reported to occur under the following conditions:

* During temperature cycling through a phase change where it is referred to as "transformation superplasticity".

* During temperature cycling of a thermally anisotropic material

* During neutron irradiation.

Of the three types mentioned, transformation superplasticity has received most of the attention.

## 1.5 OCCUPANT PROTECTION DURING CAR ACCIDENTS

In every collision, the collision forces – in other words, the energy generated in the collision – have to be absorbed in some way, to protect car occupants and reduce car damage.

The development and detail design of mechanical devices or systems for dissipating kinetic energy in a controlled manner at a pre- determined rate has increasingly become more important to all engineers in general and to mechanical engineers in particular. Advances in technology have led to higher speeds and more massive vehicles ( e. g. motor cars and aircraft ) which can cause more serious damage to people and to the costly structures themselves. People, now more than ever, are educated and vocal enough to be able to demand higher degrees of personal safety and protection, (Nader 1973). This makes up-to-date acquaintanceship with the design of safety measures, especially energy absorbers, a prerequisite for their application in this field.

The ideal situation for the car to deal with these forces is by deforming in a controlled manner so that the forces are "eaten up". The crumple zones and protective systems, such as seatbelts, airbags and energy absorbing interior material, must interact so that as much of the collision force as possible is absorbed before it reaches the occupants of the car.

Developing this interaction between the structure of the car and its interior protective systems in a way that provides maximum protection is the fundamental principle upon which crash safety should be based. Different designs have been used commercially and in research for reducing damages caused by these accidents.

The types of injuries which the vehicle occupants may be subjected to as a result of a collision depend upon the collision whether it is frontal, rear end or side collision.

According to a study on the distribution of accident types conducted by Volvo Car Corporation (Volvo, 1992), more than one accident in two is a frontal collision. The head, legs, chest and arms are the parts of the occupant body, which are most frequently injured in frontal collisions. To avoid this, different systems have been developed.

In frontal collision, the front of the car deforms and the car is retarded rapidly, while the occupants continue to move forwards. The crash is over in one – tenth of a second. Some of the protective systems usually used for such cases are:

1- Crumple zones with a number of energy absorbing members at different points in the front of the car.

2- Safety cage.

3- Self – adjusting, inertia – reel seatbelts with pretensioners on all seats.

4- Anti – submarining guard on all seats.

5- Airbags.

6- Energy – absorbing interior.

One in every ten car-accidents is a rear – end collision. The neck is most frequently injured in a rear – end collision.

In rear end collisions, the rear of the car deforms. The backward movement of the occupants can result in the neck being subjected to a catapult movement, otherwise known as a whiplash. The collision takes place in about one – tenth of a second. Some of the protective systems used in such cases are:

1- Self – adjusting, inertia – reel seatbelts with pretensioners on all seats

2- Crumple zone.

3- Safety cage.

4- Head restrains on all seats.

Three in every ten car-accidents are side impacts. The head, chest and arms are the parts of the body, which are most frequently injured in a side impact.

In side impact the side of the car is pushed into the cabin and hits the occupants. The time it takes until the collision sequence ends can be less than one – tenth of a second. Some of the protective systems used in such cases are:

1- Self – adjusting, inertia – reel seatbelts with pretensioners on all seats.

2- Side impact protection systems.

3- Side airbags.

4- Energy – absorbing interior.

## 1.6 OBJECTIVES OF THE THESIS

Crashworthiness is a well- established subject of study, although its treatment as a single discipline has yet to be generated. It can be seen from the available literature that different designs have been used to reduce the damage caused in car accidents. The design aim is to dissipate kinetic energy irreversibly rather than convert and store it elastically. The aim is to safeguard people, machinery or the vehicle itself from suffering a high degree of damage. Devices used for this purpose are usually one shot items, i.e. once having been deformed, they are discarded and replaced. Their repeatability and reliability in use are of great importance.

Most of the cases described in literature used engineering materials with reference to their quasi- static characteristics, while the actual situation occurs under dynamic or high strain rate. The implication of designing an energy absorbing device on the basis of its quasi- static loading response is that inertia effects within the device itself are unimportant and therefore is neglected and hence the kinetic energy is considered to be converted into plastic work in a quasi- static deformation mode. Therefore, it is anticipated that the use of a rate sensitive material within the quasi-

static range of deformation (from $10^{-4}$ / s to $10^0$ / s) will be beneficial in treating this problem.

It is therefore decided in this research work to utilize superplastic Tin- Lead material as a model material to simulate the behavior of other engineering materials in systems designed to be used as means for protection in car collisions. The advantage of using the Tin- Lead superplastic material is firstly its superior ductility, which allows large deformations to take place and secondly, its rate sensitivity at very low strain rates ($10^{-2}$ - $10^0$ /s) which falls in the range of strain rate available on all universal testing machines. Two metal forming processes were proposed, namely extrusion process and tube inversion process. The effectiveness of these systems as energy absorbing systems is to be investigated.

models for side impact simulation can be developed directly from the crash measurement data and the physical insight of the crash event. Uncoupled lumped parameter models for the automobile structure based on the study of distribution of crash energy was developed. The model parameters were estimated in a constrained environment. The estimation approach was verified using simulated data as well as test data. The modeling and application of the data based model was demonstrated in the actual design environment (Gandhi and Hu, 1996).

An analysis of the rigid-body model was presented for frictional three-dimensional impacts, which were originally studied by Routh. Using Coulomb's law for friction, a set of differential equations describing the progress and outcome of the impact process for general bodies was obtained. The differential equations induced a flow in the tangent velocity space for which the trajectories cannot be solved for in a closed form, and a numerical integration scheme was required. At the point of sticking, the numerical problem became ill conditioned and the flow at the singularity should be analyzed to determine the rest of the process. A local analysis at the point of sticking provided enough information about the global nature of the flow to allow enumerating all the possible dynamic scenarios for the sliding behavior during impact. The friction coefficients, and the mass parameters at the point of contact, determined the particular sliding behavior that would occur for a given problem. Once the initial conditions were specified, the possible outcome of the impact could then be easily determined (Bhatt and Koechling, 1995).

In his paper intitled 'Impulsive loading of structures', Symonds made an extension to large visco- plastic deflections of bound and mode approximation techniques. The aim was to determine the main response features of strain-rate sensitive

structures, when subjected to impulsive loads causing large plastic deflections. Experimental results were presented for both transversely loaded circular plates, which stiffen with increase in transverse deflection, and for simple rectangular frames, where their stiffness decreases with increase in deflection. Reasonable agreement was found between the theoretical predictions and both sets of experimental results ( Jones, 1976).

Explicit solutions for the dynamic die loads generated during high-speed plane strain and axi- symmetric compression with a free-flight impact-forging device were obtained. The influence of both axial and radial inertial forces were included and the die loads were evaluated for zero, full sticking, intermediate and mixed frictional boundary conditions. The manner in which inertial effects operate was exemplified for a range of impact velocities and interface frictional conditions.

A comparison was drawn between three types of impact forming devices on the basis of the effects of inertia on the die loads in a "real" forging operation (Sturgess and Jones, 1971).

Dolinski examined the dynamic response of structures with a modified mode approximation method. The reliability was regarded as the probability that the random displacement vector due to a continuous random load process remains inside a region of admissible displacements at any given time. With the introduction of some simplifications the problem was reduced to the consideration of random load impulses and some numerical simulations were presented for a two-dimensional random vector (Jones, 1976).

## 2.1.2 Specimen Geometry

### 2.1.2.1 Theoretical Work

An analytical solution for the impact response of a simply supported anisotropic composite cylinder was developed. The contact force was obtained from the compatibility condition between the elastic impactor and the cylinder. The analysis also incorporated the terms that raised in the expressions for stress resultants and stress couples due to the trapezoidal shape of an elemental section of a-shell. These trapezoidal terms could cause significant effects on the strain response of thick shell elements if the composite lay-up was non-symmetric (Matemilola and Stronge, 1997).

Anew model for the progressive crushing of circular tubes in which an active zone plastic deformation contains two folds or buckles was developed. The model captured with great realism several features of the crushing process, which were unaccounted for in all previous computational models of progressive folding. These include finite values of the load peaks, alternating heights of the peaks, unequal distances between peaks, reduced crush distance, realistic final shape of crushed tubes and a longer distance between the two first peaks. Closed-form solutions were derived for the length of the plastic folding wave and the mean crushing force (Wierzbick *et al.*, 1992).

The equivalent structure technique was developed to account for some of the effects of strain- hardening in structures undergoing plastic bending. The lateral compression of symmetrically deforming braced rings was analyzed and the results were compared with corresponding experimental data. The effects of strain- hardening on the analytical results both in the small deformation post-collapse regime and at large

deformations prior to the onset of unstable deformations were discussed (Reddy *et al.*, 1987).

In-extensional collapse mechanisms for the axial crumpling of thin-walled circular cones and frusta (truncated circular cones) were presented. Shortening of the thin shell height was achieved by folding in a non-symmetric diamond mode about stationary circumferential and inclined plastic hinges. Collapse proceeded progressively from the narrower end of the conical shell during the passage of a travelling hinge. Expressions for the various mean-crushing loads, when collapsing frusta of rigid-perfectly-plastic material were developed. Theoretical collapse modes and predicted loads were compared with those obtained experimentally by collapsing rigid PVC conical shells of constant axial length, of various wall-thickness and semi-apical angles, as well as metal (aluminum alloy and low-carbon steel) conical shells of similar geometry and good agreement was found (Mamalis *et al.*, 1986).

The mechanics of the large deformation of a square tube under axial load was discussed. Theoretical results were substantiated by experimental results. The elastic buckling load was predicted by assuming the tube to be composed of four plates simply supported at their edges. The highest load the tube can sustain was predicted by allowing for the development of plastic deformation near the corners. The mean crushing load was predicted from an incremental plasticity analysis, which allows for travelling plastic hinges. Comparison with circular tube behavior was considered and an attempt to explain some of the peculiarities was made (Meng *et al.*, 1983).

An efficient method for the accurate collapse analysis of thin steel plates subjected to in-plane compression was developed. The developed numerical technique was based on a variational principle in which a particular energy function was

minimized within a Rayleigh- Ritz type of procedure. The stress- strain behavior of the material was calculated from a plastic flow theory (Little, 1977).

The stress distribution in an elastic thin strip of finite length subjected to a transverse impact loading was examined by Okrouhlik. The problem was solved by the method of physical discretisation, which replaces the continuum by a system of particles and elastic constraints. The equations of motion were solved by numerical integration (Mamalis, 1976).

Recent interest in occupant safety has given the impetus for much research into the energy absorbing potential of metal structures in the automotive and light aircraft industries. Lightweight sheet metal constructions were not particularly amenable to simple collapse analysis procedures using the well-known limit theorems of plasticity because of the occurrence of local buckling. A computer analysis, particularly designed to deal with this situation was developed. Compound beam-spring elements were introduced which were capable of describing the reduction in the moment of resistance of thin-walled members after bending failure has occurred. Geometrical non-linearities arising from gross distortions were also accounted for. The validity of the program was supported by a number of laboratory test results.

The method was based upon experimental data that should be previously obtained for particular beam cross-sections. The approach was therefore limited to beams that can be tested to destruction in the laboratory (Miles, 1976).

Buckling loads of circular cylindrical laminated composite panels were obtained using shell theories with a first- order, shear-deformation approach and a Rayleigh-Ritz method that accounts for different boundary conditions and material anisotropy. The results obtained using these theories were compared with those obtained from finite element simulations. The curved panels were modeled using nine-node quadrilateral

continuum-based shell elements that were independent of any shell theory (Jaunky and Knight Jr, 1999).

The behavior of some simple models consisting of masses, elastic-plastic springs and bars subjected to sinusoidal loading were examined in some detail by Ceradini and Gavarini. The influence of second-order effects was briefly examined, and it was concluded that there is no guarantee of shakedown when finite-deflections were present (Jones, 1976).

An investigation was undertaken by Mikkola *et al.* into the efficiency and accuracy of some direct integration methods of ordinary differential equations, which arise in the finite-element analysis of dynamic structural problems. Numerical tests were conducted on a one-degree of freedom oscillator, axial impact of rods and transverse impact of beams. It was found that in a variable step formulation the central difference method was the most efficient for the tolerances employed (Jones, 1976).

Stolarski considered the axi symmetric response of a shallow spherical shell, impacted by a rigid mass, traveling with an initial velocity $Vo$. A kinematics method of solution was employed, and geometrical nonlinear effects were retained in the basic equations. This particular problem is related to the impact of an aircraft on the outer shell of a nuclear reactor (Jones, 1976).

Some recent work on the dynamic plastic behavior of ideal fiber-reinforced, highly anisotropic beams was described. It indicated that the permanent transverse deflections and response duration were less than the corresponding values for similar rigid, perfectly plastic isotropic beams. It was also shown that simple rigid-plastic methods could be used to predict the failure of dynamically loaded structures (Jones, 1976).

A structural theory was presented for the large static plastic deformation of space frames composed of thin walled members. Displacements comparable to the overall structural dimensions were contemplated. The frame was considered to consist of an arbitrary number of beam elements connected at node points. The analysis assumed that plastic deformation is confined to idealized hinges located at the node points. As a basis for a general frame computer program, the equations for a beam element were derived as a relationship between appropriate generalized force and deformation rates. The structural constitutive theory employed for the plastic hinge included bi-axial bending, torsion, and axial extension. It accounted for reduction in the load carrying capacity of the hinge due to local deformation. Predicted force-deformation curves for a space frame were in good agreement with experimental results (Mcivor *et al.*, 1977).

The extended Hamilton's principle was proposed to investigate the dynamic plastic behavior of a beam or a plate under an impact loading. Material was assumed to be rigid perfectly plastic. The impact loading was given in the form of initial velocity (Taya and Mura, 1974).

The effects of changes of geometry on the load-carrying capacity were studied. Using the equations of moderately large deflection shell theory, two methods for estimation of the load- deflection relations for perfectly plastic shells were discussed. Results for cylindrical pinned and clamped shells were given and certain experimental results concerning post-yield behavior of clamped shells were discussed (Duszek and Sawozuk, 1970).

## 2.1.2.2 Experimental Work

A detailed experimental investigation of the quasi-static lateral crushing of composite cylindrical tubes was carried out between flat platens. These tubes were made of glass fiber reinforced with epoxy having diameter to thickness ratio ranging from 7.33 to 39. The histories of their deformation were presented. Behavior of tubes as regards the peak-crushing load, post collapses load, energy absorbed and mode of crushing were discussed. Taking into consideration the mode of collapse of these tubes, as observed in experiments. Amathematical model for predicting the peak collapse load and the post collapse load was introduced. The load-deformation response computed from the mathematical model was compared with the experiments (Gupta and Abbas, 2000).

An experimental investigation to study the collapse mechanisms and the energy absorption capacities of glass/polyester composite hemi-spherical shells under both quasi-static and drop hammer loading was carried out. The shells were made of randomly oriented glass fiber mats and polyester resin. Influence of test speed, impact velocities and radii of the shells on the mechanism of deformation were discussed. Experiments on 45 shells showed that their progressive crushing occurred due to the formation of successive zones of fracture. Based on these observations an analytical model was developed for the prediction of load-deformation and energy-compression curves (Gupta and Easwara Prasad, 1999).

The initial collapse behavior of elliptical tubes subjected to lateral compression was investigated. Both non braced and braced tubes were analyzed, and the main factors which affect the initial collapse behavior were discussed and interpreted. The initial collapse loads for braced circular tubes, as a special case of elliptical tubes, were

compared to previous research results. The results and concepts presented can be useful in the development of design criteria for energy dissipating devices (Wu and CarneyIII, 1997).

A series of experiments were conducted for braced, elliptical tubes to verify the theoretical results presented in a previous paper by the same authors (Wu and Carney III, Int. J. Mech. Sci., 1997). In that paper, mathematical models and finite element analyses were employed to study the initial collapse behavior of braced elliptical tubes. These mathematical and numerical predictions were compared with experimental results in this paper (Wu and CarneyIII, 1998).

Experiments on short aluminum and steel round tubes were performed to study the nature of their axi - symmetric folding and the extent by which a tube folds internally. The mean diameter to thickness (D/ t) ratios of these tubes varied from 12 to 30. Typical histories of specimen deformation and load- compression curves obtained in these tests were presented. It was found that the fold formation was not symmetric about its mid plane and the extent of internal folding in each tube was dependent on its D/ t ratio. Based on the experimental observations and considering the formation of plastic hinges in a perfectly plastic material, a simple analysis was presented by assuming the fold formation to be symmetric. The effect of the non- symmetric fold formation was then considered. Various features like the fold length, the mean collapse load and the load- compression curve were derived from the analysis and the computer results were compared with the experiments (Gupta and Velmurugan, 1997).

Experimental results for the quasi-static and dynamic axial crushing of thin-walled square and rectangular tubes manufactured from sheet metal were published. The tubes were tested both empty and filled with polyurethane foam of various densities.

Both the stability and the energy absorbing characteristics of the tubes were described and discussed. Simple theoretical models were proposed to explain and quantify the interaction between the foam and the sheet metal tubes (Reid *et al.*, 1986).

Results of an experimental investigation of the axial crushing modes and energy absorption properties of quasi- statically compressed aluminum alloy tubes were presented. In particular the influence of tube length on these properties was discussed and quantified and classification chart was presented. This chart together with other experimental data enables a designer to predict the energy absorbing properties of a given tube as well as its mode of crushing (Andrews *et al.*, 1983).

Two different thin-walled closed sections, one square shape and the other rectangular were tested in bi-axial bending using displacement-controlled cantilever bending tests. Two different constraint conditions were used; the first kept the deflection axis fixed while the direction of the load axis was free. The second kept the load axis direction fixed and allowed the beam to deflect freely, Each configuration was repeated at 15° axis intervals and was performed twice to assure repeatability.

The results were used to compare the beam behavior in the transition and collapse stages between the two constraint conditions. The behavior was also compared with thick-walled theory predictions (Brown and Tidbury, 1983).

Experimental results mainly concerning the fracture of brittle cylinders due to impulsive loading were presented. Fracture Patterns and the development of cracks and spalls in spheres, plates and bars of variable sections, with or without holes or other forms of irregularity due to point explosive loading were tested and photographed by high-speed photography. An interpretation of the fracture patterns in terms of wave propagation and reflection was attempted (Johnson and Mamalis, 1976).

The collapse and energy dissipation characteristics of metal tubes braced with tension members were considered experimentally. The results were applied in the full scale crash testing of a vehicle impact attenuation device composed of clusters of steel tubes and subjected to high-speed roadway collisions (Reid *et al.*, 1983).

Aluminum rings of varying height, outside diameter and inside diameter ratios, machined from extruded solid bars and subjected to static axial compression were investigated and the modes of deformation were reported (Janardhana and Biswas, 1979).

Molnar carried out an experimental program, which examined the stability of thin-walled tubes with rectangular cross-sections subjected to static or dynamic axial loads. His results were employed to predict the collision behavior of buses with frames constructed from similar tubes (Jones, 1976).

### 2.1.2.3 Theoretical and Experimental

The crumpling of thin-walled frusta, under axial compression was studied. The energy expended in bending at the plastic hinges and in stretching the metal between the hinges was minimized for the total decrease in height due to collapse. The thinning of the cross-section due to stretching was neglected. A theoretical model was developed, which showed the effect of the semi-apical angle of the frusta and the effect of the slenderness ratio defined as the ratio of height to diameter. A good qualitative agreement was obtained between the experimental results and those obtained from the theoretical model (Mamalis *et al.*, 1984).

The bending collapse behavior of rectangular and square section tubes was studied theoretically and experimentally. A limit analysis technique was employed and a set of formulae relating the hinge moment and associated angle of rotation was derived.

The theoretical predictions were verified by comparison with 56 quasi-static bending tests for different sections, aspect ratios and width to wall thickness ratios. Very good agreement was found between the theoretical predictions and experimental results for the whole range of sections (Kecman, 1983).

The plastic response of a chain of circular aluminum rings due to an axial tensile impact load at one end was investigated both experimentally and analytically. High-speed photography was employed to record the development of the deformation process, a simplified approach was adopted which assumed rigid- perfectly plastic behavior of the ring material and arrived at an equation of the same form as the classical one-dimensional elastic wave equation (Silva- Gomes *et al.*, 1978).

### 2.1.3 Processing Parameters

An analysis of the response of a right-angled bent cantilever beam subjected to an out of plane impulsive load i.e., suddenly imposed velocity, applied to concentrated mass at its tip was provided. The history of deformation was described following importation of the load (Wang *et al.*, 1996).

Axial crushing of foam-filled tapered sheet metal tubes was studied. Following earlier work on the axial crushing of foam-filled sheet metal tubes of square and rectangular cross-sections and empty tapered tubes, the behavior of foam-filled tapered tubes was considered. Theoretical estimates of the variation in the mean crushing loads for both quasi-static and dynamic loading conditions were provided and compared with experimental data (Reid and reddy, 1986).

Mittal *et al.* examined the problem of the transverse impact of a slow speed striking mass hitting a clamped circular plate. The outhers presented a simplified theory supported with experimental measurements for impact force, bending strain and

deflection for the multiple contacts, which took place during the period of collision. They claimed that the impact forces corresponding to the different contact intervals had a greater influence on the discontinuous bending strains than the deflection (Mamalis, 1976).

Farlik demonstrated changes in the structure of polycrystalline metals due to the interaction of stress pulses for specific conditions of applied loading, specimen geometry and boundary conditions. These changes resulted in the appearance of anisotropic zones of "manifold form" with grains containing twins and possibly the appearance of micro- cracks. The anisotropic zones were thought to represent sources of residual stresses. An attempt to explain the mechanism of interaction of the stress pulses was presented; certain zones were suggested to grow in relation with the so-called stabilized and unstabilized barriers (Mamalis, 1976).

Application of the two-dimensional finite element method to the problem of the impact of conical pistons (with equal end diameters having different apex angles) on cylindrical rods was presented. Iso-parametric finite elements with bilinear displacement approximation were used in the numerical calculations. Experimental measurements of the axial force were also reported (Nilsson *et al*, 1976).

Cern investigated the influence of reflection from curved boundaries on the stress distribution of a thin elastic disc loaded by an impact radial force. The equation of motion of the two-dimensional continuum was solved by means of a Laplace-Carson transformation and by the method of separation of variables (Mamalis, 1976).

The higher modal dynamic plastic response of impulsively loaded, fully clamped beams was examined using various rigid perfectly plastic theoretical procedures and numerical elastic-plastic computer code (Jones and Soares, 1978).

Some experimental tests on copper specimens loaded dynamically at various strain rates were described. The experimental results were compared with existing visco plastic theories, and a new dynamic yield condition of a quadratic type was proposed which describes the principal features of the experiments (Baltov and Vodenitcharov, 1976).

## 2.1.4 Materials Used

The failure modes, criteria and thresholds of plastic structural members (beams, rings, plates and thin shells, etc.) subjected to intense dynamic loads, such as impulsive velocities or impact were surveyed. Besides the three basic failure modes for impulsively loaded beams, namely, *large inelastic deformation* (Mode I), *tensile tearing* (Mode II) and *transverse shear failure at the supports* (Mode III), more complicated failure behaviors observed in the cases of complex structural members and / or dynamic loading conditions were summarized and discussed. All the failure criteria used in the relevant theoretical analyses including *elementary' failure criterion, energy density criterion* and *quasi- static equivalent energy criterion,* etc., were commented upon. The threshold impulsive velocities for the onset of Mode III failure of fully clamped beams predicted from various approaches were compared with each other, as well as with the relevant experimental results. Particular attention was paid to structural members with macro imperfections (for example, containing cracks or notches), where failure which usually originate from the imperfections are fracture-dominant so that local fracture criteria, such as the j-integral criterion, should be incorporated into the global structural failure description. In addition, some most recent results of the authors studies were briefly presented (Yu and Chen, 2000).

An axi- symmetric, two-dimensional finite difference code was used by Glenn to study the behavior of a brittle solid under intense impulsive loading. The development of the fracture zone was predicted to have an important influence on the stress field and this was confirmed by dynamic photo- elastic experiments in which steel projectiles were caused to impact on glass targets (Mamalis, 1976).

## 2.2 SECOND SECTION

In this section, review of the available literature on the superplasticity, superplastic materials and strain rate sensitive materials is given. They are classified according to the subtopics they concentrated on

### 2.2.1 Methods of Loading

Lipkin and Campbell examined the influence of strain-rate history on the flow stress of copper and titanium using a torsional split Hopkinson-bar apparatus. Unlike previous dynamic shear tests, the strain rates were suddenly decreased to a lower value. Their experiments indicated that strain-rate history effects must be considered in order to obtain a suitable description of the response (Jones, 1976).

Equal channel angular pressing (ECAP) which is a processing procedure where a sample is pressed through a die containing a channel bent into an L shaped configuration was used. This procedure introduces a high strain into the sample without any change in the cross-sectional area and it may be used to attain an ultra fine grain size with dimensions lying typically within the sub micrometer range. This paper described a series of experiments where ECAP was applied to a commercial Al-Mg-Li-Zr alloy having an initial grain size of ~400 μm were described (Furukawa *et al.*, 2000).

A numerical and experimental study that has been undertaken into the dynamic elasto-plastic behavior of a single fuel sub-assembly resting on liquid sodium was reported (Zehlein, 1976).

## 2.2.2 Specimen Geometry

The combined effects of material strain-rate sensitivity and anisotropy on necking or "limit" strain predictions were examined for thin sheets with transversely isotropic properties. Various rate dependent constitutive laws based on flow theory and deformation theory of plasticity were also considered (Neale and Chater, 1980).

Mechanical anisotropy and stress-strain rate characteristics in superplastic deformation of titanium alloys were studied. Uni-axial tension and compression tests were carried out on two titanium-based alloys; Ti-6Al -4V in the form of extruded tubes and forged plates and Ti-3Al- 10V-2Fe sheets, to study anisotropic behavior during superplastic deformation. New constitutive equations for describing anisotropic superplastic deformation have been proposed to explain the effect of strain rate or stress on anisotropy (Bai *et al.*, 2001).

The results of experiments on strain-rate behavior for technically pure lead were reported. Experiments were performed in compression using cylindrical specimens of different slenderness ratios over a wide range of strain-rate $2x\ 10^{-3}\ s^{-1} < \dot{\varepsilon} < 2\ x\ 10^{3}\ s^{-1}$ (Malatynski and Klepaczko, 1980).

The deformation of hollow cylinders of different internal to external diameter ratios, made of superplastic tin-lead eutectic alloy was investigated under the effect of axial compression. The deformation was studied under two different conditions. One with the cylinders collapsing in an open die and the other with the cylinders constrained in a closed die. Graphs were obtained showing the effect of di/do and rate of loading on the capacity of energy absorption in the collapse of the cylinders (Abdullatif and Zaid, 1984).

A research on uniformly thin circular cylinders and frusta (truncated circular cones) made of low carbon steel subjected to axial loading at elevated strain-rates was conducted. Their initial axial length and the outside diameter of the cylinders and frusta (the larger top end) were kept constant whilst their uniform wall thickness was varied. The load-deformation or compression behavior of the cylinders and frusta for the two semi-apical angles used were recorded and the modes of collapse were provided and are discussed. Initial axi- symmetric rings ('ring', 'bellows' or 'concertina') developed into non-symmetric 'diamond' patterns (elliptic, triangular and square, etc.) as loading progressed and initially non-symmetric diamond buckle patterns were observed to characterize the modes of frustum collapse (Mamalis *et al.*, 1984).

The effect of a layered microstructure and its evolution on superplastic behavior of this alloy was examined depending on the fact that superplastic forming grade sheets of AA 8090 Al - Li alloy were observed to contain layers of different microstructure and micro texture across the thickness cross-section. Superplastic behavior and its relationship to the concurrent micro structural and micro textural evolution of this sheet were studied at by tensile testing of specimens taken from the full thickness and the near surface and mid thickness layers (Fan *et al.*, 2001).

High strain rate bi-axial superplastic forming of complex shapes was studied. Forming envelope has been defined and post-forming mechanical properties were investigated. Formed specimens were sectioned to investigate cavitation and cross-sectional thinning. Tensile tests were performed on parent and formed material to investigate the effect of superplastic forming on mechanical properties (Styles, 2000).

Results of a series of rolling I-section beam tests in the first two passes, using lead as a model material, were presented. Measurements of relative spread, natural

elongation, roll load and roll torque were made together with the observed changes in deformation modes with variation in shape factors (height to width ratios) of the specimens and the relative draughts were discussed. Comparison of these results was made with those obtained using empirical formulae suggested by earlier research workers. The observed rolling loads were compared also with measurements made of the die loads when rectangular specimens with the same shape factors as in these rolling tests were compressed between shaped dies having grooves similar to that in rolling and compressed under conditions of plane strain and in open-die compression (Chitkara and Hardy, 1977).

Augusti and Focardi carried out an experimental program to study the dynamic response of rigid-plastic one-story frames with displacements that were not constrained to remain in a fixed plane. The results were hoped to assist in determining the behavior of buildings excited by earthquakes (Jones, 1976).

The blow- forming of a flat superplastic metal sheet to a spherical surface was analyzed with a mathematical model based on the classical theory of liquid bubbles. The model enabled a quantitative account to be given for the effect of the strain-rate sensitivity, flow stress and temperature of the metal on the rate of blow- forming. Formulae were derived which enabled the superplastic flow stress and strain-rate sensitivity to be calculated from simple blow-forming tests (Belk, 1975).

Superplastic zinc aluminum eutectoid alloy sheet blanks were bulged from a square die using pneumatic pressure. Methods of describing the bulge centerline and diagonal profiles were proposed and the predicted profiles were in good agreement with the experimental profiles. "Boxes " of various heights and of various degrees of

deformation were formed and their associated strain distributions were determined (Clemas *et al.*, 1975).

An analysis was presented for the bulging by lateral pressure of a superplastic alloy sheet that has a flow equation, in uni-axial tension or compression, given by $\sigma = K\acute{\epsilon}^m$, where $\sigma$ is the flow stress, $\acute{\epsilon}$ the strain rate and K and m are material parameters. Two cases were dealt with: (1) the bulging of a flat circular sheet clamped at its perimeter and (2) the bulging of a sheet into $90^\circ$ V grooves. The latter process is pertinent to the problem of molding a sheet to a die contour so as to achieve detail. Bulge profile and sheet thickness distribution were predicted as a function of the variables pressure, geometry, time, K and m. Results were in good agreement with experimental findings (Holt, 1970).

The phenomenon of superplasticity in metals and the behavior of superplastic alloys in simple tension were described. The advantage of using these materials in forging processes and the possibility of developing, for superplastic alloys, vacuum forming, pressure forming and blow- molding techniques similar to those used in the plastics industry was investigated. Part II of the same paper described experiments in which tubes and sheet of superplastic tin-lead eutectic alloy were formed using various pressure –forming techniques. These include free forming of tube, forming a tube into die, production of a bottle from a backward extruded pre-form, stretch-forming sheet either freely or into a female die and the drawing of a very deep cup using pressure-augmented deep drawing. The material used was Tin- Lead superplastic alloy, which deforms superplastically at low strain-rates and at room temperature (AL- Naib and Duncan, 1970).

Tubes and circular rods of superplastic tin- lead alloy were produced by extruding cast billets of eutectic composition. Specimens of extruded material were

tested in simple Tension, compression and torsion. The tests on tubular specimens could be satisfactorily correlated using the usual representative stress, σ, and strain-rate, ἐ, functions. It was also shown that a σ/ἐ curve can be obtained from torsion tests of a solid rod using an analysis similar to that used for obtaining secondary creep data from torsion tests.

Simple equipment was described which could be used to obtain material properties over a wide range of strain-rate from a single test on a superplastic alloy in bar form at room or at elevated temperature (Ghosh and Duncan, 1970).

The superplastic deformation of thin circular diaphragms subjected to one-sided hydrostatic pressure was examined both theoretically and experimentally. Special attention was given to the thickness variations in bulged shapes of simple geometry (domes) and also in more complex shapes related to those encountered in practical forming operations (Cornfield and Johnson, 1970).

### 2.2.3 Processing Parameters

The Effects of strain rate and test temperature on flow behavior and microstructural evolution in AA 8090 Al-Li alloy were studied. Tensile specimens of superplastic forming grade AA8090 Al- Li alloy were deformed at constant strain rates and at constant temperatures to investigate their effects on the nature of stress- strain curves and on the concurrent microstructures, substructures, and micro textures (Fan *et al.*, 2001).

The two-dimensional plane strain equation of plastic flow in accordance with the Levy-Mises constitutive relation was expressed in terms of stream functions of complex variables. Expressions for the stress, strain-rate and velocity were derived, assuming the stream function in the form of both the summation and product of conjugate flow

functions, for plastic flow in a nonlinear viscous (strain-rate sensitive) medium. The plastic states were also derived using a mixed mode solution expressed in terms of non-separable, independent conjugate complex variables. Application of the summation form solution was illustrated through the block indentation problem. Calculations were made on the effect of variation of the strain-rate sensitivity exponent on the contact stress (Lee and Male, 1982).

A numerical method for analyzing the plane strain deformation of rate sensitive materials was presented. A rate of energy functional was introduced which was thought to take adequate account of the strain rate sensitivity of the material. In the numerical technique, the functional was minimized with respect to a kinematically admissible velocity field and used in a discretized form in a finite element analysis. The frictionless, plane-strain, side extrusion process was considered as an example to simulate actual side extrusion processes. Friction was incorporated into the analysis by assuming a constant fraction of the current shear stress of the material (Tomita and Sowerby, 1979).

For superplastic forming of aluminum to break out of the market that it currently occupies, alloys will be required to possess a higher strain rate capability, appropriate in service properties, and a significantly lower price and to be capable of volume production. An approach that has been developed in an attempt to address these fundamental requirements was described. A series of Al-Mg-Zr alloys with increasing levels of zirconium has been prepared via extrusion consolidation of cast particulate. The superplastic properties of the resultant cold rolled sheet have been evaluated as a function of thermo mechanical treatment and zirconium addition (Grimes et al., 2000).

The two-dimensional plane strain equation of plastic flow in accordance with the Levy-Mises constitutive relation in terms of stress functions of complex variables was expressed. Expressions for the stress, strain rate and velocity were derived for plastic flow in a non-linear viscous medium assuming the stress function in the form of both the summation and product of conjugate stress functions. The plastic states were also derived using a mixed mode solution expressed in terms of non-separable, independent conjugate complex variables. In their analysis, the block indentation associated with a nonlinear viscous (strain rate hardening) material under plane strain condition using the product form solution was performed. The effect of the variation in the strain-rate-hardening exponent on the contact stress was investigated (Lee and Patel, 1980).

The superplastic bulging of circular sheets damped against axi-symmetrical cylindrical dies using a rigid-visco-plastic finite element method was analyzed numerically. Four node quadrilateral iso-parametric elements were used with a Newton-Raphson non-linear solution scheme. Both effects of normal anisotropy and strain hardening in the material were considered and a modified Coulomb friction law was adopted. At the same time, the yield criterion suited for the superplastic forming process and the cavity damage evolution models, deduced from continuum damage mechanics, was applied to a finite element formulation. The influence of material parameters i.e. the strain rate sensitivity exponent $m$, the strain hardening exponent n, and the coefficient of normal anisotropy $R$ and processing parameters (pressure cycle, lubrication condition, die geometry) on the inhomogeneity of the thickness distribution were studied and discussed. A selection of the simulated results was compared with the experimental results and good agreement was found (Xiang et al., 2001).

Inconel 718 is a nickel-based alloy, used extensively in the aerospace industry. It has good service capabilities in terms of strength and fatigue resistance at high

temperatures. This alloy, in the form of sheet, has the capability of being shaped using gas pressure forming techniques similar to those used for a number of aluminum and titanium based alloys. An extensive research program has been carried out to investigate the high temperature formability of this alloy. This has involved both uni-axial tensile testing to determine such parameters as flow stress and strain rate sensitivity, and micro structural examination to investigate grain stability under both static heating and deformation. The forming characteristics of the material have been correlated with the δ phase solvus temperature. Optimum forming temperatures and strain rates were discussed (Huang *et al.*, 2000).

The influence of copper additions on the superplastic forming behavior of the Zn- Al eutectoid was studied. Measurements of the flow stress ($\sigma_f$) and strain-rate sensitivity (m) over a wide range of strain rates ($\dot{\varepsilon}$) and at temperatures have been made. Basically the Zn-Al eutectoid, (78 Zn-22 Al) was used, but with additions of copper up to 1.0% (Naziri and Pearce, 1970).

## 2.2.4 Superplastic Materials Used

A study on rate-dependent plasticity, linear visco elastic constitutive equations, was performed. The study was based on the previous work for the authors in which generalized constitutive equations and evolution laws for rate-independent plasticity were developed from the theory of internal state variables in irreversible thermodynamics. It established rate-dependent constitutive relations, which have more generality than those proposed by other authors. As a particular case, generalized linear visco-elastic constitutive relations were derived under the assumption that the process was isothermal, which were found to be identical with those obtained from the general linear visco elastic model analysis (Woo *et al.*, 1995).

Deformation of semi-solid dendritic alloys was studied from a mechanical standpoint. At low strain rates, the behavior of the solid skeleton controls the deformation. It can be described using a compressible visco plastic constitutive model. An upper-bound method was used to model the parallel plate compression experiment and to explain the role of friction in semi-solid forging. An analysis of axi-symmetric extrusion was seen to provide information for the design of fractional re-melting purification units (Charreyron and Fleming, 1985).

Microstructure and high strain rate superplasticity of *in situ* composite synthesized from aluminum and nano-$ZrO_2$ particles by powder metallurgy was studied. Pure aluminum matrix composites reinforced mainly with a fine needle-like $Al_3 Zr$ phase were synthesized by the reaction between nanocrystalline $ZrO_2$ particles and pure aluminum using powder metallurgy followed by hot extrusion and hot rolling (Geng *et al.*, 2001).

The research conducted in Japan in the field of high strain rate superplasticity was reviewed (Higashi, 2000).

The phenomenon of superplasticity was explored at high strain rates where it is economically more attractive. True tensile superplasticity in nano- crystalline materials was demonstrated. The difference in the details of superplasticity between the nano-crystalline and micro- crystalline state was emphasized (Mcfadden *et al.*, 2000).

A modified Hopkinson bar was used to compress specimens of commercially pure titanium, and titanium alloys, at natural strain rates ranging between $3x \, 10^3 \, s^{-1}$ and $3x \, 10^4 \, s^{-1}$. All materials deformed in a viscous manner with a linear increase of flow stress with strain rate (Wulf, 1979).

images, the variation of the number of cavities per unit volume with strain was measured for various strain rates. Hence an inter linkage parameter was introduced (Martin *et al.,* 2000).

Superplastic forming of conventional titanium alloy sheet is limited commercially by the relatively long cycle times imposed by the high temperatures and slow strain rates required. In order to minimize cycle times, material with a fine grain size is required to allow either, an increase in the forming rate or a reduction in the deformation temperature. For this purpose, the manufacture of Ti-6Al-4V-0.5B powder with a nano crystalline grain size, which was produced by mechanical milling, was detailed. The material was consolidated by hot iso- static pressing at a range of temperatures during which ~2.5 vol.-%TiB was formed by an *in situ* reaction between the titanium and boron. The consolidated material was hot tensile tested (Godfrey *et al.,* 2000).

# 3. MATERIALS, EQUIPMENT AND PROCEDURES

## 3.1 MATERIALS

### 3.1.1 Die Materials

All the dies used in this research work, namely; compression, extrusion and tube inversion die blocks were manufactured from die steel D-2 of the chemical composition shown in Table (3-1) and some of its mechanical characteristics shown in Table (3-2) (Bohler, 1995). The material was received as cylindrical rods of 75 mm and 30 mm diameter and 500 mm length. The dies and die blocks were all machined from these rods to the required shapes and dimensions.

Table (3-1): Chemical analysis by weight of die steel D-2 (Bohler, 1995).

| Element | C | Si | Mn | Cr | Mo | V | Fe |
|---------|------|------|------|------|------|------|-------|
| Weight % | 1.51 | 0.32 | 0.27 | 11.6 | 0.75 | 0.91 | 84.64 |

Table (3-2): Some characteristics of die steel D − 2 (Bohler, 1995).

| Density | 7.79 g / cm$^3$ |
|---------|-----------------|
| Hardness after annealing | 235 HB |
| Modulus of elasticity | 2.1 x 10$^5$ Mpa |
| Thermal conductivity | 20 W / m K |
| Specific heat capacity | 460 J / Kg K |

### 3.1.2 Workpiece Materials

All workpieces, used throughout this work, were made of superplastic Tin – Lead alloy which was prepared in the laboratory from granular Tin of 99.7 % purity and Lead of 99.97 % purity with a weight percentage of each corresponding to the eutectic

composition which is 61.9 % Tin and 38.1 % Lead. The details for preparation of this alloy will be given in the procedure section.

## 3.2 EQUIPMENT

Different pieces of equipment were designed and manufactured to allow the superplastic material to deform plastically i.e. consuming energy which is supposed to be caused by the automobile collision to avoid damage and to protect the occupants during accidents.

Two forming processes were suggested to investigate this, namely the extrusion process and the tube inversion process. Two main dies were designed and manufactured. One for the extrusion process and the other for the tube inversion process.

### 3.2.1 Extrusion Die Set

These dies were designed and manufactured to utilize the energy consumed in extrusion of metal as a mean of absorbing the energy resulting from collision. They were used with the extrusion die set shown in Fig. (3-1). A list of the main components of this die is given in Table (3-3). This die consists of the Container (part No. 1), which contains the material to be extruded in a billet form. This part was made of a solid cylinder of tool steel D-2 material, turned to an external diameter of 80 mm, 26 mm bore and 100 mm length. The container was fitted to the female extrusion die, which in turn was fitted to the lower shoe or base of the die set by four bolts. The lower shoe was raised from the machine platen by a hollow mild steel cylinder of 114 mm bore, 11-mm thickness and 150 mm height.

Fig. (3-1): Schematic drawing of the main extrusion die set

All dimensions are in mm.

Table (3-3): List of the components of the main extrusion die set

| PART NO. | PART NAME | PART MATERIAL | QUANTITY |
|---|---|---|---|
| 1 | Container | Die steel | 1 |
| 2 | Die | Die steel | 1 |
| 3 | Plunger | Die steel | 1 |
| 4 | Dummy block | Die steel | 1 |
| 5 | Guide bushing | Brass | 1 |
| 6 | Base | Mild steel | 1 |
| 7 | Cylinder | Mild steel | 1 |
| 8 | Billet | Superplastic material | 1 |
| 9 | Screws | Cast iron | 1 |

The extrusion force was applied to the billet (workpiece) from the compression machine through the plunger, part No. 3, which was made of die steel D-2 of 22 mm diameter and 150 mm length. The plunger was guided through a flange or guide bushing, part No. 5, made of brass and fitted to the upper part of the container. The pillow or the dummy block, part No. 4, is a solid disk of die steel D-2 of 26-mm diameter and 10 mm thickness. This pillow separates the die block from the plunger to protect the later when the workpiece material is completely extruded. A photograph of the exploded extrusion die showing all its parts is shown in Fig. (3-2).

To allow more energy to be absorbed, the superplastic material was allowed to be extruded through a high extrusion ratio defined as the original cross sectional area of the billet, $A_o$, to the final cross sectional area of the extruded part, $A_f$, i.e. ($A_o / A_f$), and to use a series of holes, die orifices, in one die block.

All Rights Reserved - Library of University of Jordan - Center of Thesis Deposit

Fig (3-2): Photograph of the exploded extrusion die

Two female die blocks were used; all made of die steel D-2 and of the dimensions shown in Fig. (3-3) and Fig. (3-4) to serve this purpose.



Fig. (3-3): Extrusion die used for grain refinement
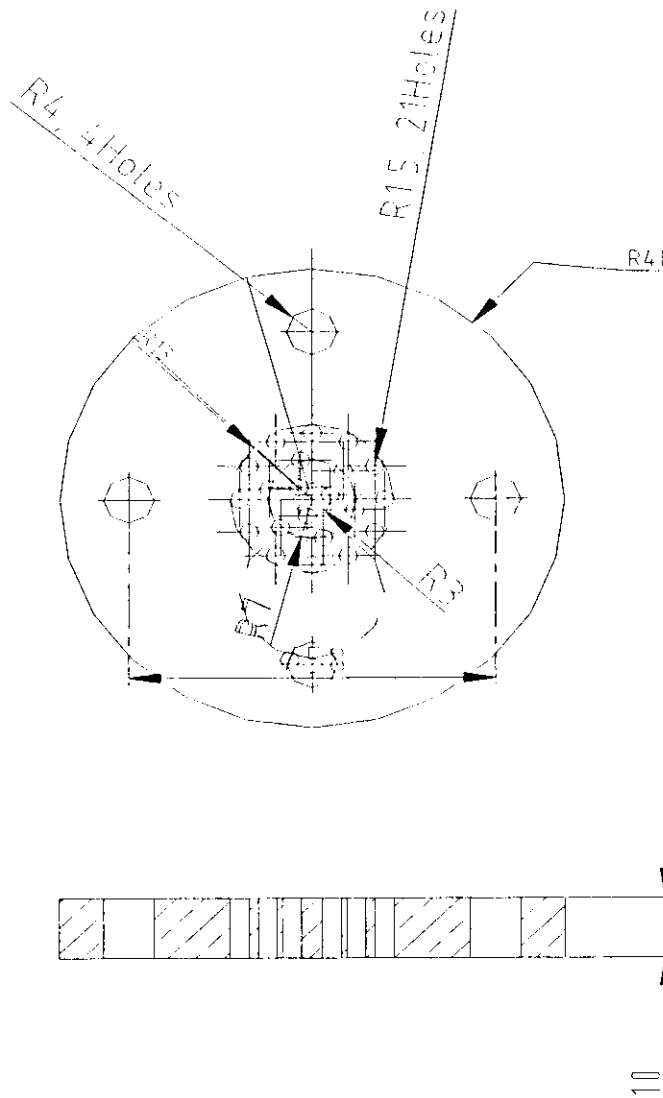
All dimensions are in mm.

Fig (3-4): Extrusion die with series of holes
All dimensions are in mm.

### 3.2.2 Tube Inversion Die Set

This die set was designed and manufactured to utilize the energy consumed in inverting a hollow tube plastically around radiused profile die blocks during its axial compression between the middle main die and the upper and lower die blocks.

Two sets of die blocks were manufactured for this purpose with the dimensions shown in Fig (3-5) and Fig (3-6) for the first set and in Fig. (3-7) and Fig. (3-8) for the second set. Fig. (3-9) shows the frame holding co-axially these parts together with the

workpiece. Fig. (3-10) shows a photograph of the main die, the die blocks and the

frame, whereas Fig. (3-11) shows a drawing of the assembled die set.
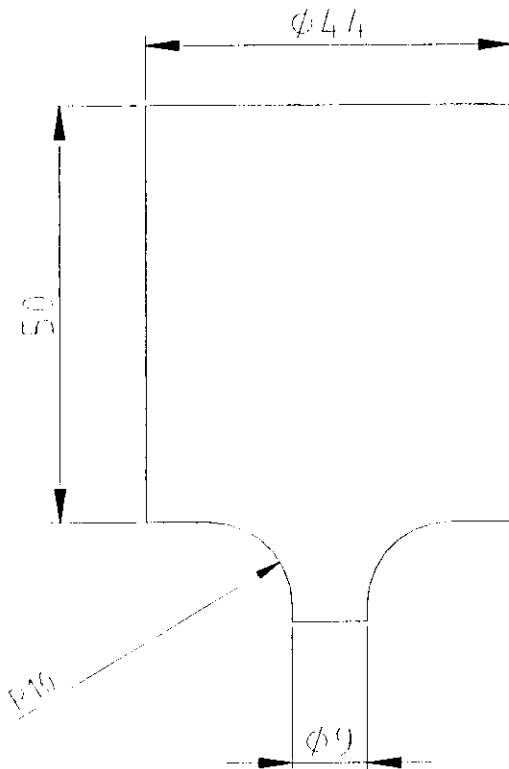
Fig. (3-5): Inversion die block (First set)

Part No. 1

2 pieces are required
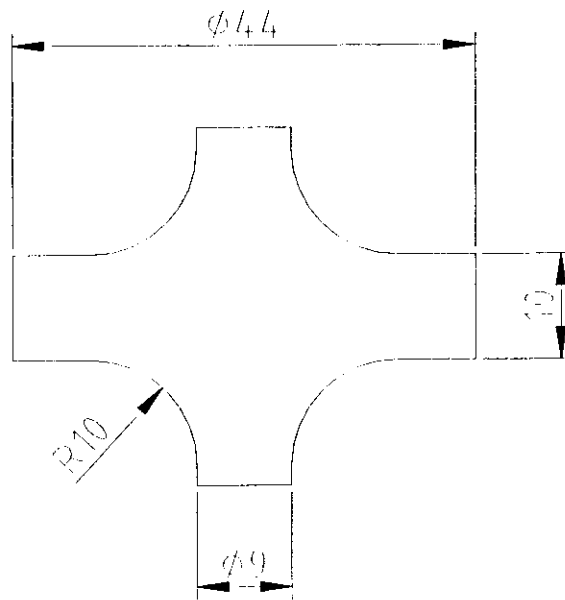
All dimensions are in mm.

Fig. (3-6): Inversion die block (First set)
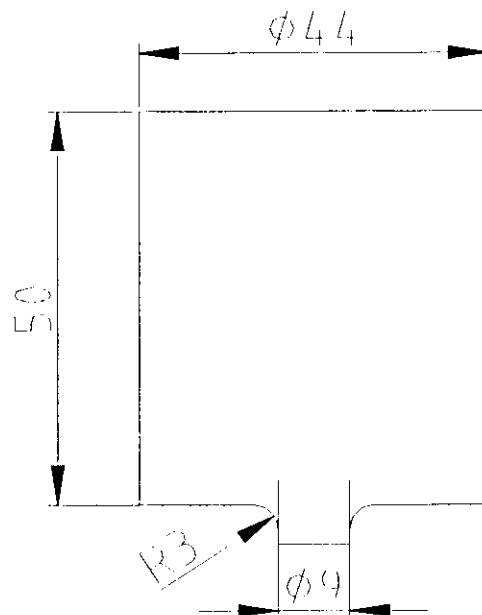
Part No. 2

All dimensions are in mm.



Fig. (3-7): Inversion die block (Second set)

Part No. 1

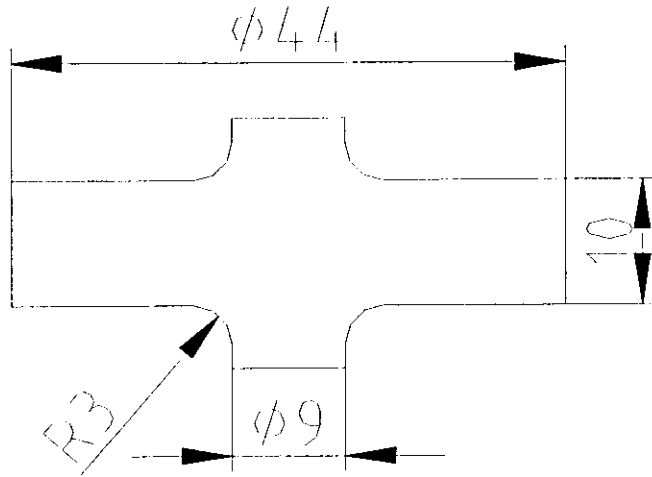2 pieces are required

All dimensions are in mm.

Fig. (3-8): Inversion die block (Second set)
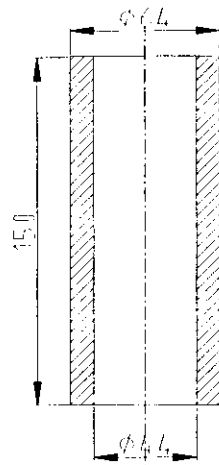
Part No. 2

All dimensions are in mm.



Fig. (3-9): The cylindrical frame of the die set (Both sets)
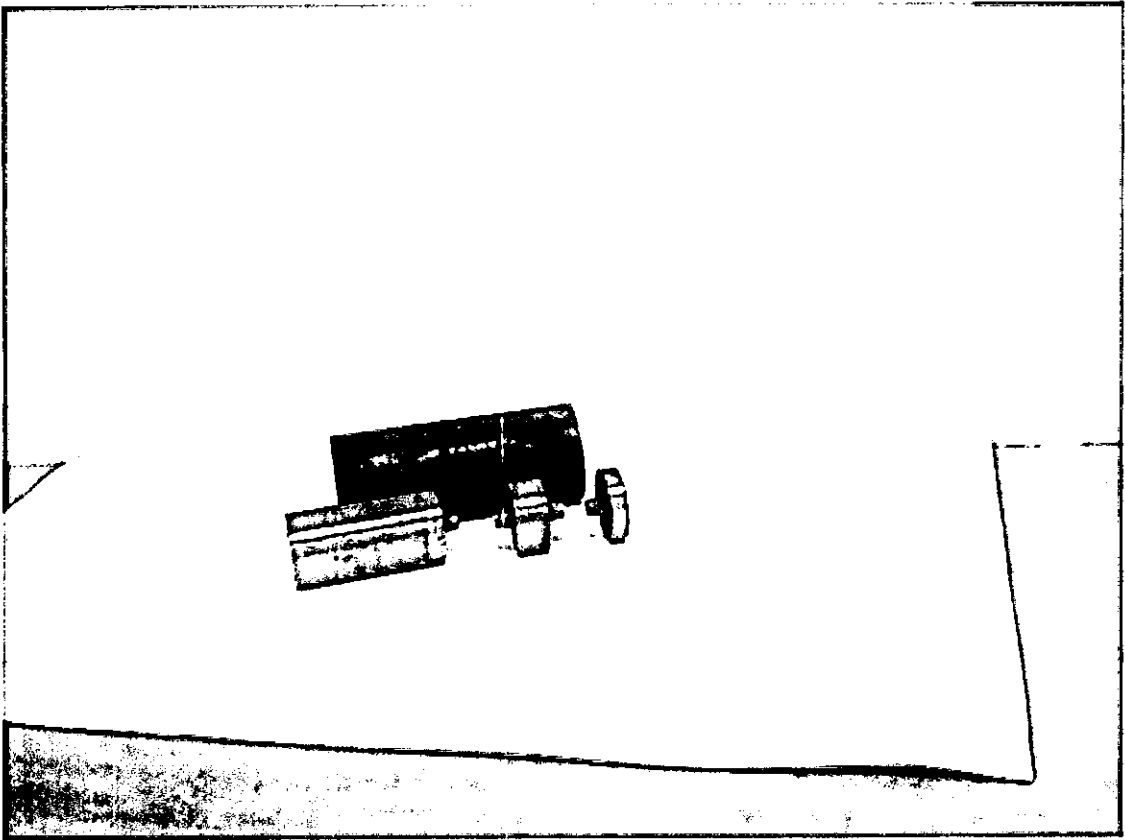
Part No. 3

All dimensions are in mm.

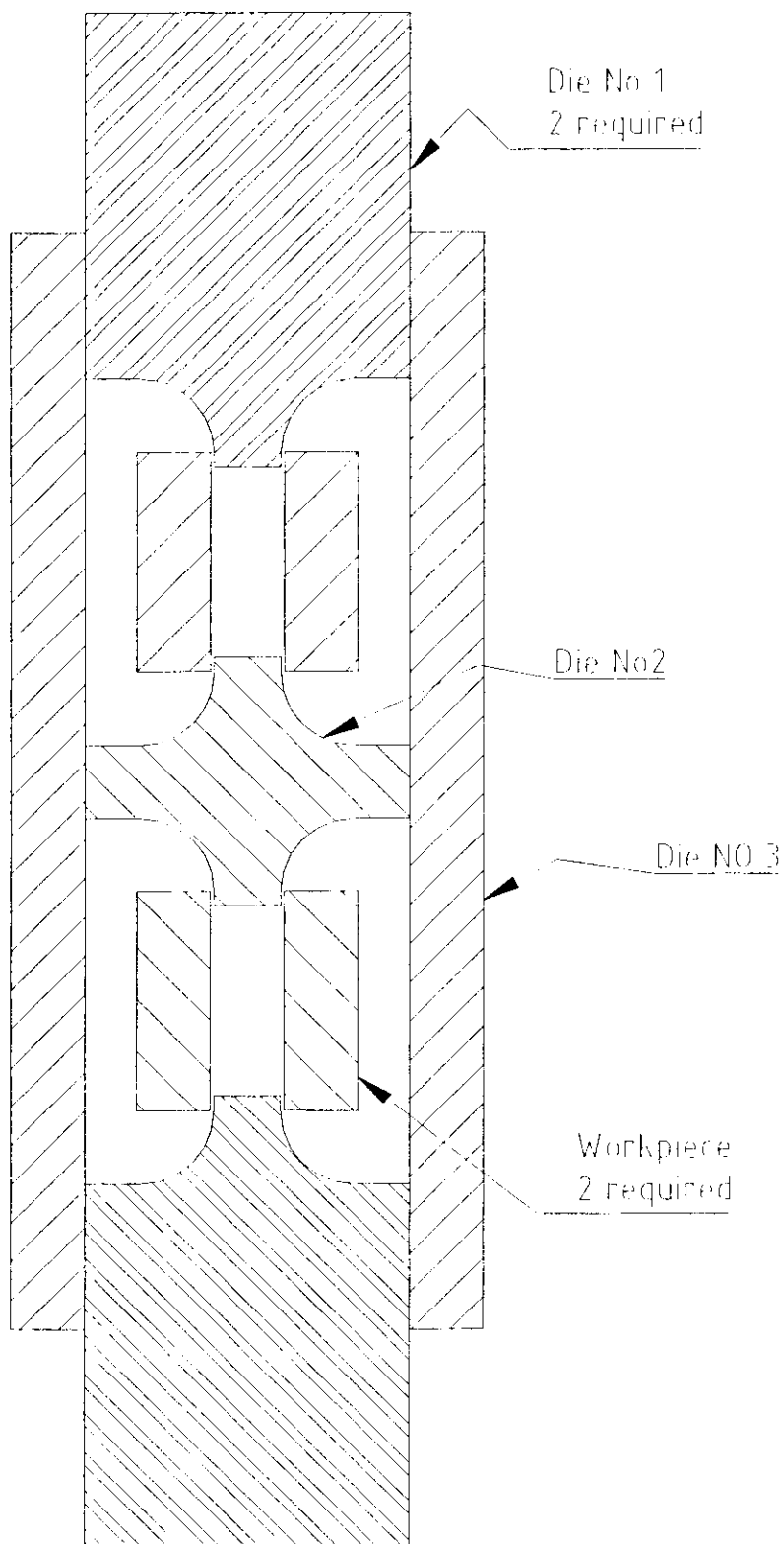Fig. (3-10): A photograph showing the parts of the inversion die set

Die No 1
2 required

Die No2

Die NO 3

Workpiece
2 required

Fig. (3-11): Schematic drawing of the tube inversion test apparatus

## 3.3 PROCEDURES

The procedures followed in this work were first to produce the superplastic material Lead- Tin and second to test it under different loading conditions.

### 3.3.1 Preparation of the Superplastic Tin – Lead Alloy

The precalculated weights of Tin and Lead were weighed using a digital balance machine to an accuracy of 0.05 milligram. These were then placed in a graphite crucible and charged into an electric furnace which was preheated to 400° C. After melting, the mixture was stirred by a graphite rod and then poured in hollow brass cylinders of 26 mm inside diameter, 70 mm height and 10 mm thickness, then left to solidify and cool in air. Finally, the first 20-mm from the top of the cast cylinder was removed to avoid any oxide or impurities in the produced superplastic alloy.

To increase the degree of superplasticity of the produced alloy, it was extruded from 26-mm diameter to 22-mm diameter followed by further compressing the extruded cylinder into 25-mm diameter. By this, the grains of the superplastic Tin – Lead cast alloy were reduced in size due to plastic deformation i.e. grain refinement takes place resulting in improvement of the degree of superplasticity.

The specimens were kept in a deep freeze until they were tested to avoid grain growth, as suggested by Al – Naib *et al.* (1970).

### 3.3.2 Testing Procedures

The following different types of tests were carried out on the superplastic Tin – Lead alloy. All the tests were carried out either on the universal testing machine, type Dartec having a capacity of 250 KN (in Albalqa Applied University) or on TI/EMC universal testing machine of capacity of 300 KN at Al- Hashemiyya University.

### 3.3.2.1 Compression tests

Thirteen tests were carried out on cylindrical specimens of 10-mm diameter and 10 mm height at different cross head speeds to determine the mechanical behavior of the produced alloy. The following cross head speeds were used 0.12, 0.2, 2, 20 and 50 mm / min giving strain rates of $3.33 \times 10^{-4}$, $5.55 \times 10^{-4}$, $5.55 \times 10^{-3}$, $5.55 \times 10^{-2}$ and $1.39 \times 10^{-1}$ / s respectively. The autographic record i.e. load – deflection curve for each test was obtained from which the true stress – true strain at each strain rate was determined. Each test was repeated twice to guarantee the repeatability of the results and when differences of more than ±2% was found, a third test was carried out. A typical autographic record of one of these compression testes at a strain rate of $5.55 \times 10^{-3}$ /s is shown in Fig. (3-13).

### 3.3.2.2 Extrusion tests

Two groups of extrusion tests were carried out, the first group was carried out in an ordinary circular cross sectional die to increase the degree of superplasticity and the second group was carried out through a series of circular cross sectional dies as means of energy absorption device.

The first group of extrusion tests were carried out at reduction from 26 to 22 mm diameter i.e. to an extrusion ratio of 1.4 whereas the second group was carried out at a reduction from one simple cylinder of 26 mm diameter to 21 cylinders of 3 mm diameter each i.e. at 75 extrusion ratio.

The tests were performed at three crosshead speeds, namely: 0.24, 5 and 120 mm / min corresponding to strain rates $3 \times 10^{-4}$, $5 \times 10^{-3}$ and $1 \times 10^{-1}$ / s respectively.
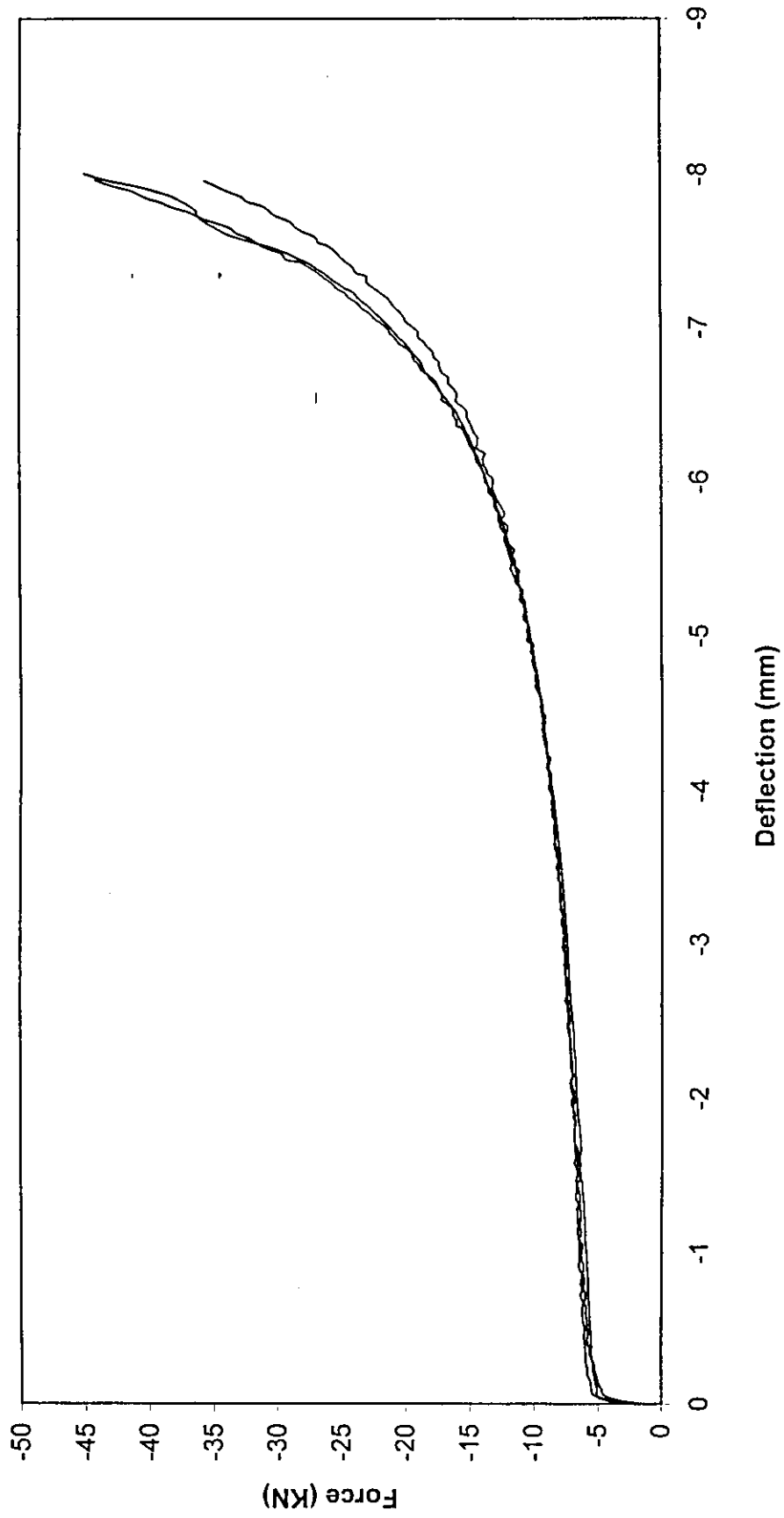
Fig. (3-13): Autographic record of compression test of superplastic Tin- Lead alloy at strain rate of 5.55 E-3/s

A typical autographic record of the second group of extrusion tests is shown in Fig. (3-14)

### 3.3.2.3 Tube inversion tests

These tests were carried out to investigate an other mean of utilizing the plastic work consumed in inverting tubes as energy dissipation system to protect vehicle occupants during accidents.

To perform these tests, hollow cylindrical specimens of superplastic Tin – Lead were first produced by extrusion of the material around a mandrel fixed in the middle of the extrusion die set, where the die opening served to produce the outer diameter of the tube, 26 mm diameter, and the mandrel diameter served to produce the inside diameter which is 10 mm.

The produced tubes were then cut to heights of 40 mm which confirms to the dimensions of the designed and manufactured die set for the tube inversion tests, Fig. (3-15).

After the tubes were placed in position, the whole assembly was placed between the two platens of the universal testing machine and were subjected to loading by applying a compressive load to the upper and lower die blocks, causing the tube to be inverted and bent around the profile radius of the upper, middle and lower die blocks.

These tests were carried out at crosshead speeds of 0.4, 8.3 and 200 mm /min corresponding to strain rates $1.2 \times 10^{-4}$, $2.5 \times 10^{-3}$ and $6 \times 10^{-2}$ /s using die blocks of profile radii of 3 and 10 mm.

Fig.(3-14): Autographic record for extrusion of Tin-Lead alloy

Strain Rate = 0.1/s

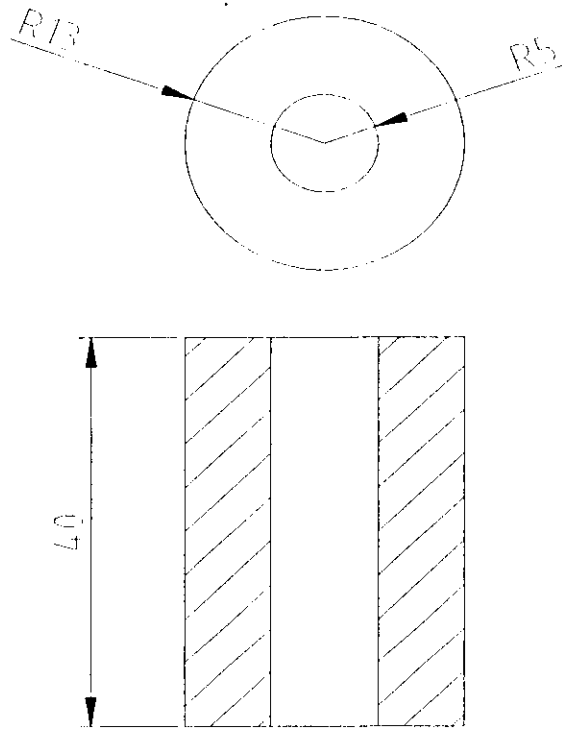deflection (mm)

Force(KN)
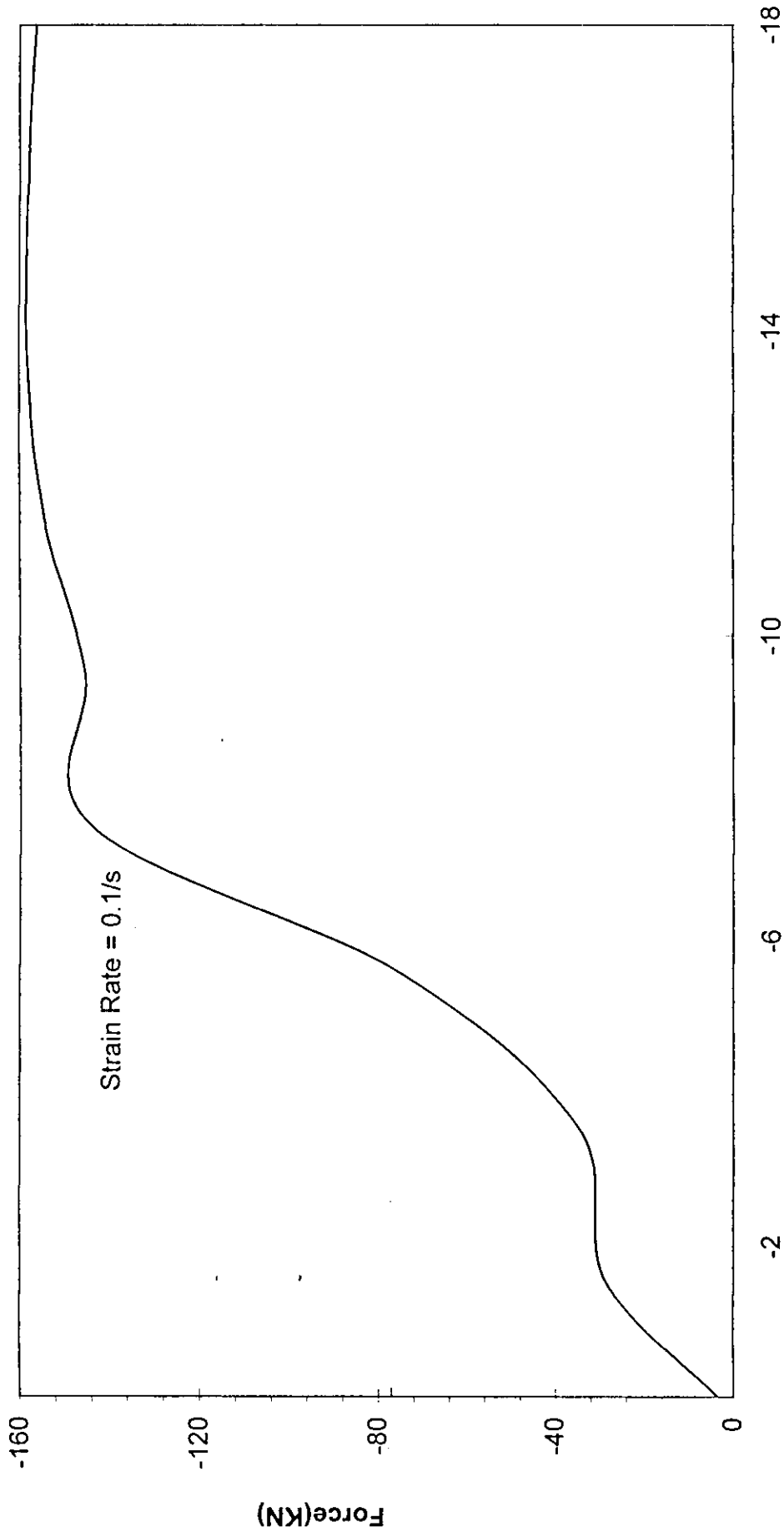
Fig. (3-15): A hollow cylinder produced by extrusion for inversion tests

All dimensions are in mm.

# 4. THEORETICAL CONSI DERATIONS

In this chapter, the basic terms and concepts that may be used in any theoretical aspects on the subject are discussed

## 4.1 BASIC DIFINITIONS:

### 4.1.1 Stress

The engineering Stress, *S*, is defined as:

$$S = \frac{F_c}{A_o} \tag{4.1}$$

Where:

*S: engineering stress*

*$F_c$: the current force applied on the specimen in a tension or compression test*

*$A_o$: the original cross sectional area of the specimen*

While the actual or true stress is defined as:

$$\sigma = \frac{F_c}{A_c} \tag{4.2}$$

Where:

*σ : actual or true stress*

*$A_c$: the current cross sectional area of the specimen*

### 4.1.2 Strain

The engineering strain, *e*, is defined as:

$$e = \frac{\Delta l}{l_o} \tag{4.3}$$

Where:

*e: engineering strain*

$\Delta l$ : *change in length of the specimen*

$l_o$: *original length of the specimen*

While the actual or true strain, $\varepsilon$, is defined as:

$$\varepsilon = \int_0^\varepsilon d\varepsilon = \ln\frac{l_f}{l_o} = \ln\frac{l_o + \Delta l}{l_o} = \ln\left(1 + \frac{\Delta l}{l_o}\right) = \ln(1 + e) \qquad (4.4)$$

Where:

$\varepsilon$: *actual or true strain*

$l_f$: *the final length of the specimen*

### 4.1.3 Autographic record

Autographic record is the force- deflection curve in any loading process

### 4.1.4 Perfectly plastic, or rigid plastic material

A perfectly plastic or rigid plastic material is a material for which $\sigma = \sigma_y$ for any strain

### 4.2 Representative Stress ($\bar{\sigma}$) and representative strain ($\bar{\varepsilon}$)

In the general case of a three dimensional stress system, there will be three true principal stresses $\sigma_1$, $\sigma_2$, and $\sigma_3$. If the loading system is such that the stresses $\sigma_1$, $\sigma_2$, and $\sigma_3$ does not reach or exceed the elastic limit, there will be a change in volume of the material, and poison's ratio will have a value depending on the loaded material but never equals 0.5. However if the loading system represented by the stresses $\sigma_1$, $\sigma_2$, and $\sigma_3$ and the strains $\varepsilon_1$, $\varepsilon_2$ and $\varepsilon_3$ is such that yielding takes place at any part of the material, then poison's ratio for all materials at and after yielding i.e. over the whole plastic region will be equal to 0.5 i.e. $\upsilon = 0.5$.

This is known in the theory of plasticity as the constant volume principle or the incompressibility of the loaded material in the plastic region. This may be represented as the sum of the three principal strains being equal to zero i.e.

$$\varepsilon_1 + \varepsilon_2 + \varepsilon_3 = 0 \qquad (4.5)$$

Furthermore, in the plastic region, the three stresses are represented by one principal stress component referred to as the representative stress σ and determined from

$$\bar{\sigma}^2 = \frac{1}{2}\left[(\sigma_1 - \sigma_2)^2 + (\sigma_2 - \sigma_3)^2 + (\sigma_3 - \sigma_1)^2\right] \qquad (4.6)$$

and the strains are represented by a principal strain component referred to as representative strain ε, determined from (Caddell, 1993).

$$\bar{\varepsilon}^2 = \frac{2}{9}\left[(\varepsilon_1 - \varepsilon_2)^2 + (\varepsilon_2 - \varepsilon_3)^2 + (\varepsilon_3 - \varepsilon_1)^2\right] \qquad (4.7)$$

It is worth noting that for a uniaxial stress system, whether pure tensile or pure compression, namely $(\sigma_1, 0, 0)$ or $(0, 0, -\sigma_1)$ respectively, the representative stress $\bar{\sigma}$ for these two systems will be equal to $\sigma_1$ and the representative strain $\bar{\varepsilon}$ will be equal to $\varepsilon_1$. As the strain systems will be $(\varepsilon_1, -0.5\varepsilon_1, -0.5\varepsilon_1)$ or $(0.5\varepsilon_1, 0.5\varepsilon_1, -\varepsilon_1)$ respectively and by substituting the corresponding values of stresses and strains for each of the two systems in equations (4.6) and (4.7) respectively, these results were obtained.

### 4.3 Strain Rate, $\dot{\varepsilon}$

Strain rate is usually defined as

$$\dot{\varepsilon} = \frac{d\varepsilon}{dt}\left(s^{-1}\right) \qquad (4.8)$$

In manufacturing processes in general and forming in particular, the instantaneous strain rate is extremely difficult to determine and as its effect becomes only pronounced when it varies by orders of magnitude, therefore the average strain rate is the one, which is always used in these processes. This is defined as $\bar{\varepsilon}$ and equals the representative strain over the forming time, t i.e. (Zaid, 1997)

$$\bar{\dot{\varepsilon}} = \frac{\bar{\varepsilon}}{t} \tag{4.9}$$

Where $\varepsilon$ is the representative strain and $t$ is the forming time.

## 4.4 Energy Consumed in Plastic Deformation

As mentioned earlier, for uniaxial stress system, the true stress is a representative stress and the true strain is a representative strain. Then the true stress-true strain curve from uniaxial loading will be a representative stress- representative strain curve.

Referring to Fig. (4-1), the differential small quantity of plastic work $dw_p$ per unit volume is determined from

$$dW_p = \bar{\sigma} \, d\bar{\varepsilon} \tag{4.10}$$

$$Plastic \ work(W_p) \Big/ Unit \ volume = \int_0^{\bar{\varepsilon}_p} \bar{\sigma} \, d\bar{\varepsilon} \tag{4.11}$$

$$Plastic \ work(W_p) = \int_v \int_0^{\bar{\varepsilon}_p} \bar{\sigma} \, d\bar{\varepsilon} \, dv \tag{4.12}$$

For an engineering material where the general equation representing its mechanical behavior is given by:

$$\bar{\sigma} = k_1 \bar{\varepsilon}^n \tag{4.13}$$

Where

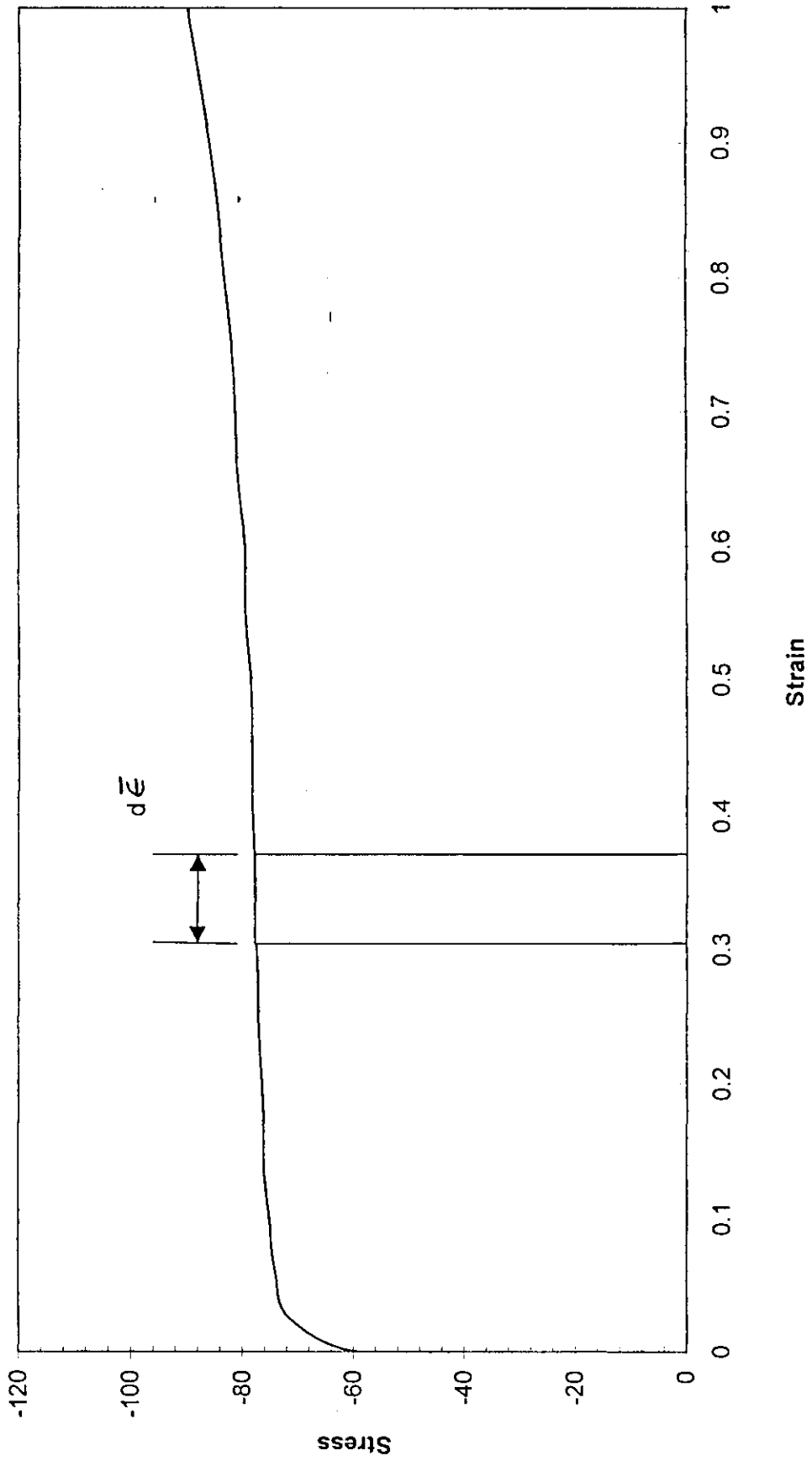$K_1$ : material constant

$n$ : strain hardening index

Fig (4-1): Definition of the differential plastic work

Whereas for a superplastic material

$$\overline{\sigma} = k_2 \dot{\overline{\varepsilon}}^m \qquad (4.14)$$

Where

$K_2$ : material constant

$m$ : strain rate sensitivity index

Hence to determine the plastic work per unit volume $W_p$, the value of $\sigma$ is substituted from equation (4.13) or (4.14) in equation (4.11) for an ordinary engineering material or superplastic material respectively and carryout the integration. The total theoretical energy consumed in plastic work i.e., just to overcome the mechanical strength of the material, can be determined using equation (4.12).

To determine the actual energy consumed in any forming process, the work consumed in friction between the die and the workpiece ($W_f$) which varies from 15% to 35% of the total work depending on the effectiveness of the lubricant used and the redundant work ($W_r$), which ranges from 5% to 15% of the total work being maximum in the extrusion and wire drawing processes, should be added to the theoretical work value obtained from equation (4.12).

## 4.5 Extrusion Processes

The following terms are usually used in extrusion processes

$$Extrusion\ ratio\ (R) = \frac{A_o}{A_f} \qquad (4.15)$$

$$Reduction\ percentage\ (r) = \frac{A_o - A_f}{A_o} \times 100\% = (1 - \frac{A_f}{A_o}) \times 100\% = (1 - \frac{1}{R}) \times 100\% \qquad (4.16)$$

container decreases as the extrusion process proceeds. These three forces sum together to give the total extrusion force.

The theoretical work per unit volume for any extrusion process can be derived by assuming the process to be equivalent to a uniaxial stress system and using equation (4.11), where the representative stress for this case is the average flow Stress ($Y_f$)

$$Plastic\ work\ (W_p)/Unit\ volume = Y_f \ln\frac{l_f}{l_o} = Y_f \ln\frac{A_o}{A_f} = Y_f \ln R = Y_f \ln\frac{1}{1-r} \qquad (4.20)$$

The extrusion pressure (P) can be related to the plastic work per unit volume as follows

Plastic work = (Force) x (distance along the force) = (P) x ( $A_o$ ) x ( $l_o$ )

$$= Volume \int_0^{\bar{\varepsilon}_p} \bar{\sigma}\ d\bar{\varepsilon} = A_o\ l_o \int_0^{\bar{\varepsilon}_p} \bar{\sigma}\ d\bar{\varepsilon} \qquad (4.21)$$

$$\Rightarrow P = \int_0^{\bar{\varepsilon}_p} \bar{\sigma}\ d\bar{\varepsilon} = Plastic\ work\ /\ Unit\ volume \qquad (4.22)$$

Experimental formulae were suggested by Johnson and Watkin to determine extrusion pressures. Both have identical form to equations (4.20) and (4.22).

### 4.5.1 Johnson's Formula

$$\frac{P}{Y} = a + b\ln\frac{1}{1-r} = a + b\ln R \qquad (4.23)$$

where

a = 0.8          b = 1.5          Y = Average flow stress

### 4.5.2 Watkin's Formula

$$P = a + b \ln \frac{1}{1-r} = a + b \ln R \qquad\qquad (4.24)$$

Where P is the extrusion pressure in tons and the value of the constants a and b depend on the extruded material. Their values for Lead are 2.7 and 8 respectively, while they are 6 and 3 respectively For Tin.

### 4.6 Tube Inversion Processes

### 4.6.1 Mechanism of Deformation

The tube inversion process can be divided to three subsequent steps

1-Bending of the tube around the die profile radii.

2-Unbending of the bent part.

3- Expansion of the unbent part from the original tube diameter (d) to the final Expanded diameter which is d+4r+2t.

The plastic work consumed in this system will be that consumed in the previous three processes i.e.

Total work = Bending work + Unbending work + Expansion work $\qquad$ (4.25)

### 4.6.2 Calculation of Energy Consumed in Bending a Tube

In the case of bending a tube, the existing true strains are

1- Circumfrential strain i.e. hoop or tangential strain ( $\varepsilon_0$ ).

2- Radial strain ( $\varepsilon_r$ ).

3- Thickness strain ( $\varepsilon_t$ ).

Maximum tangential engineering strain in bending a straight part of a tube around a radius ( r ) with the neutral plane remaining in the geometrical center of the tube is given by

$$e_{\theta_{max}} = \frac{2\Pi\left(r + \frac{t_o}{2}\right) - 2\Pi r}{2\Pi r} = \frac{t_o}{2r} \qquad (4.26)$$

Substituting for $e_{\theta max}$ from equation (4.26) in equation (4.4) to get the maximum true tangential strain, $\varepsilon_{0max}$ as

$$\varepsilon_{\theta_{max}} = \ln\left(1 + \frac{t_o}{2r}\right) \qquad (4.27)$$

This is the maximum value of the tangential strain, while the tangential strain at the undeformed part of the specimen is zero. Hence the average value of the tangential strain is half the maximum i.e.

$$\varepsilon_\theta = \frac{1}{2}\ln\left(1 + \frac{t_o}{2r}\right) \qquad (4.28)$$

Experimental measurements of the thickness strain at different positions along the deformed tube were carried out. The thickness strain variation was found to be very small along the major part of the tube and does not exceed a maximum value of 10% at a very small part of the tube. Therefore it is justified with very good approximation to consider that the inversion process takes place without change in thickness i.e. $\varepsilon_t = 0$.

Substituting this result in equation (4.5), to get

$$\varepsilon_r = -\varepsilon_\theta = -\frac{1}{2}\ln\left(1 + \frac{t_o}{2r}\right) \qquad (4.29)$$

Substituting the values of the strains in equation (4.7), the representative strain in the bending stage $\varepsilon_{bending}$ is

$$\overline{\varepsilon}_{bending} = \frac{2}{\sqrt{3}}\varepsilon_\theta = \frac{1}{\sqrt{3}}\ln\left(1+\frac{t_o}{2r}\right) \tag{4.30}$$

The energy consumed in bending stage can be calculated using equation (4.12). In this equation the value of the representative stress from equation (4.13) is substituted if the material is an ordinary engineering material or from equation (4.14) if the material is superplastic. The value of representative strain is then calculated by substituting the corresponding values of $t_o$ and $r$ in equation (4.30).

### 4.6.3 Calculation of the Energy Consumed in Unbending a Tube

The energy consumed in the unbending stage is equivalent to that consumed in the bending stage because

- The material is a non-work-hardening material being superplastic.

- The bending and unbending are symmetric.

### 4.6.4- Calculation of the Energy Consumed in the Expansion of the Tube

After the tube is unbent, it will continue to expand. The true strains in the tube in this stage will be

1- Circumfrentiol strain i.e. hoop or tangential strain ( $\varepsilon_\theta$ ).

2- Longitudinal strain ( $\varepsilon_l$ ).

3- Thickness strain ( $\varepsilon_t$ ).

The engineering tangential strain for this case is given by

$$e_\theta = \frac{d+4r+2t-d}{d} = \frac{4r+2t}{d} \tag{4.31}$$

And the true tangential strain is calculated using equation (4.4) as

$$\varepsilon_\theta = \ln\left(1+\frac{4r+2t_o}{d}\right) \tag{4.32}$$

The thickness strain $\varepsilon_t$ can be assumed to be zero depending on experimental measurements as explained before

Substituting this result in equation (4.5), to get

$$\varepsilon_l = -\varepsilon_\theta = -\ln\left(1 + \frac{4r + 2t_o}{d}\right) \qquad (4.33)$$

Substituting the values of the strains in equation (4.7), $\varepsilon$ for the tube expansion is obtained as

$$\bar{\varepsilon}_{exp\,ansion} = \frac{2}{\sqrt{3}}\varepsilon_\theta = \frac{2}{\sqrt{3}}\ln\left(1 + \frac{4r + 2t_o}{d}\right) \qquad (4.34)$$

The energy consumed in the expansion stage can be calculated using equation (4.12). By substituting in this equation, the value of the representative stress as obtained from Equation (4.13) for an ordinary engineering material or as obtained from equation (4.14) for a superplastic material. The value of representative strain is calculated by substituting the corresponding values of $t_o$, $d$ and $r$ in equation (4.34).

Finally the total theoretical energy consumed in the tube inversion is simply the summation of the energy consumed in the three stages, namely bending, unbending and the expansion stages.

# 5. RESULTS AND DISCUSSION

In this chapter , the obtained results for each of the investigated systems together with discussion of these results will be presented

## 5.1 Mechanical behavior

Fig. (5-1) gives the compression autographic record for the superplastic Tin-Lead alloy which was grain refined by extrusion and compression. Specimens of 10 mm diameter and 10 mm height i.e. of an aspect ratio equals one, were compressed at different cross head speeds namely 0.12, 0.2, 2, 20 and 50 mm/ min corresponding to strain rates 3.33 x $10^{-4}$, 5.55 x $10^{-4}$, 5.55 x $10^{-3}$, 5.55 x $10^{-2}$ and 1.4 x $10^{-1}$ /s.

The mechanical behavior of this alloy represented by the true stress- true strain curve i.e. $\sigma$- $\varepsilon$ curve which is the representative stress, $\sigma$,- representative strain, $\varepsilon$, is shown in Fig. (5-2).

It can be seen from this figure that although the material is compressed within the quasi-static range i.e. 3.33 x $10^{-4}$ to 1.4 x $10^{-1}$ /s, the material has shown a high degree of strain rate sensitivity. For example, at a compression strain of 0.6, the flow stress, $\sigma_f$, at 3.33 x $10^{-4}$ /s is 45 Mpa, whereas the flow stress is 100 Mpa at 0.14 /s strain rate, indicating a rate sensitivity of 2.2.

It is worth noting in this respect that if an engineering material like steel or aluminum was tested at these two strain rates, the flow stress would not have been altered (Baraya, 1971).

To determine the rate sensitivity range of this material, the previous data was reproduced as log $\sigma$ versus log $\acute{\varepsilon}$ as shown in Fig. (5-3) from which the rate sensitivity
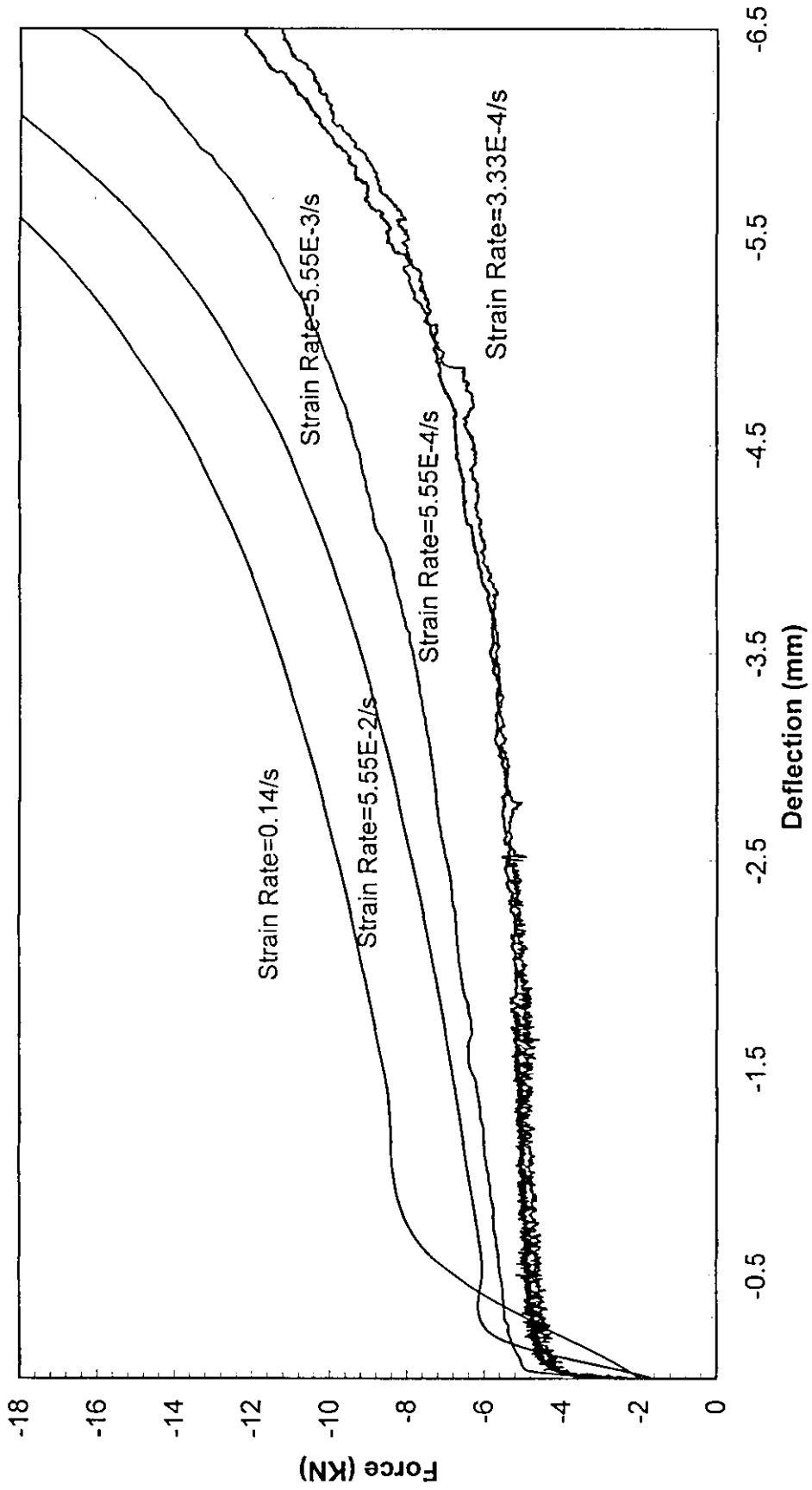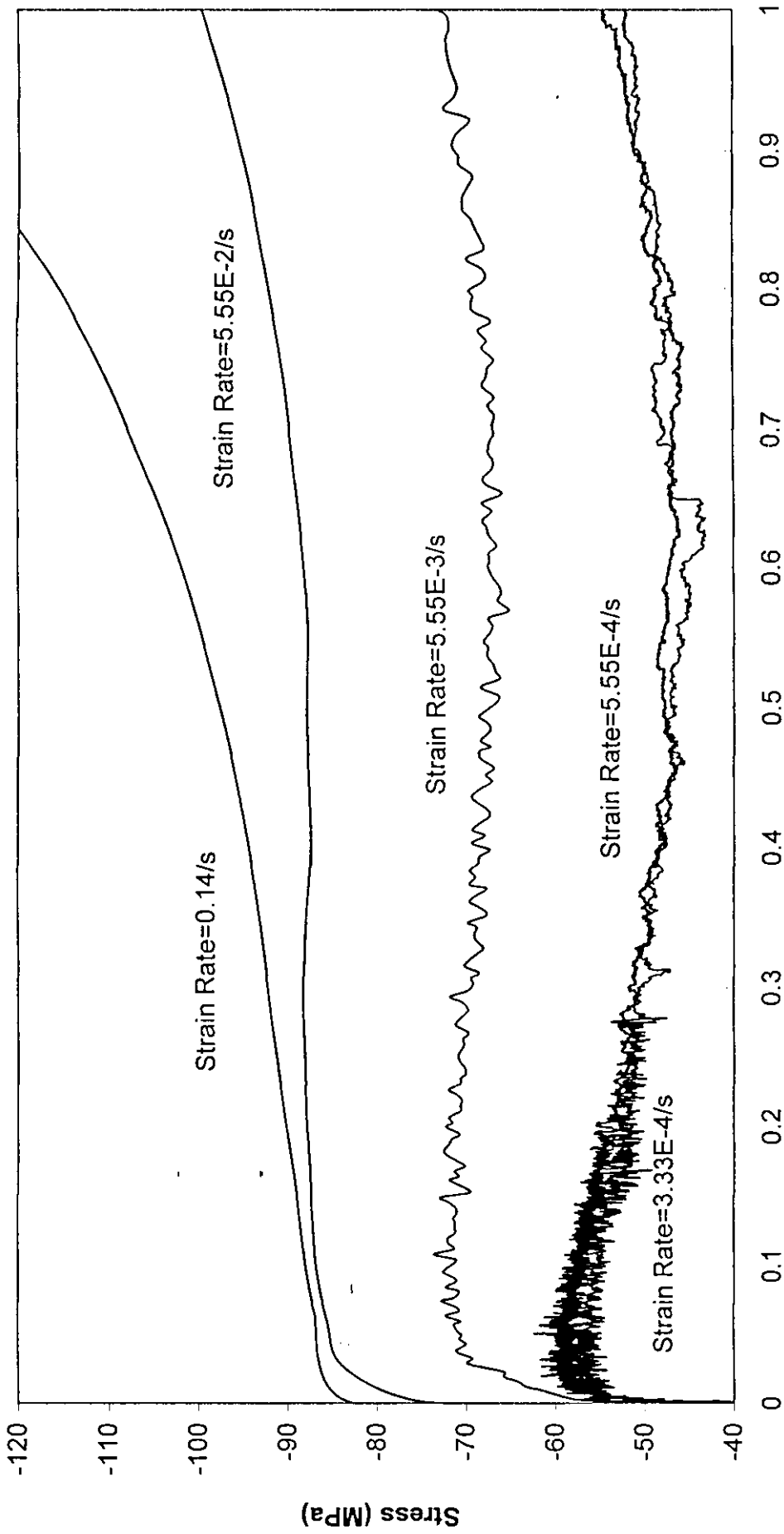
Fig. (5-1): Autographic record for compression experiments
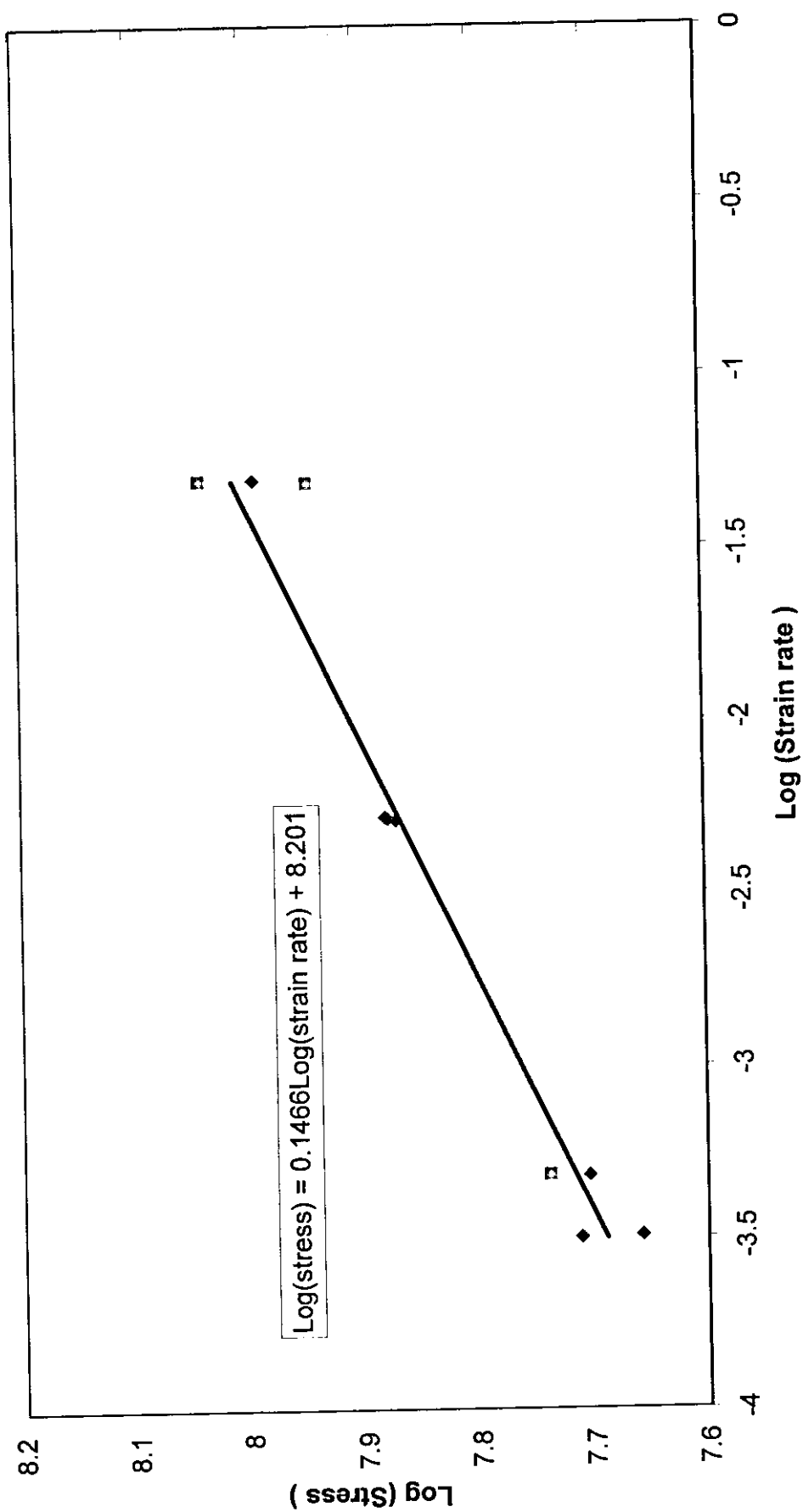
Fig. (5-2): Stress-Strain curves for Tin-Lead alloy

Fig. (5-3): Log stress-log strain curve for Tin-Lead alloy

Log(stress) = 0.1466Log(strain rate) + 8.201

index was found to be 0.1466. Hence, the mechanical behavior of the prepared superplastic Tin- Lead alloy can be indicated by the following relationship

$$\sigma = 158.85(\dot{\varepsilon})^{0.1466} \tag{5.1}$$

Where $\sigma$ is in Mpa.

## 5.2 Energy Dissipation System Based on Extrusion Process

### 5.2.1 Preliminary Experiments

Before the actual system was investigated, preliminary tests were carried out on plasticine and pure lead to test the performance of the system. Fig. (5-4) and Fig. (5-5) show the autographic records for the extrusion system for plasticine and lead respectively. It was concluded that the system worked successfully and hence it was later used on the superplastic mateial.

### 5.2.2 Experiments on the Extrusion of Superplastic Material

After the preliminary results on plasticine and lead, the extrusion die set was tried on the superplastic Tin- Lead alloy. Fig. (5-6) shows the autographic record of the test, at three different strain rates, namely $3 \times 10^{-4}$, $5 \times 10^{-3}$ and $1 \times 10^{-1}$ /s. The photograph of Fig. (5-7) shows the female die with the twenty one extruded cylinders, coming out of the die.

It is clear from Fig. (5-6) that the energy consumed increases with the increase of strain rate for the same plunger displacement, which again reflects the rate sensitivity of this alloy.

To determine the effect of strain rate on the energy absorbed by this system, the energy was calculated at each strain rate for a constant value of deflection, at 17.5 mm. The energy which is represented by the area under each curve was determined using the trapezoidal rule. These results are shown in Table (5-1).
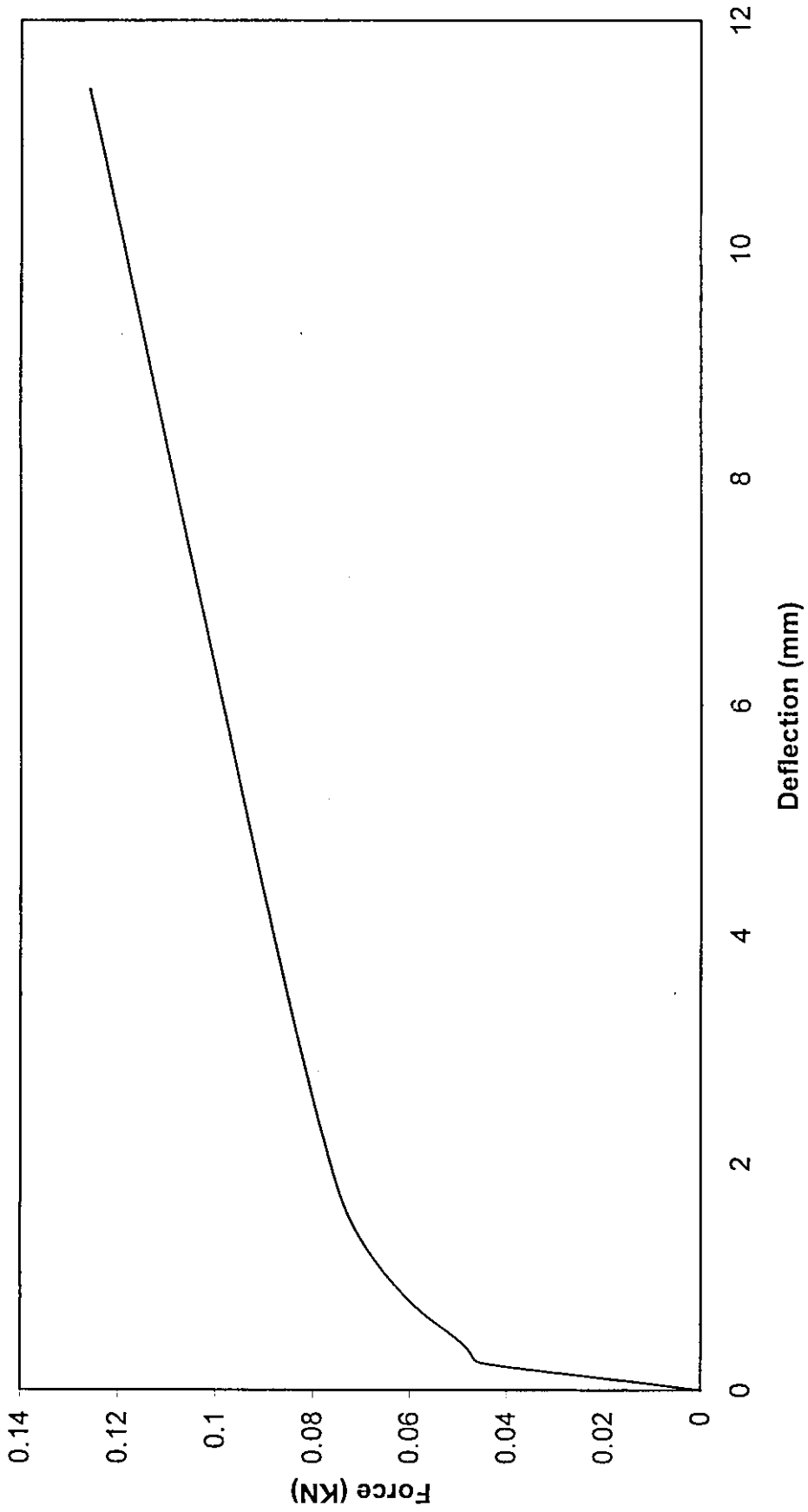
**Fig. (5.4): Autographic record for extrusion of plastecine through a single die**
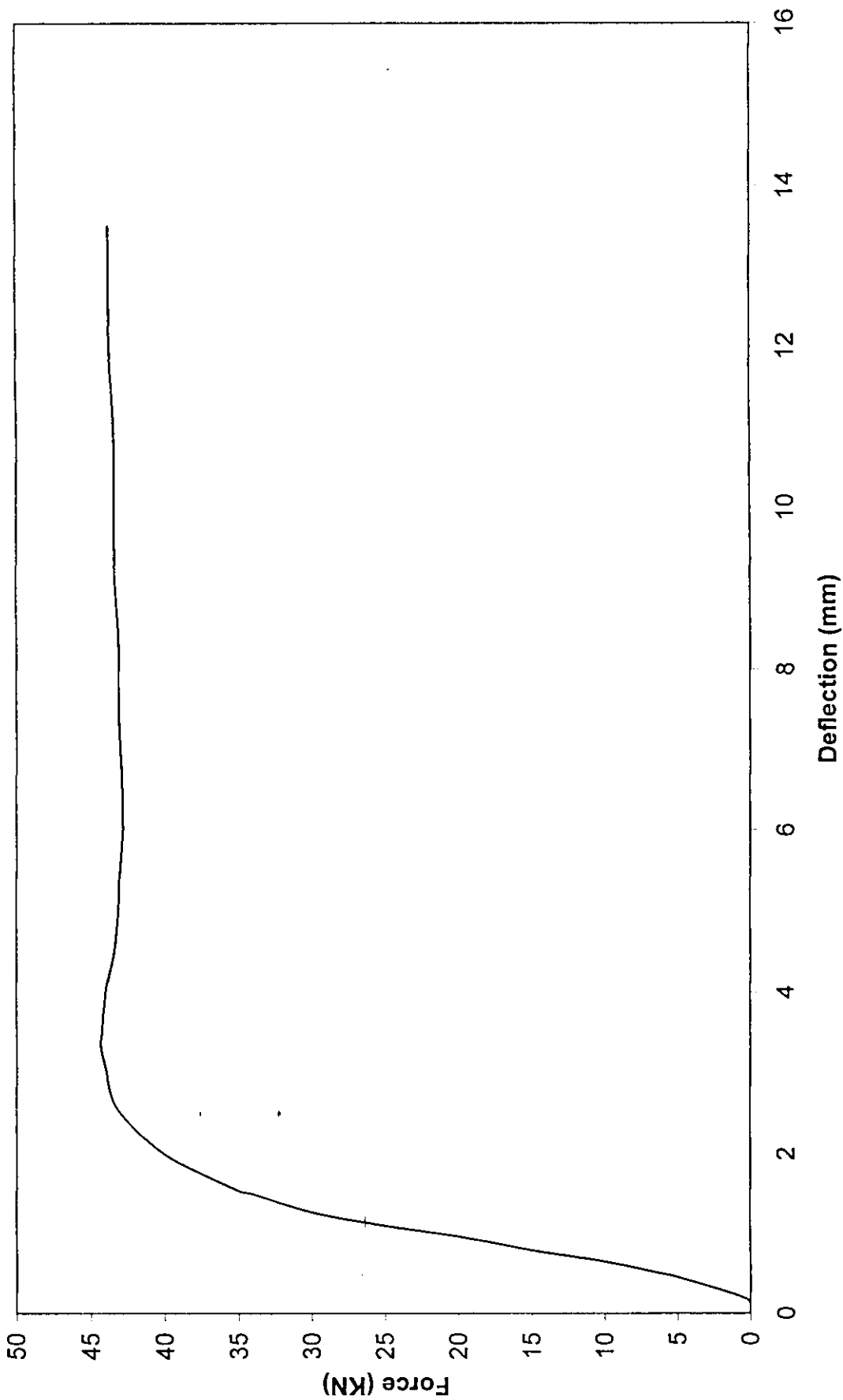
Fig. (5-5): Autographic record for extrusion of lead through a single die
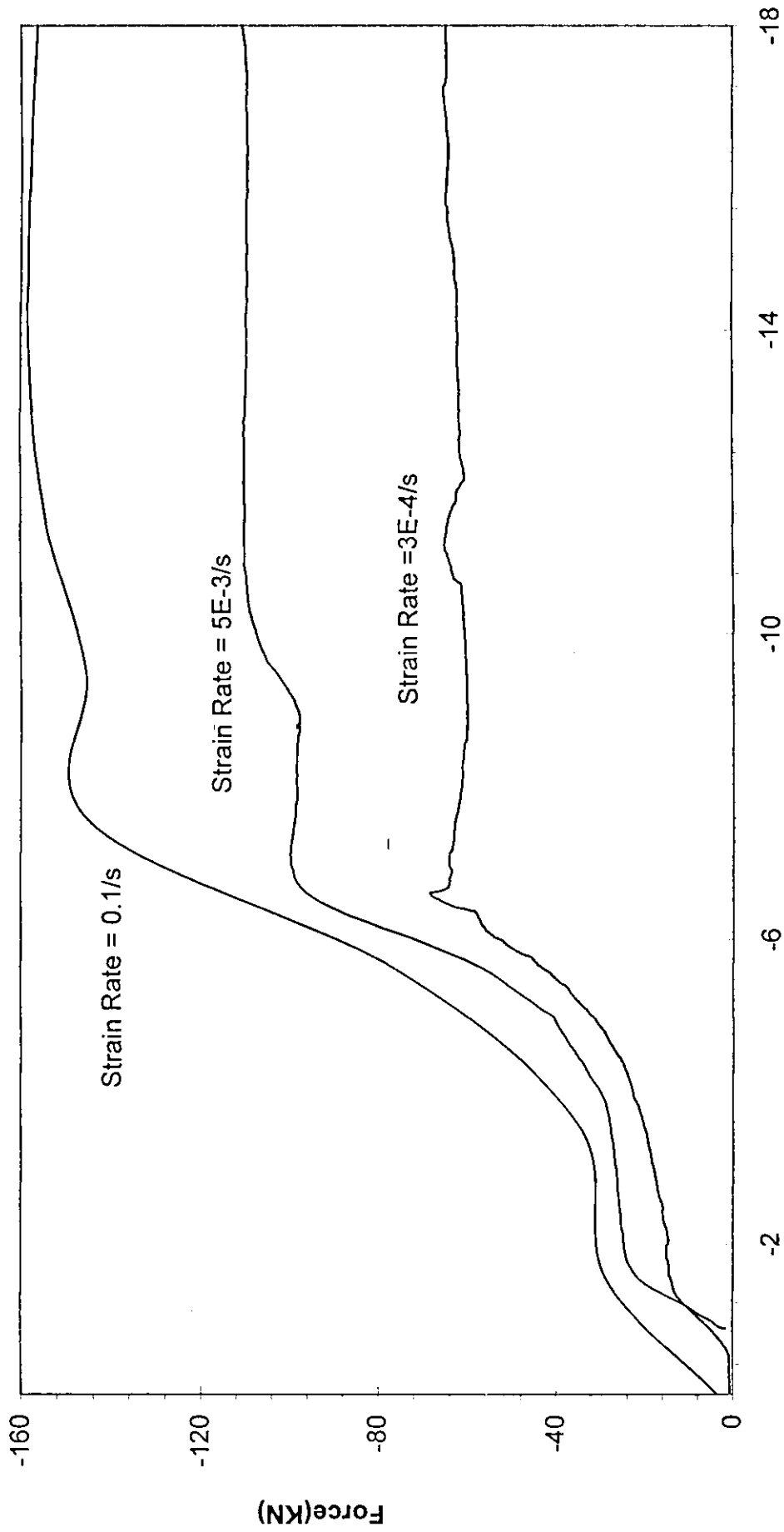
Fig.(5-6): Autographic record for extrusion of Tin-Lead alloy
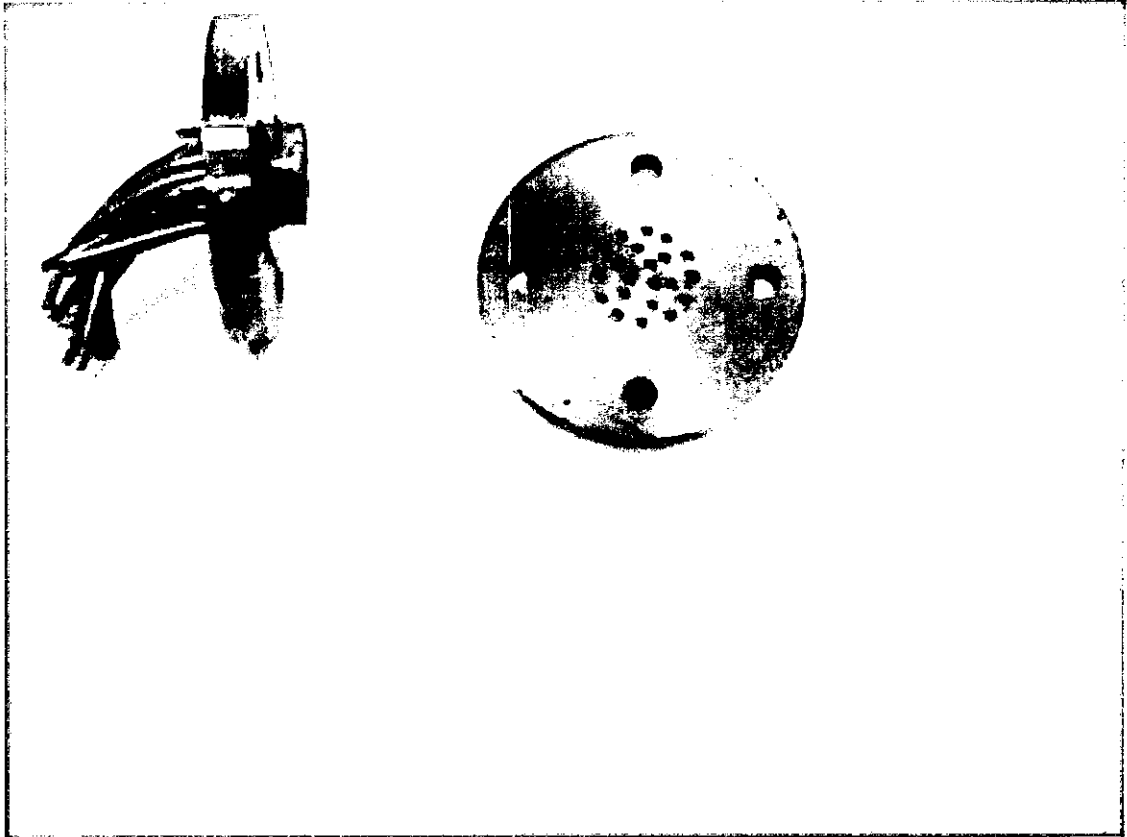
Fig. (5-7): A photograph showing the extrusion die with the extruded material coming out of it

Table (5-1): Variation of energy with strain rate at 17.5 mm deflection

| Cross Head Speed (mm/min) | Strain Rate $s^{-1}$ | Energy Absorbed (Joule) |
|---|---|---|
| 0.24 | $3 \times 10^{-4}$ | 835 |
| 5 | $5 \times 10^{-3}$ | 1376 |
| 120 | $1 \times 10^{-1}$ | 1944 |

It can be seen from table (5-1) that although the strain rate was increased from $3 \times 10^{-4}$ to $5 \times 10^{-3}$ /s i.e. by 17 times, the energy consumed was increased by about 65%, whereas increasing the strain rate from $5 \times 10^{-3}$ to $1 \times 10^{-1}$ /s i.e. by 20 times, the energy has increased only 41.3%. This indicates that this alloy is more sensitive at the lower values of strain rates and becomes less sensitive at the higher values. This is a typical behavior of a superplastic material as it behaves like an ordinary material after it surpasses its rate sensitive range, (Zaid and abdullatif, 1984).

### 5.2.3 Experiments with Offset Extrusion Dies

To increase the energy consumed by the previous die system at any strain rate, other systems utilizing the extrusion through two and three offset multiple dies were investigated as shown in Fig. (5-8) and Fig. (5-9) respectively.
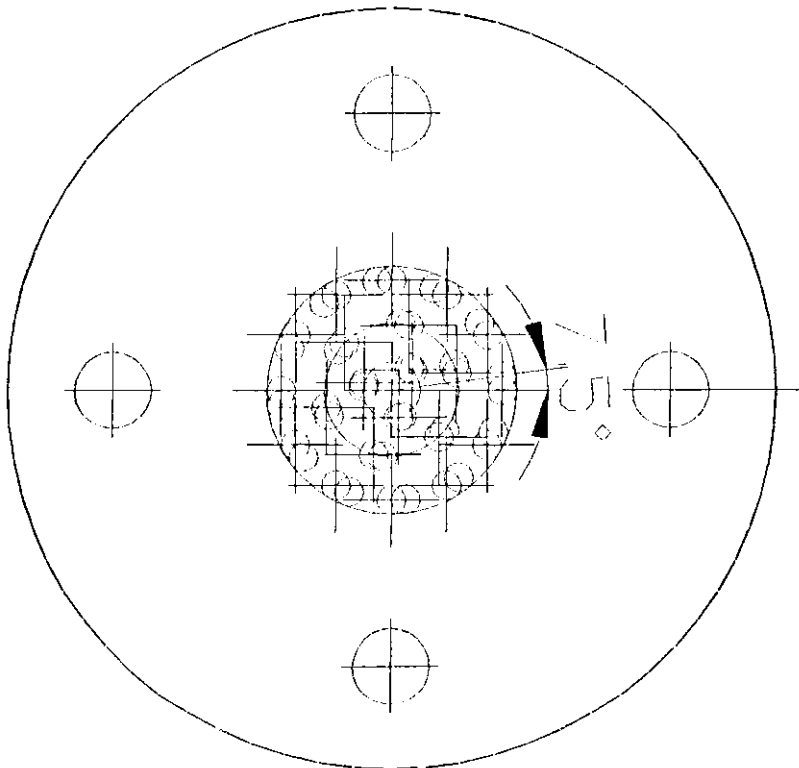


Fig. (5-8): Two offset extrusion dies
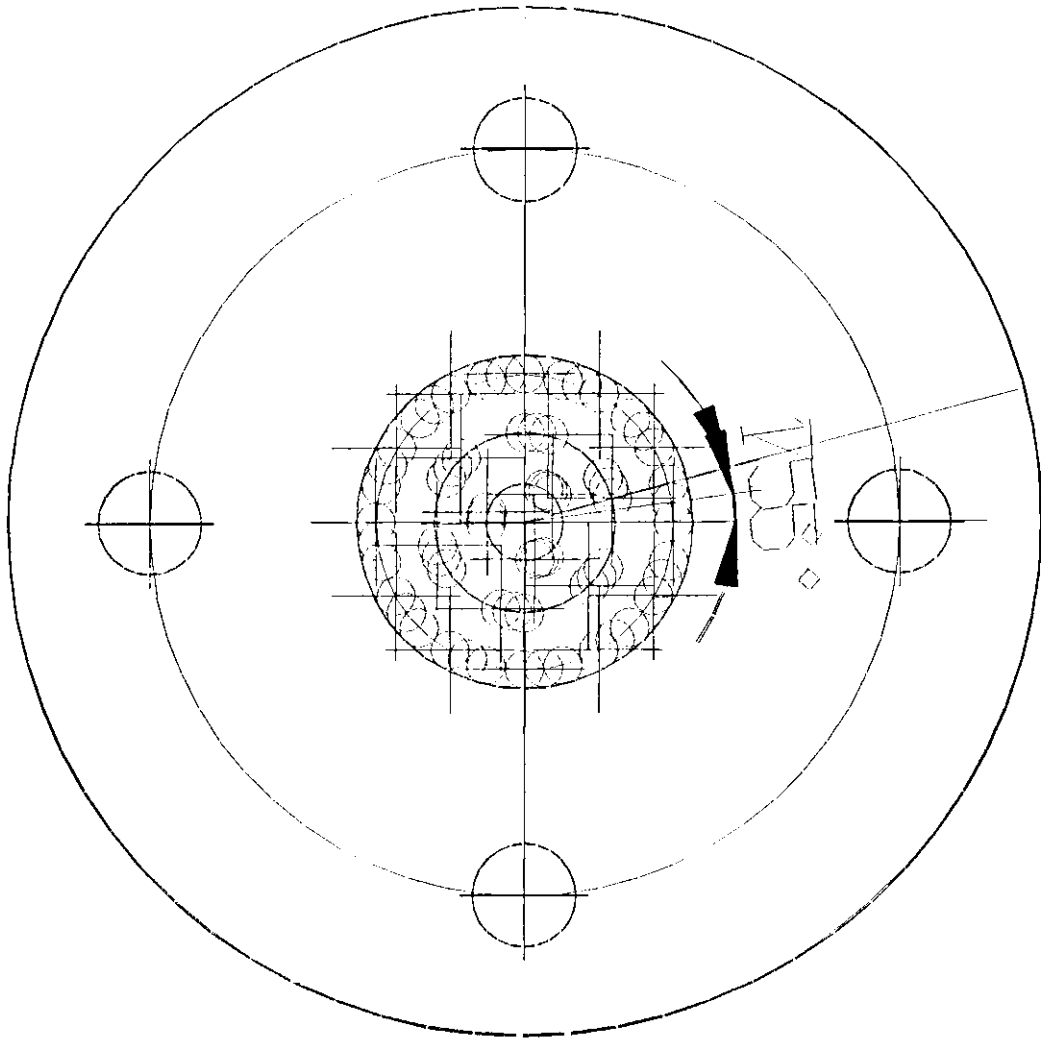
Fig. (5-9): Three offset extrusion dies

As in the case of the one multiple die, offset type dies were first tried on plasticine and lead. The outographic records for plasticine using the two and three offset die set are shown in Fig. (5-10) and Fig. (5-11) respectively, whereas, the autographic records for Lead are shown in Fig. (5-12) and Fig. (5-13) respectively.

Fig. (5-10): Autographic record for extrusion of plastecine through two dies set

Fig. (5.11): Autographic record for extrusion of plastecine throgh three dies set

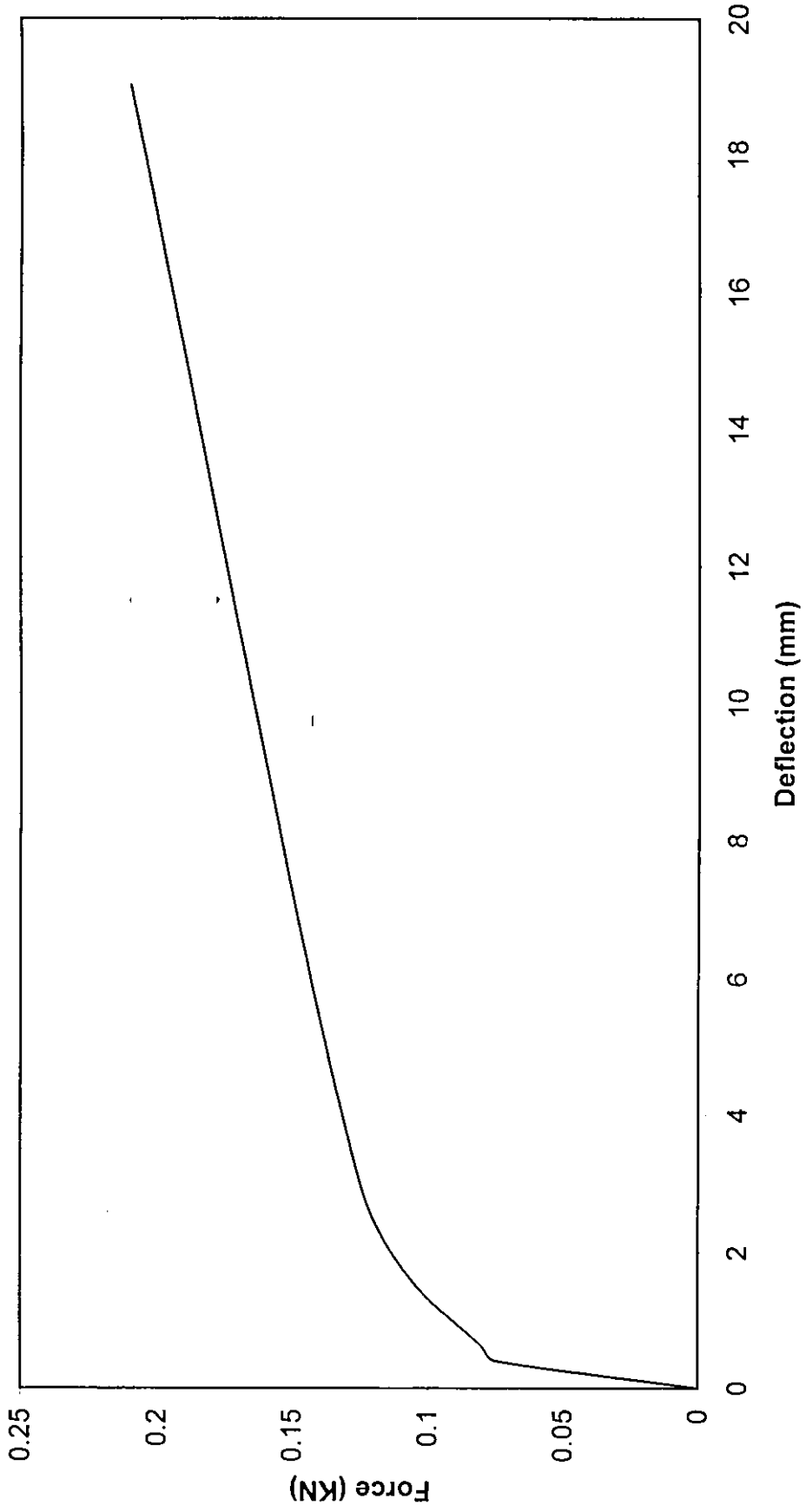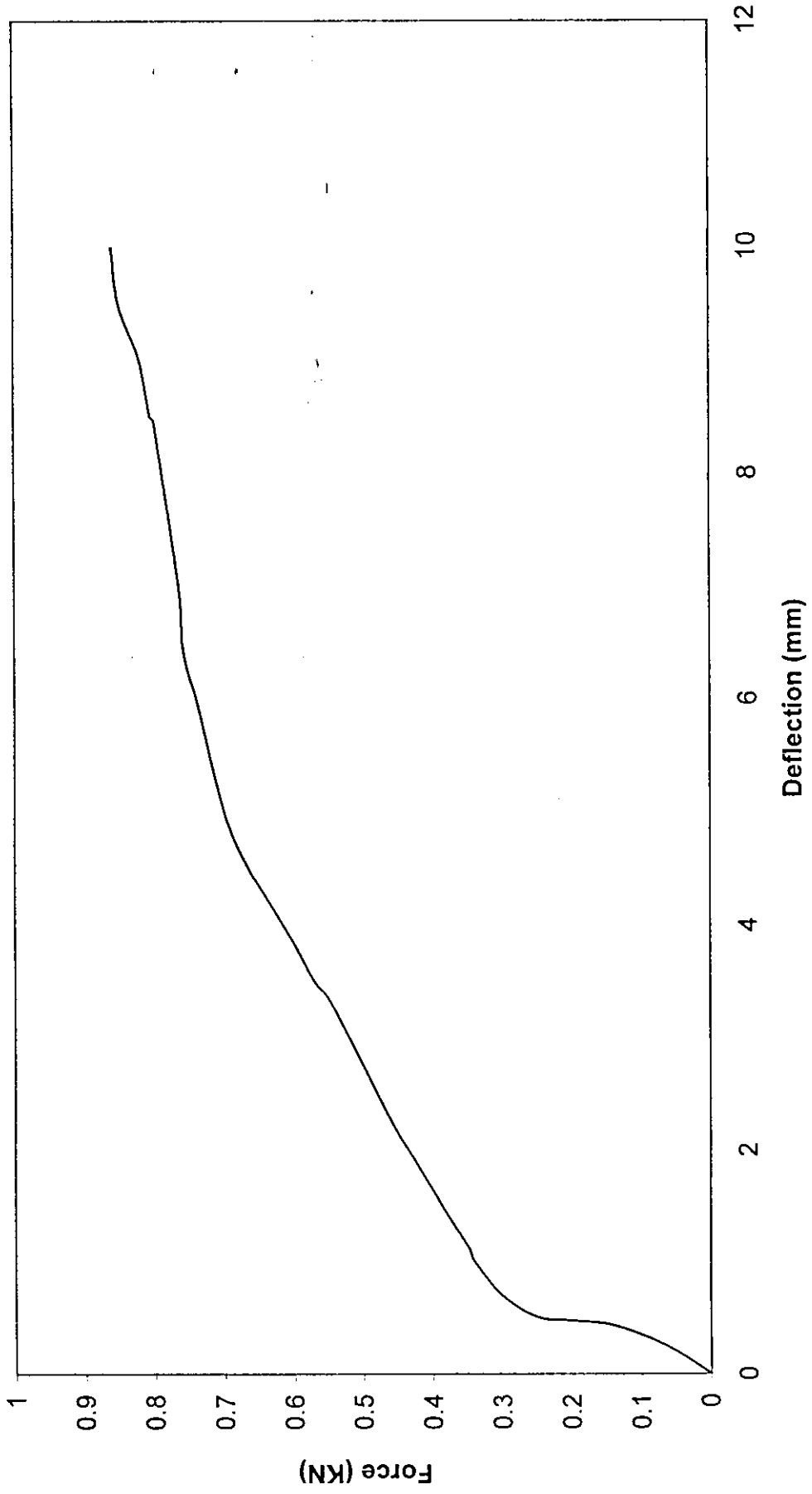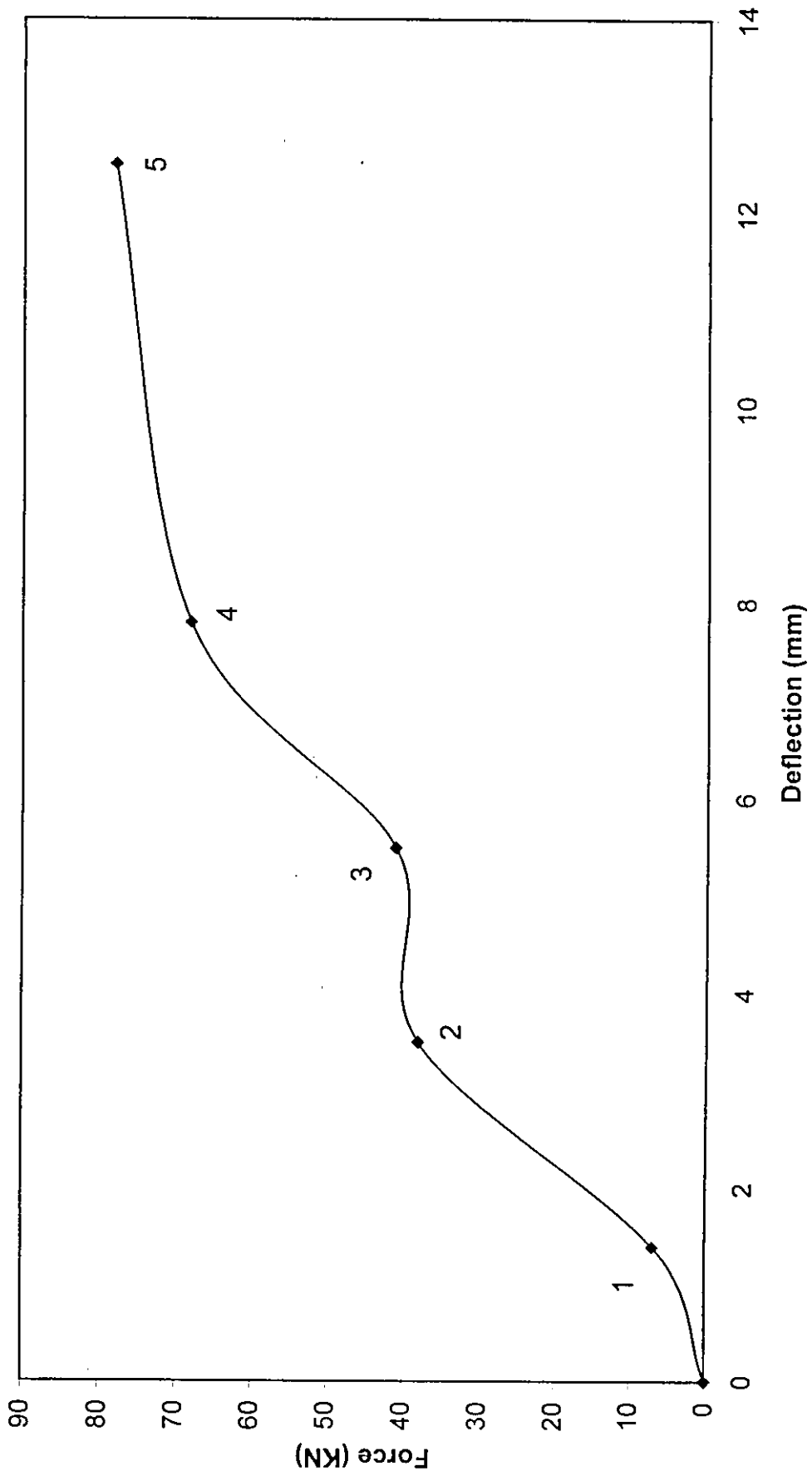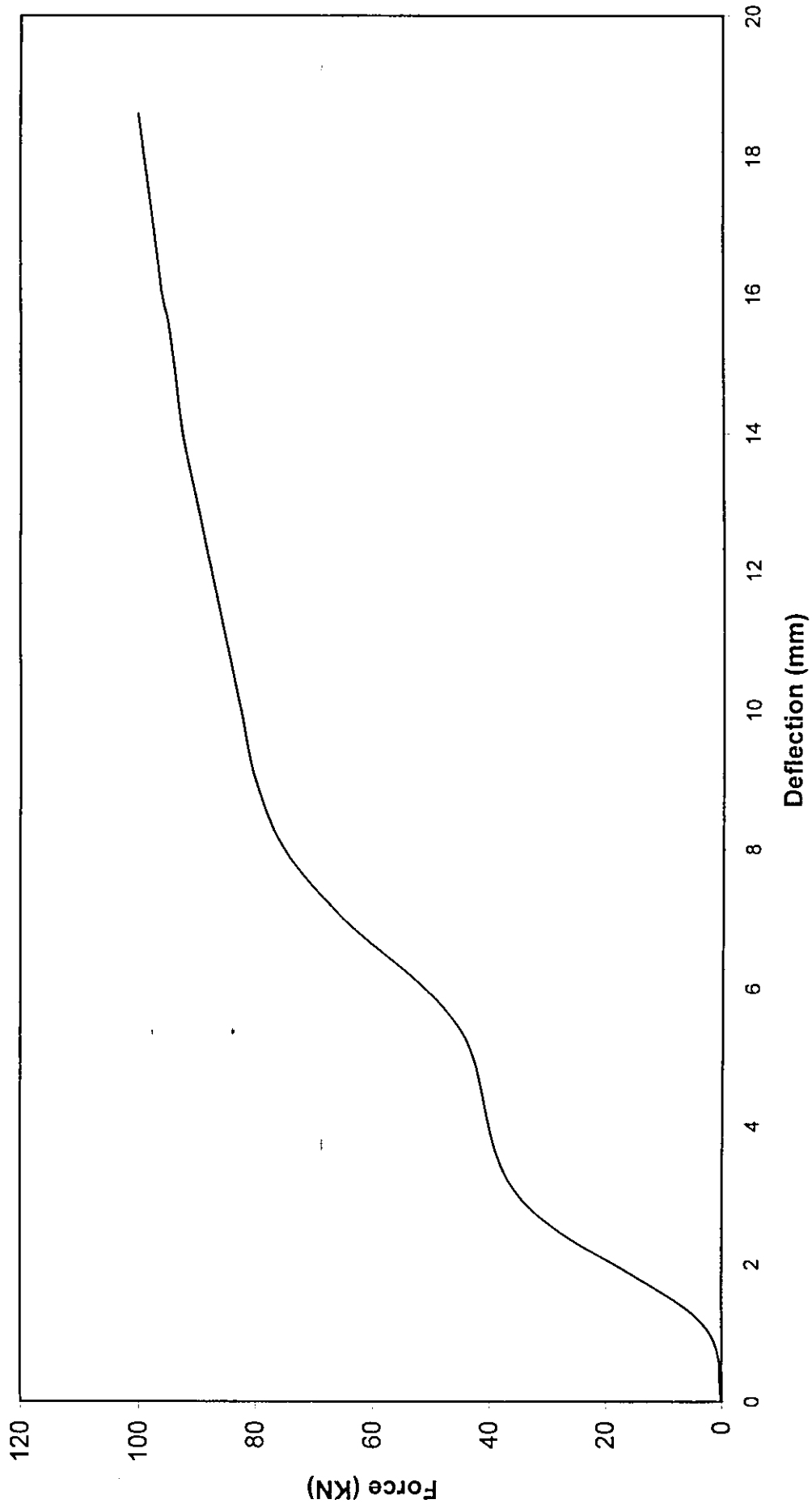Fig. (5.12): Autographic record for extrusion of lead through two dies set

**Fig. (5-13): Autographic record for extrusion of lead through three dies set**

The two offset die set was tried on the superplastic Tin- Lead alloy, at the lowest strain rate $3\times10^{-4}$ /s and the autographic record for this alloy is shown in Fig. (5-14). It can be seen from this figure that the maximum reached force is 240 KN which is near to the maximum capacity of the available universal testing machine, therefore the test was stopped, although the deflection was only 18 mm and the billet was not completely extruded and just came out of the second die.

### 5.2.4 Mechanism of Deformation in the Two Offset Extrusion Die Set with Lead

The mechanism of deformation may be studied with reference to the autographic record, Fig. (5-12) for lead. The part 0-1 of the autographic record represents the filling of the container by the Lead specimen , which is a compression process. At point 1 the material starts to fill the die cavity. At point 2, the die is completely filled with lead, and starts to be extruded out of the die opening. Line 2-3 represents the extrusion process of the lead material through the openings of the first die. At point 3, the extrusion process is completed through the first die, and starts to fill the orifices of the second die. It completes filling of the die at point 4, after which it starts to be extruded through the second die. Line 4-5 represents the extrusion process through the second offset die.
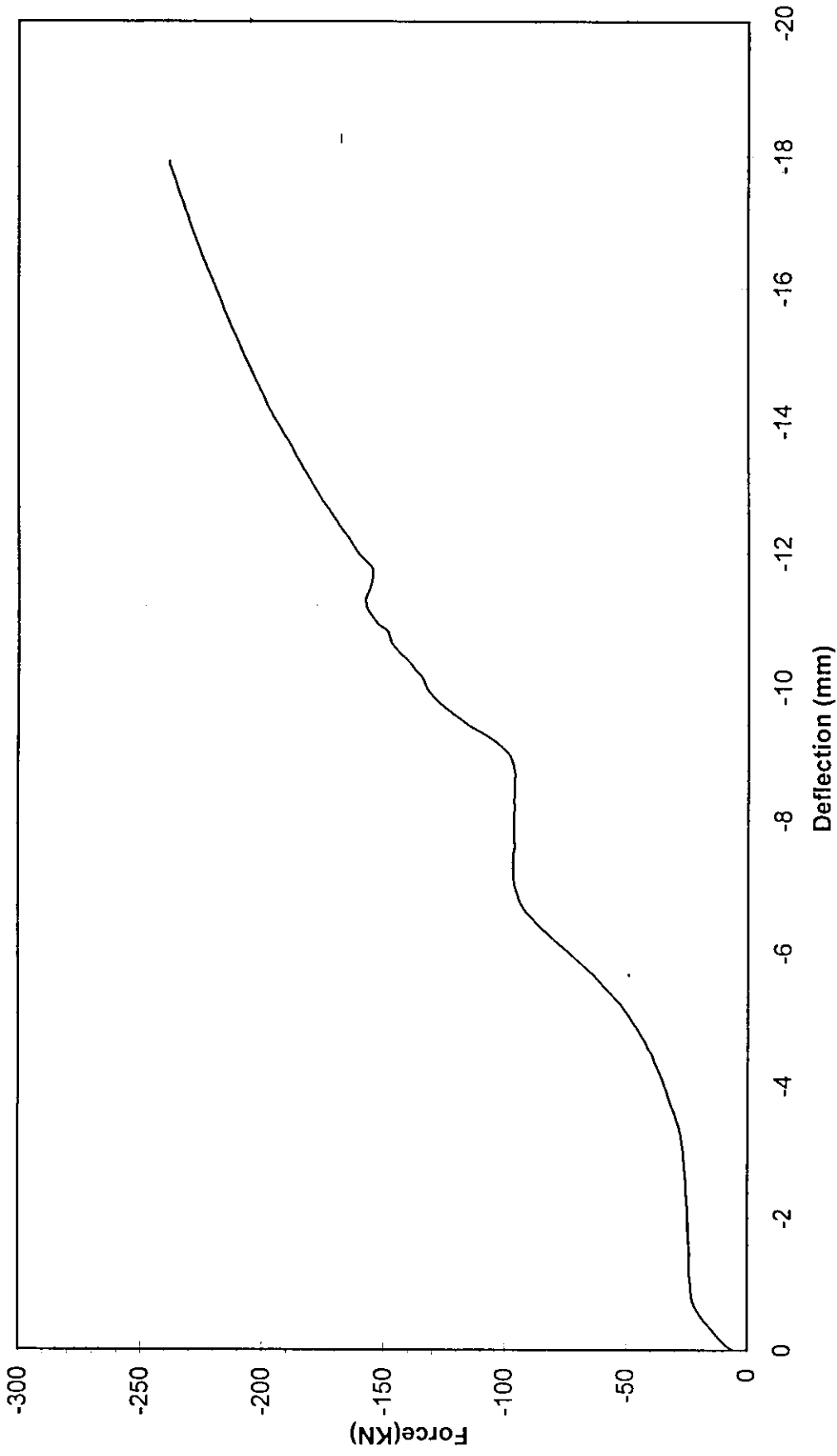
Fig. (5-14 ): Autographic record for extrusion of Tin-Lead alloy through two offset dies set

## 5.3 Energy Dissipation System Based on Tube Inversion Process

Experimental observations on the tube deformation around the die profile radius indicated that the mode of deformation in the case of the large die profile radius (10 mm) is somewhat different from that of the 3 mm die profile radius. This is reflected by the shape of the autographic records i.e. load- deflection curve of each case, Fig. (5-15), at $\dot{\varepsilon} = 4.2 \times 10^{-2}$ /s. Therefor each mode is discussed on its own merits.

### 5.3.1 Tube Deformation Around 3 mm Die Profile Radius

As discussed earlier, the deformation of the tube around 3 mm die profile radius takes place through three independent stages, first, reduction in length or the height accompanied simultaneously by bending of the tube end around the die profile radius, part 0-1 on Fig. (5-15). As the bending around the die profile continues, the bent part of the tube starts to open up (i.e. unbending takes place to staighten up the previously bent part of the tube). This is represented by part 1-2 on Fig. (5-15). It can be seen from this figure that point 1 represents an inflection point on the autographic records. Finally, after the straightening of the tube, expansion of the tube takes place from the internal diameter, d, to d + 4r + 2t, where r is the bending profile radius And t is the thickness of the tube. This is represented by part 2-3 on the autographic record. It can also be seen from This figure that the relationship between the force and deflection is linear during the expansion process.

This mode of deformation has not changed by the change of strain rate in the process as indicated by Fig. (5-16). It can be seen from this figure that increasing the strain rate by 500 times, the mode of deformation as reflected by the shape of the autographic records was not altered.
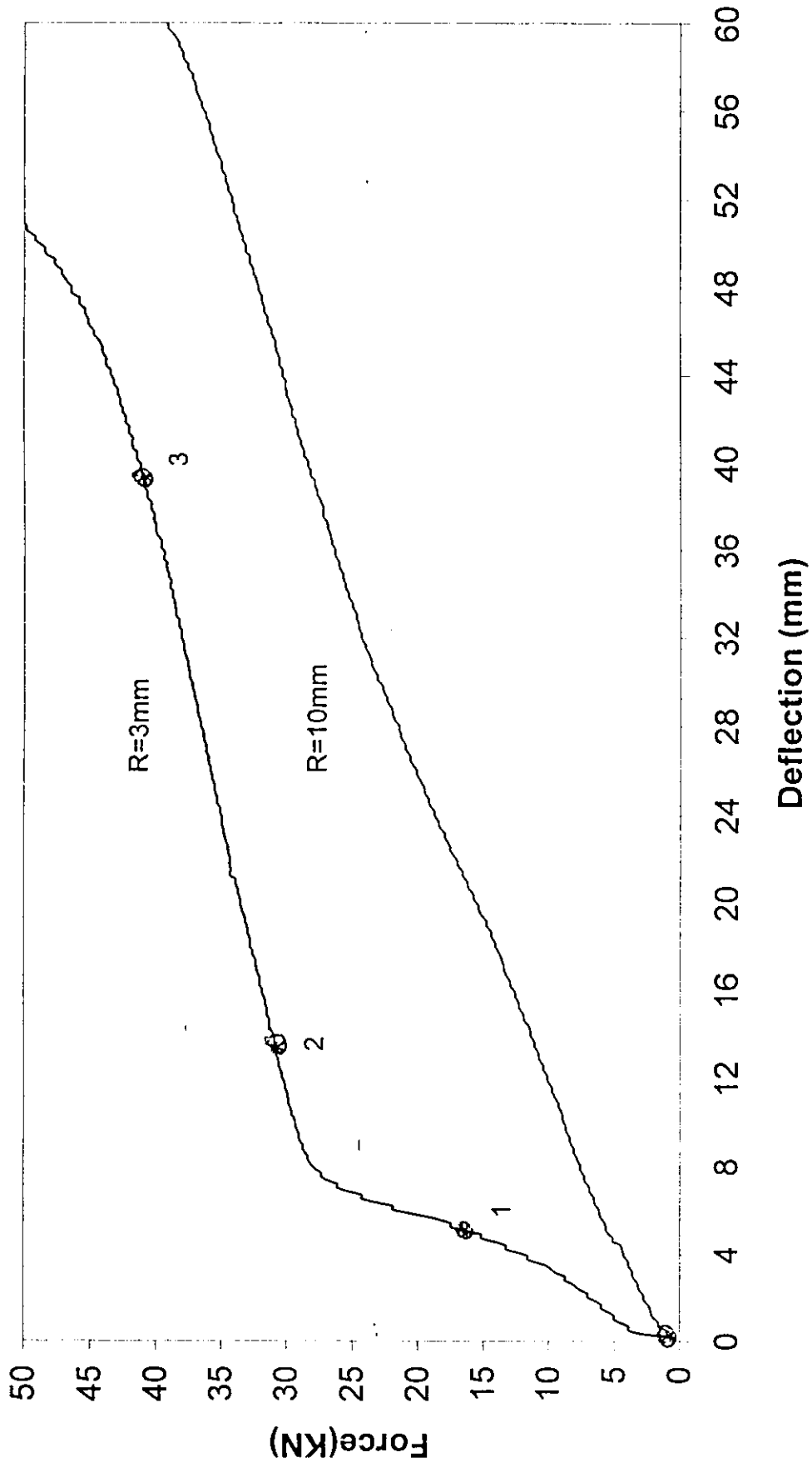
**Fig. (5-15):** Autographic record for tube inversion process at strain rate of 4.2 E-2/s
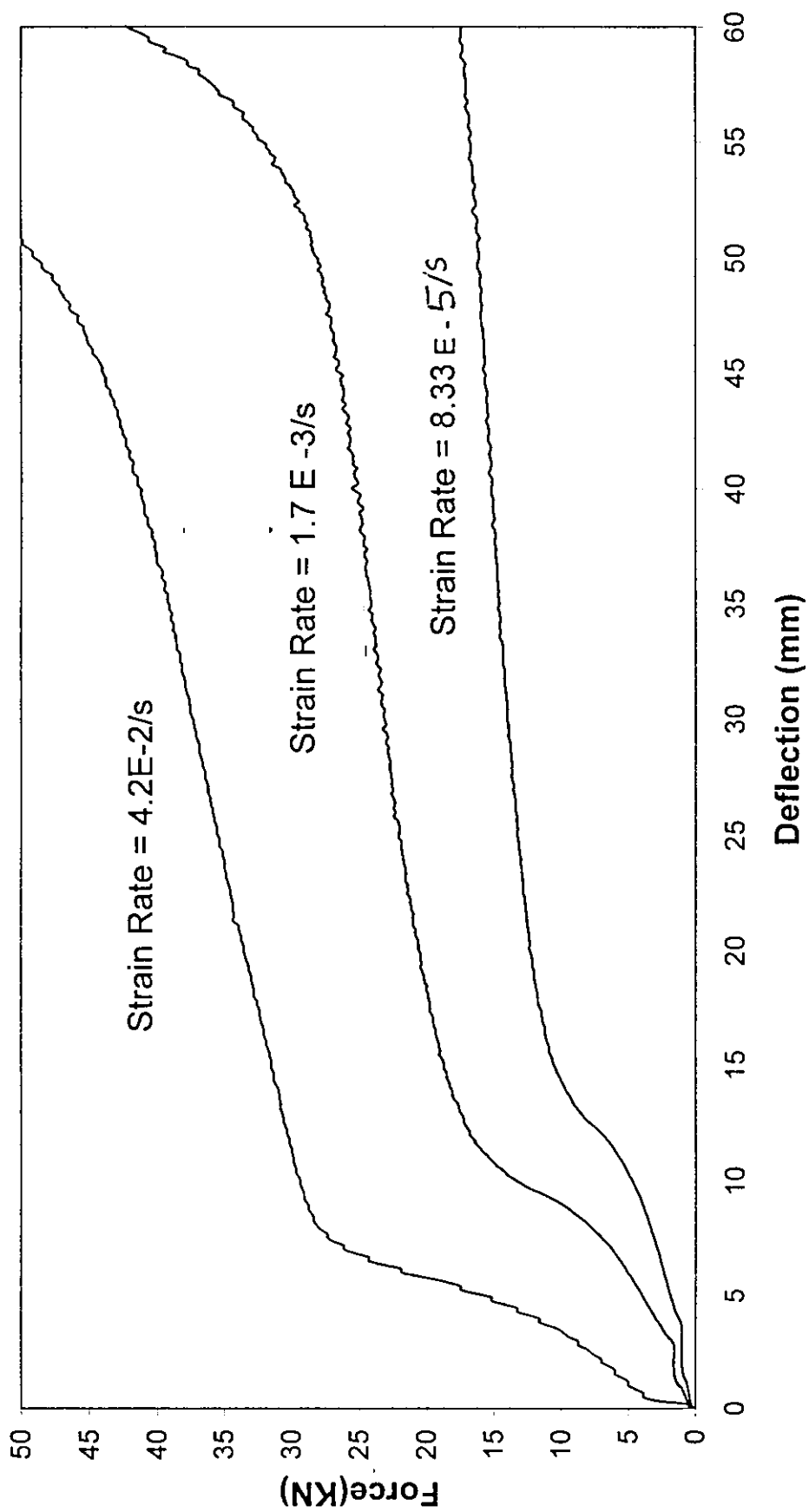
Fig. (5-16): Autographic record for tube inversion process using 3 mm die profile radius

Furthermore, it was noted on all the deformed tubes that the outer diameter has increased whereas the inner diameter has been reduced, even complete closure has taken place in some tubes as shown in Fig. (5-17). This behavior is similar to compression of hollow cylinders under flat platens, where the internal diameter increases or decreases depending on the end friction at the workpiece - platens interface and the geometrical ratio of the inner to outer diameter for an ordinary engineering material (Male, 1966), (Hawkyard and Johnson, 1967), (Biswas and Travis, 1971) and for superplastic Tin-Lead alloy (Zaid and Abdullatif, 1984), (Zaid and Belal, 2003).
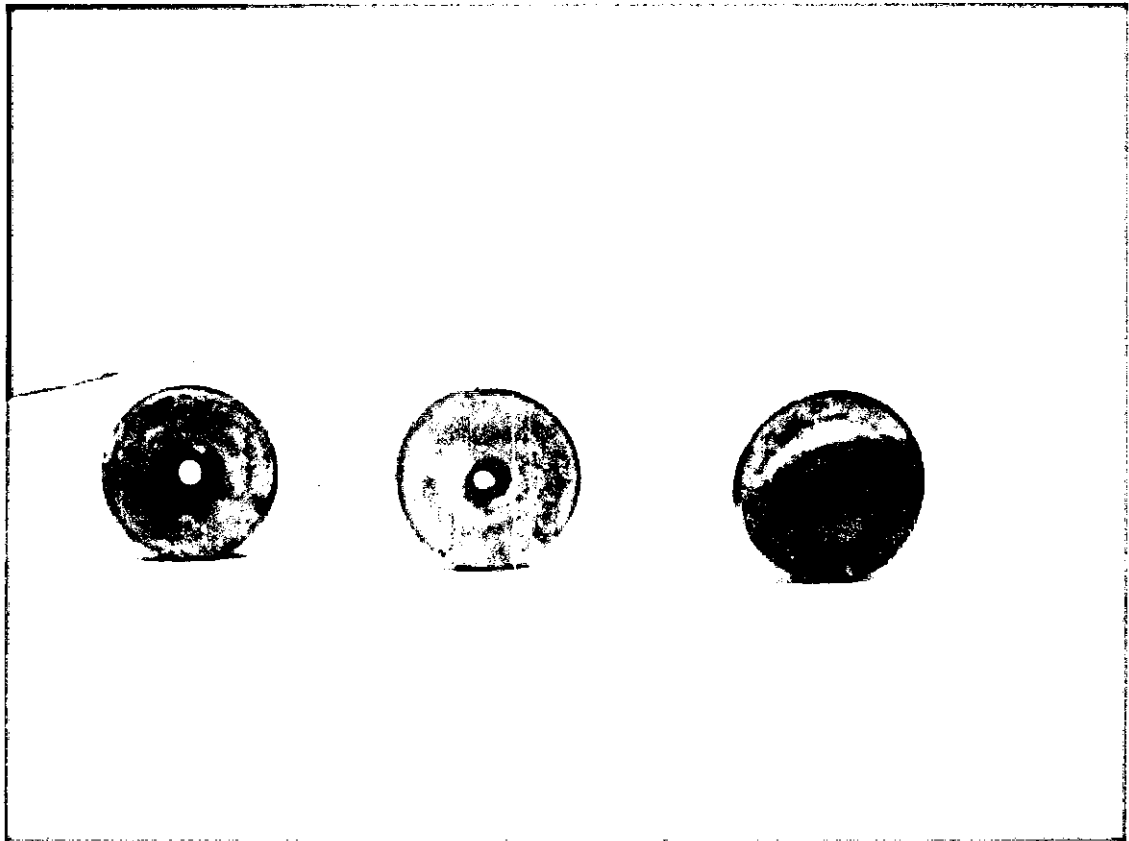


Fig. (5-17):A photograph showing some of the bent tubes
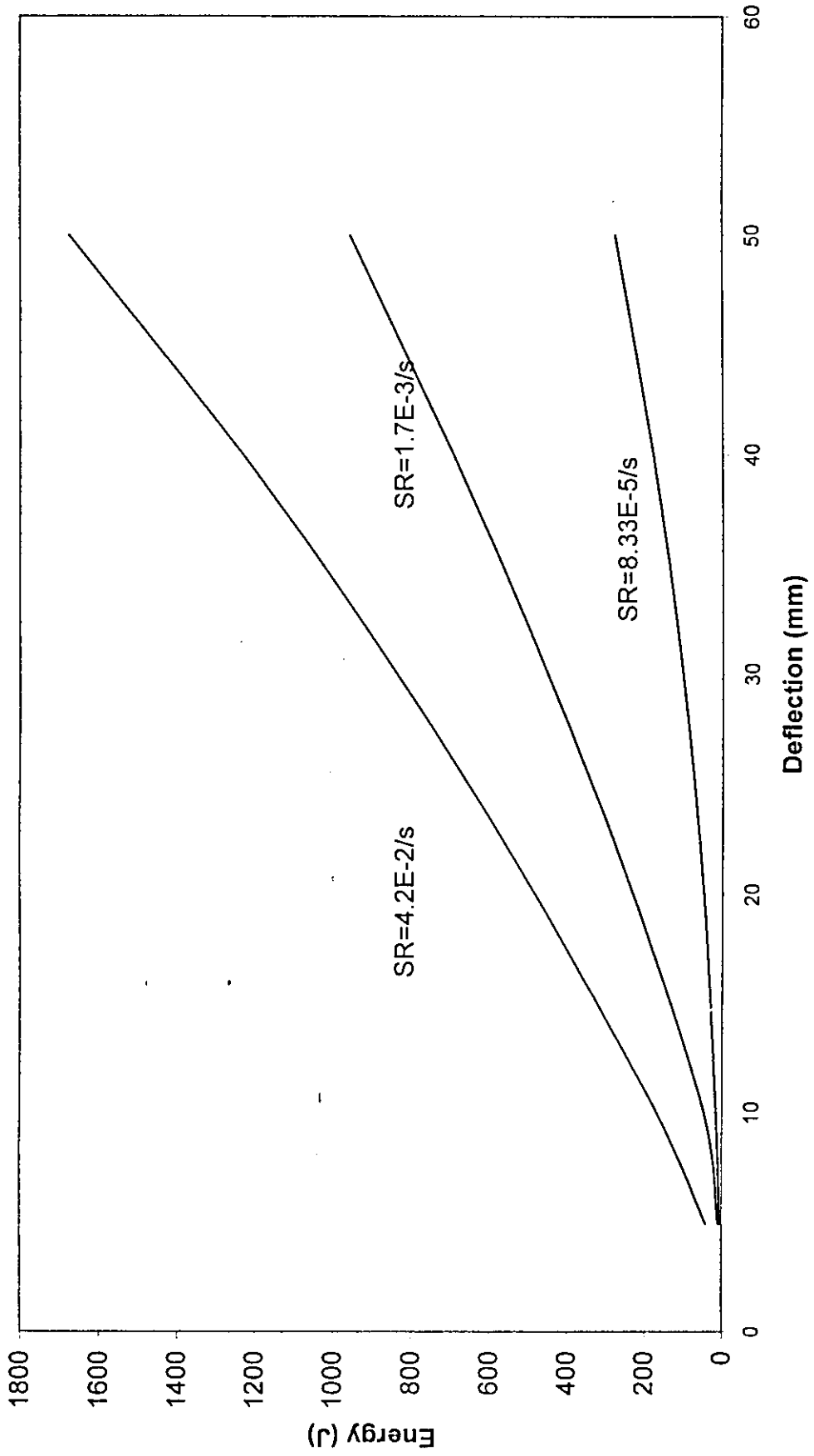
Fig. (5-18): Variation of energy with deflection for 3mm die profile radius

resulted in 14% increase, whereas increasing the displacement from 40 to 50 mm resulted in 18.9% increase. From this it can be concluded that the deformation force increases with displacement at all values of strain rate. However the increase is more pronounced at small displacements and lower values of strain rates.

Similarly, regarding the energy consumed in deformation, it also increases with displacement and with strain rate, Table (5-3). It can be seen from this table that the rate of increase of energy with the displacement is more pronounced at lower values of strain rate. for example, at strain rate, $\acute{\epsilon} = 8.33 \times 10^{-5}$ /s, increasing the displacement from 10 to 20 mm, the energy increased from 15.9 J to 47.7 J, i.e. by about 200%, whereas increasing the distance from 40 to 50 mm resulted only in 54.5% increase. On the other hand, at high strain rates, $\acute{\epsilon} = 4.2 \times 10^{-2}$ /s, increasing the displacement from 10 to 20 mm resulted in 184.3% increase, whereas increasing the displacement from 40 to 50 mm resulted in 36% increase.

Table (5-3): Variation of energy with displacement for 3 mm die profile radius

| Deflection (mm) | ENERGY ( J ) | | |
|---|---|---|---|
| | SR =8.33 X $10^{-5}$ /S | SR = 1.7 x $10^{-3}$ /s | SR = 4.2 x $10^{-2}$ /s |
| 5 | 5.1 | 9.8 | 41.5 |
| 10 | 15.9 | 47.1 | 169.5 |
| 20 | 47.7 | 229.7 | 481.9 |
| 30 | 101.7 | 449.6 | 836.3 |
| 40 | 178 | 691.2 | 1231.6 |
| 50 | 275.9 | 956.7 | 1675.3 |

From this, it can be concluded that if the collision force is high, it is better to utilize multi system in parallel, whereas if the object is to absorb the energy of collision rather than force, it is advisable to invest in the axial displacement.

### 5.3.2 Tube Deformation around 10 mm Die Profile Radius

Experimental observation indicated that the mode of deformation for the 10 mm die profile radius is quite different from the 3 mm one. This is clearly indicated by reference to Fig. (5-15). This figure shows the autographic record for both dies at the same strain rate. It can be seen from this figure that the relationship between the deformation force and displacement is almost linear for the 10 mm die profile radius over the 60 mm deflection. This behavior was found to be the same at the three different strain rates, namely $8.33 \times 10^{-5}$ /s, $1.7 \times 10^{-3}$ /s and $4.2 \times 10^{-2}$ /s as shown in Fig. (5-19).

It is worth mentioning in this respect that the internal diameter of the undeformed part of the tube has not been affected, i.e. remained constant, during the deformation. The only effect of strain rate is the increase in the deformation force at the same displacement, which again emphasizes the rate sensitivity of this alloy (Tin-Lead).

To investigate further the mechanism of deformation, the deformed tube was sectioned diametrically, along its length and projected. The thickness of the tube, hence the thickness strain was obtained at different positions along the tube wall. Fig. (5-20) shows the sectioned deformed tube together with the projected original thickness. The measurements of the thickness indicated that the tube suffered thickening, i.e. the thickness increased at all the sections. However, the increase in thickness was almost the same along the tube. The variations of increase in thickness along the tube did not exceed $\pm 11\%$ on a small portion of the deformed part of the tube as can be seen in table (5-4). The increase in thickness is expected as a result of compression for this particular tube having a ratio of internal to external diameter of 0.38. This is in general agreement with the results of the work of (Zaid and Abdullatif, 1984) where the authors found that the mode of deformation varies with the $d_i / d_o$ ratio.
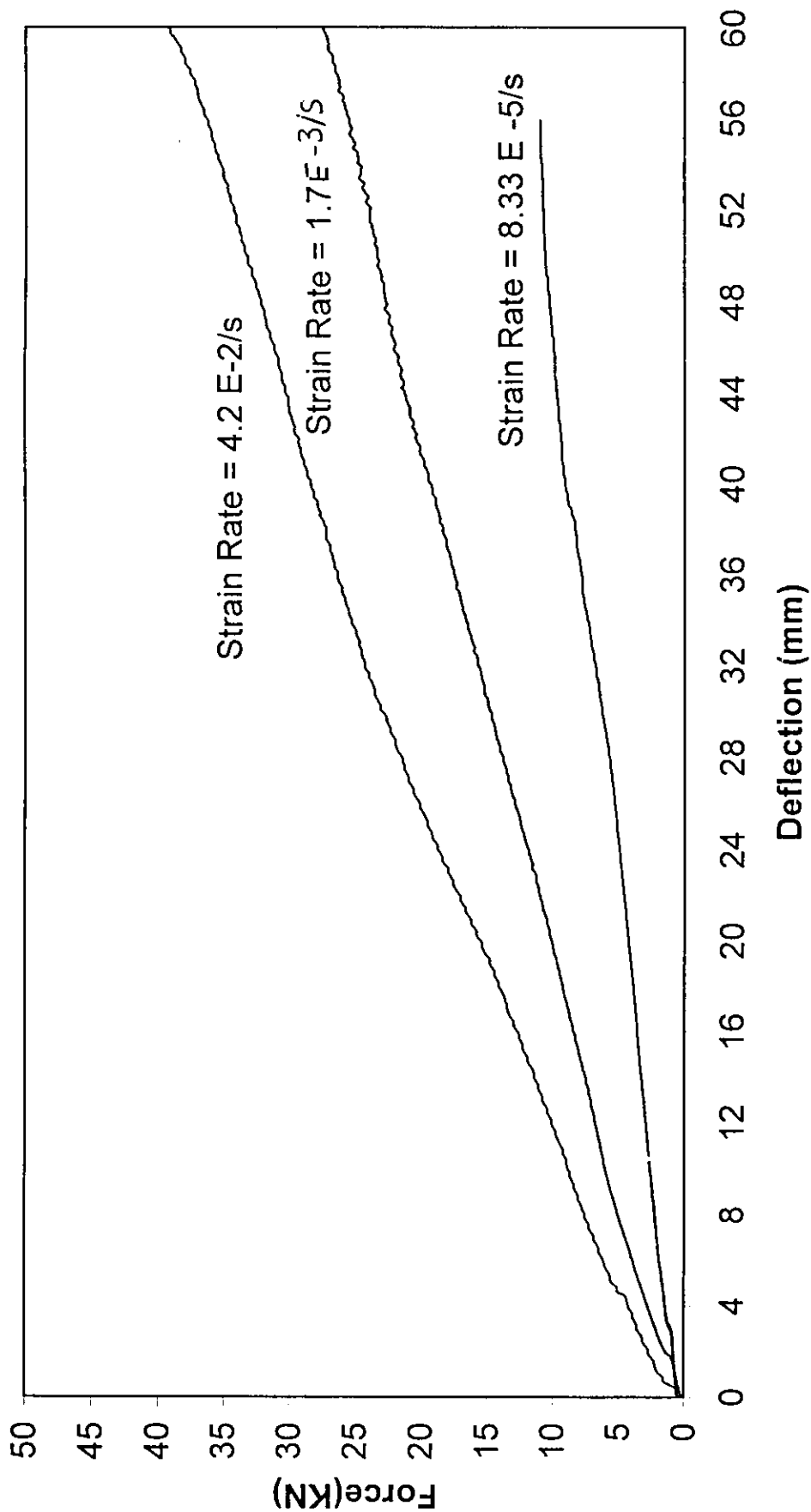
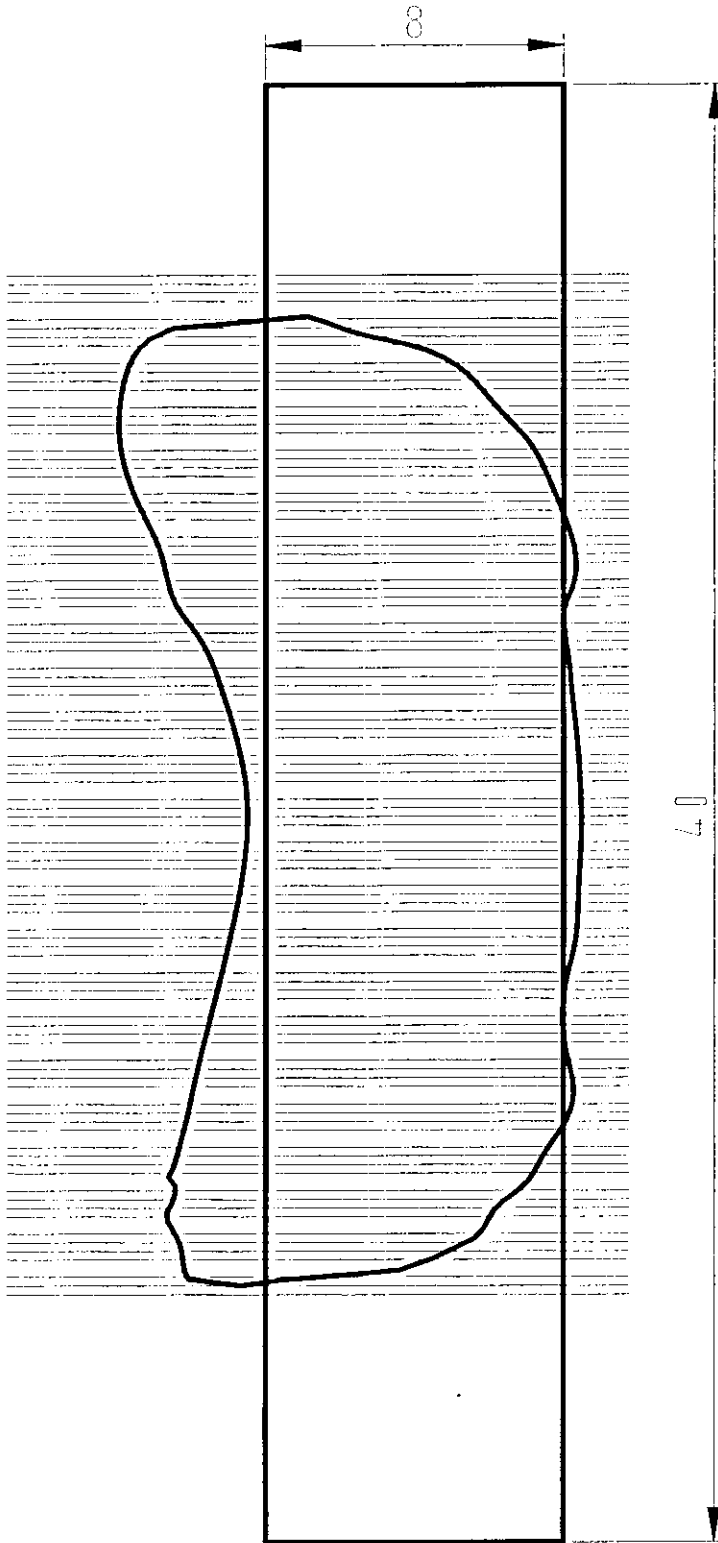**Fig. (5-19): Autographic record for tube inversion process using 10 mm die profile radius**

Fig. (5-20): Sectional view of the inverted tube showing original and final thickness (dimensions are in mm)

## Table (5-4): Thickness variations in the bent tube

| tangential strain | %change in thickness | actual final thickness | tickness | y2 | y1 | |
|---|---|---|---|---|---|---|
| 0.109843691 | 11.61036002 | 8.928828801 | 37.4 | 190.5 | 153.1 | 1 |
| 0.164473659 | 17.87725189 | 9.430180151 | 39.5 | 190.9 | 151.4 | 2 |
| 0.196855068 | 21.75675638 | 9.74054051 | 40.8 | 190.9 | 150.1 | 3 |
| 0.19930305 | 22.0551798 | 9.764414384 | 40.9 | 190.2 | 149.3 | 4 |
| 0.204181108 | 22.65202665 | 9.812162132 | 41.1 | 189.8 | 148.7 | 5 |
| 0.216273154 | 24.14414376 | 9.931531501 | 41.6 | 189.7 | 148.1 | 6 |
| 0.251695984 | 28.6204951 | 10.28963961 | 43.1 | 190.4 | 147.3 | 7 |
| 0.256325622 | 29.21734194 | 10.33738736 | 43.3 | 189.7 | 146.4 | 8 |
| 0.263230137 | 30.11261221 | 10.40900898 | 43.6 | 189.3 | 145.7 | 9 |
| 0.272362621 | 31.3063059 | 10.50450447 | 44 | 189 | 145 | 10 |
| 0.272362621 | 31.3063059 | 10.50450447 | 44 | 188.6 | 144.6 | 11 |
| 0.270087307 | 31.00788248 | 10.4806306 | 43.9 | 188.2 | 144.3 | 12 |
| 0.267806804 | 30.70945906 | 10.45675672 | 43.8 | 187.9 | 144.1 | 13 |
| 0.260933925 | 29.81418879 | 10.3851351 | 43.5 | 187.6 | 144.1 | 14 |
| 0.251695984 | 28.6204951 | 10.28963961 | 43.1 | 187.3 | 144.2 | 15 |
| 0.242371907 | 27.42680141 | 10.19414411 | 42.7 | 187 | 144.3 | 16 |
| 0.230593208 | 25.9346843 | 10.07477474 | 42.2 | 186.7 | 144.5 | 17 |
| 0.221069326 | 24.74099061 | 9.979279248 | 41.8 | 186.4 | 144.6 | 18 |
| 0.209035487 | 23.24887349 | 9.859909879 | 41.3 | 186 | 144.7 | 19 |
| 0.201745054 | 22.35360323 | 9.788288258 | 41 | 185.7 | 144.7 | 20 |
| 0.196855068 | 21.75675638 | 9.74054051 | 40.8 | 185.4 | 144.6 | 21 |
| 0.187002772 | 20.56306269 , | 9.645045015 | 40.4 | 185 | 144.6 | 22 |
| 0.184524456 | 20.26463927 | 9.621171141 | 40.3 | 184.7 | 144.4 | 23 |
| 0.182039983 | 19.96621585 | 9.597297268 | 40.2 | 184.4 | 144.2 | 24 |
| 0.177052441 | 19.369369 | 9.54954952 | 40 | 184 | 144 | 25 |
| 0.174549311 | 19.07094558 | 9.525675646 | 39.9 | 183.7 | 143.8 | 26 |
| 0.174549311 | 19.07094558 | 9.525675646 | 39.9 | 183.3 | 143.4 | 27 |
| 0.174549311 | 19.07094558 | 9.525675646 | 39.9 | 183 | 143.1 | 28 |
| 0.174549311 | 19.07094558 | 9.525675646 | 39.9 | 182.6 | 142.7 | 29 |
| 0.172039899 | 18.77252216 | 9.501801772 | 39.8 | 182.3 | 142.5 | 30 |
| 0.172039899 | 18.77252216 | 9.501801772 | 39.8 | 182 | 142.2 | 31 |
| 0.164473659 | 17.87725189 | 9.430180151 | 39.5 | 181.6 | 142.1 | 32 |
| 0.161938803 | 17.57882847 | 9.406306277 | 39.4 | 181.3 | 141.9 | 33 |
| 0.156849734 | 16.98198162 | 9.35855853 | 39.2 | 181 | 141.8 | 34 |
| 0.151734633 | 16.38513478 | 9.310810782 | 39 | 180.7 | 141.7 | 35 |
| 0.146593234 | 15.78828793 | 9.263063034 | 38.8 | 180.4 | 141.6 | 36 |
| 0.144012587 | 15.48986451 | 9.239189161 | 38.7 | 180.1 | 141.4 | 37 |
| 0.138831228 | 14.89301766 | 9.191441413 | 38.5 | 179.8 | 141.3 | 38 |
| 0.136230446 | 14.59459424 | 9.167567539 | 38.4 | 179.6 | 141.2 | 39 |
| 0.133622883 | 14.29617082 | 9.143693665 | 38.3 | 179.3 | 141 | 40 |
| 0.128387269 | 13.69932397 | 9.095945918 | 38.1 | 179 | 140.9 | 41 |
| 0.128387269 | 13.69932397 | 9.095945918 | 38.1 | 178.8 | 140.7 | 42 |
| 0.125759147 | 13.40090055 | 9.072072044 | 38 | 178.6 | 140.6 | 43 |
| 0.12048209 | 12.80405371 | 9.024324296 | 37.8 | 178.4 | 140.6 | 44 |
| 0.12048209 | 12.80405371 | 9.024324296 | 37.8 | 178.3 | 140.5 | 45 |
| 0.117833081 | 12.50563028 | 9.000450423 | 37.7 | 178.1 | 140.4 | 46 |
| 0.115177037 | 12.20720686 | 8.976576549 | 37.6 | 178 | 140.4 | 47 |
| 0.11251392 | 11.90878344 | 8.952702675 | 37.5 | 177.9 | 140.4 | 48 |
| 0.115177037 | 12.20720686 | 8.976576549 | 37.6 | 177.9 | 140.3 | 49 |
| 0.11251392 | 11.90878344 | 8.952702675 | 37.5 | 177.8 | 140.3 | 50 |
| 0.115177037 | 12.20720686 | 8.976576549 | 37.6 | 177.9 | 140.3 | 51 |
| 0.115177037 | 12.20720686 | 8.976576549 | 37.6 | 177.9 | 140.3 | 52 |
| 0.117833081 | 12.50563028 | 9.000450423 | 37.7 | 178 | 140.3 | 53 |
| 0.12048209 | 12.80405371 | 9.024324296 | 37.8 | 178.1 | 140.3 | 54 |
| 0.123124099 | 13.10247713 | 9.04819817 | 37.9 | 178.2 | 140.3 | 55 |
| 0.128387269 | 13.69932397 | 9.095945918 | 38.1 | 178.4 | 140.3 | 56 |
| 0.128387269 | 13.69932397 | 9.095945918 | 38.1 | 178.5 | 140.4 | 57 |
| 0.133622883 | 14.29617082 | 9.143693665 | 38.3 | 178.7 | 140.4 | 58 |
| 0.138831228 | 14.89301766 | 9.191441413 | 38.5 | 178.9 | 140.4 | 59 |
| 0.144012587 | 15.48986451 | 9.239189161 | 38.7 | 179.1 | 140.4 | 60 |
| 0.149167238 | 16.08671135 | 9.286936908 | 38.9 | 179.3 | 140.4 | 61 |
| 0.154295454 | 16.6835582 | 9.334684656 | 39.1 | 179.5 | 140.4 | 62 |
| 0.159397506 | 17.28040504 | 9.382432403 | 39.3 | 179.8 | 140.5 | 63 |
| 0.164473659 | 17.87725189 | 9.430180151 | 39.5 | 180 | 140.5 | 64 |
| 0.169524175 | 18.47409873 | 9.477927899 | 39.7 | 180.3 | 140.6 | 65 |
| 0.177052441 | 19.369369 | 9.54954952 | 40 | 180.6 | 140.6 | 66 |
| 0.187002772 | 20.56306269 | 9.645045015 | 40.4 | 181 | 140.6 | 67 |
| 0.19930305 | 22.0551798 | 9.764414384 | 40.9 | 181.4 | 140.5 | 68 |
| 0.223458814 | 25.03941403 | 10.00315312 | 41.9 | 182 | 140.1 | 69 |
| 0.249373103 | 28.32207168 | 10.26576573 | 43 | 182.6 | 139.6 | 70 |
| 0.274632769 | 31.60472932 | 10.52837835 | 44.1 | 183.2 | 139.1 | 71 |
| 0.294835477 | 34.29054013 | 10.74324321 | 45 | 183.8 | 138.8 | 72 |

The only effect of strain rate is the increase in the deformation force at the same displacement, which again emphasizes the rate sensitivity of this alloy ( Tin- Lead).

To investigate explicitly the variation of force and energy with strain rate, values of force and energy were obtained at different values of displacement at each strain rate. These results are shown in Table (5-5) and Table (5-6) respectively.

Table (5-5): Variation of force with displacement for 10 mm die profile radius

| Deflection (mm) | Force (KN) | | |
|---|---|---|---|
| | $SR = 8.33 \times 10^{-5}$ /S | $SR = 1.7 \times 10^{-3}$ /s | $SR = 4.2 \times 10^{-2}$ /s |
| 5 | 1.9 | 4 | 5.5 |
| 10 | 2.6 | 6 | 8.9 |
| 20 | 4.3 | 10 | 15.5 |
| 30 | 6.3 | 14.8 | 23 |
| 40 | 9.1 | 19.4 | 28.5 |
| 50 | 10.6 | 23.4 | 33.3 |

Table (5-6): Variation of energy with displacement for 10 mm die profile radius

| Deflection (mm) | NERGY ( J ) | | |
|---|---|---|---|
| | $SR = 8.33 \times 10^{-5}$ /S | $SR = 1.7 \times 10^{-3}$ /s | $SR = 4.2 \times 10^{-2}$ /s |
| 5 | 5 | 8.7 | 15.4 |
| 10 | 20.7 | 32.5 | 52.1 |
| 20 | 116.9 | 112.7 | 172.1 |
| 30 | 248.8 | 237 | 365.8 |
| 40 | 395 | 407.6 | 626.4 |
| 50 | 551.6 | 623.4 | 935 |

It can be seen from this Table (5-5) that at the first stage of deformation, the force increases rapidly with displacement, and then the rate of increase decreases at all strain rates, being more pronounced at the lower values of strain rate, $\dot{\varepsilon}$. For example, at strain rate, $\dot{\varepsilon} = 8.33 \times 10^{-5}$ /s, increasing the displacement from 10 to 20 mm, the force increased from 2.6 KN to 4.3 KN, i.e. by about 65.4%, whereas increasing the distance from 40 to 50 mm resulted only in 16.5% increase. On the other hand, at high strain rates, $\dot{\varepsilon} = 4.2 \times 10^{-2}$ /s, increasing the displacement from 10 to 20 mm resulted in 74.2% increase, whereas increasing the displacement from 40 to 50 mm resulted in 16.8% increase. From this it can be concluded that the deformation force increases with displacement at all values of strain rate. However the increase is more pronounced at small displacements and lower values of strain rates.

Similarly, regarding the energy consumed in deformation, it increases with displacement and with strain rate Table (5-6). It can be seen from this table that the rate of increase of energy with the displacement is more pronounced at lower values of strain rate. For example, at strain rate, $\dot{\varepsilon} = 8.33 \times 10^{-5}$ /s, increasing the displacement from 10 to 20 mm, the energy increased from 20.7 J to 116.9 J, i.e. by about 464.7%, whereas increasing the distance from 40 to 50 mm resulted only in 39.6% increase. On the other hand, at high strain rates, $\dot{\varepsilon} = 4.2 \times 10^{-2}$ /s, increasing the displacement from 10 to 20 mm resulted in 230.3% increase, whereas increasing the displacement from 40 to 50 mm resulted in 49.3% increase.

Fig. (5-21) shows the relationship between the consumed energy and displacement. It indicates that this relation is parabolic, i.e. $E \alpha \delta^2$. Therefore the results were represented as square root of E versus displacement in Fig. (5-22). From this figure, the relationship is found to be linear and can be represented by the following equation
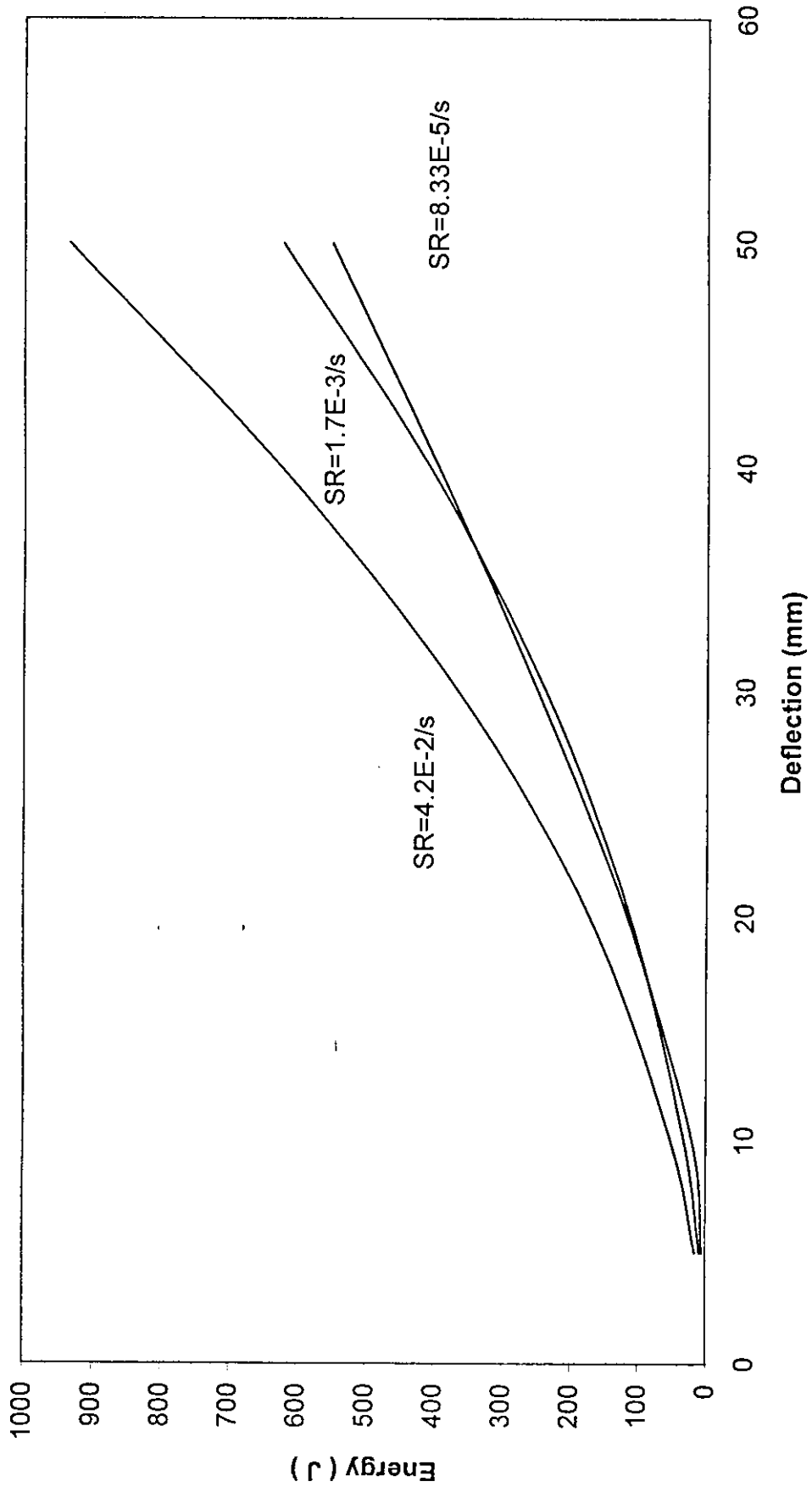
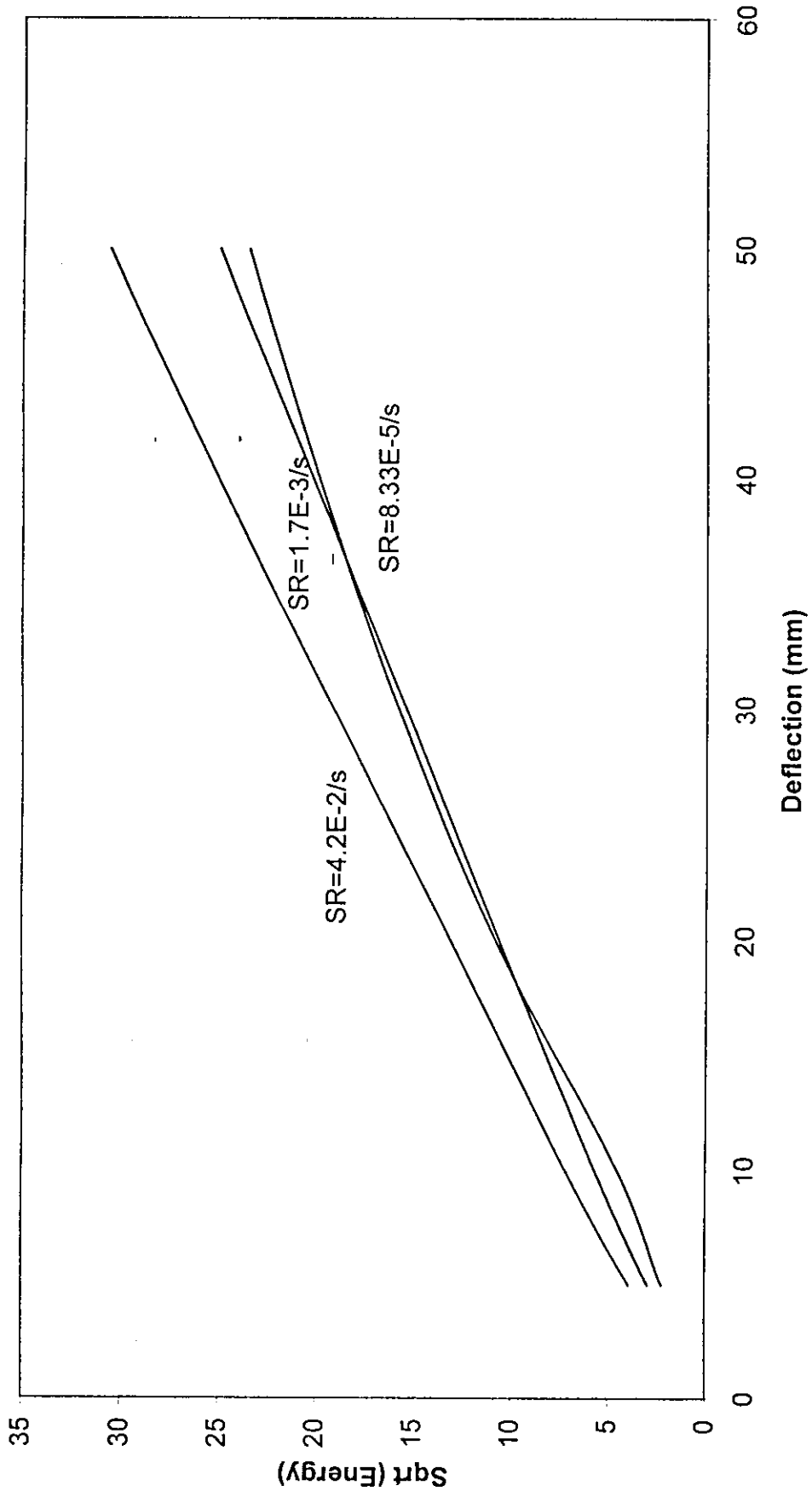Fig. (5-21): Variation of energy with deflection for 10 mm die profile radius

**Fig. (5-22): Sqrt (energy) vs deflection for 10 mm die profile radius**

$$\sqrt{E} = 0.4821\delta + 0.3348 \qquad\qquad (5-2)$$

## 5.4 Comparison Between Experimental Results and Theoretical Analysis

In this section, comparison is made between the theoretical analysis discussed in the previous chapter and the obtained experimental results.

Consider superplastic Tin- Lead alloy is to be used in the system, then substituting the appropriate values for a, b, Y and R, as obtained before, in equation (4.23), the extrusion pressure (P) can then be determined at each strain rate, from which the total theoretical work at each strain rate was determined. The calculated values of the extrusion pressure, the theoretical work and the experimental work at each strain rate are shown in table (5-7). Details of the calculations is shown in Appendix (A).

Table (5-7): Values of extrusion pressure, theoretical and experimental work

| Strain rate /s | $3 \times 10^{-4}$ | $5 \times 10^{-3}$ | 0.1 |
|---|---|---|---|
| Y(Mpa) | 48 | 74 | 104 |
| P(Mpa) | 130.1 | 200.5 | 281.8 |
| Theoretical Work(J) | 689.5 | 1062.7 | 1493.5 |
| Experimental Work(J) | 835 | 1376 | 1944 |

The difference between the experimental and theoretical results is attributed to the work consumed in both friction and redundant work. It can be seen from Table (5-8) that their percentages lies between 21.1 to 30.2% of the theoretical work, which falls within the range reported in the literature for metal forming processes in general and extrusion processes in particular.

Friction and redundant work = Experimental Work - Theoretical Work

Table (5-8): Values and percentages of friction and redundant work

| Strain rate /s | $3 \times 10^{-4}$ | $5 \times 10^{-3}$ | 0.1 |
|---|---|---|---|
| friction and redundant work(J) | 145.5 | 313.3 | 450.5 |
| %Friction and redundant work | 21.1 | 29.5 | 30.2 |

Let a car of 1000 kg weight driving at a speed of 80km / hr be stopped

Initial kinetic energy = (0.5) (1000kg) (80 km/hr)$^2$ (1000m/km)$^2$ (hr/3600s)$^2$

$= 246.9$ KJ

5.4.1 using an extrusion die set at a strain rate of 0.1/s (quasi static condition), the energy absorbed for 10 mm deflection, is 1944 J

then we need (2.469 x 10$^5$ / 1944) = 127 die set required.

These die sets are divided to 6 identical square sets, each is equivalent to 21 die sets

$A_o = 21 \times \pi \times (13)^2 = 11150$ mm$^2$

Number of holes = 21 x 21 = 441

$L_o = $ sqrt ( 11150 ) = 106 mm

5.4.2 using an extrusion die set at a strain rate of 1000/s (dynamic condition), the energy absorbed for 10 cm deflection can be calculated as follows

$$Y = 1.589 \times 10^8 \dot{\varepsilon}^{0.1466} = 1.589 \times 10^8 (1000)^{0.1466} = 437.4 MPa$$

P = 2.71 x 437.4 = 1185.4 MPa

Theoretical consumed work = 1185.4 x 10$^6$ x $\pi$ x ( 13x10$^{-3}$ )$^2$ x ( 0.1 ) = 62.9 KJ

Friction and redundant work is approximately 30% of the theoretical work =

0.3 x 62.9 = 18.9 KJ

and the total work = 62.9 + 18.9 = 81.8 KJ

Then we need (246.9 / 81.8) = 3 die set required

These die sets are divided to 3 identical sets, each is equivalent to 1 die sets

$A_o = \pi \times (13)^2 = 531 \text{ mm}^2$

Number of holes = 21

## 5.5 Simulation of the Behavior of Steel Using Superplastic Tin- Lead Alloy as a Model Material

In this section, simulation of the behavior of steel using superplastic tin- lead alloy as a model material is given.

Considering mild steel in the annealed condition to be used. Its average flow stress in the quasi-static range of strain rate is 280 Mpa (Kalpakjian, 1997). Consider the rate sensitivity of 2 in order to allow for the effect of strain rate in the impact process (1000 /s), (Zaid, 1996). Hence the average dynamic flow stress will be 600 Mpa. Substituting the values of a, b, Y and R in equation (4.23), the extrusion pressure is found to be 1626 Mpa. Allow the length of billet to be 10 cm, then the theoretical consumed work =

$$=\text{Extrusion pressure} \times \text{Cross sectional area of the billet} \times \text{Billet length}$$

$$= 1626 \times 10^6 \times 5.3 \times 10^{-5} = 86.2 \text{ KJ}$$

Consider the friction and redundant work to be approximately 30% of the theoretical work, i.e. 25.9 KJ. Then the total work will be 112.1 KJ. Details of the calculations are given in Appendix (B).

If a car of 1000 kg weight driving at a speed of 80km / hr is to be stopped by this system, then the kinetic energy of the car will be 24 6,KJ. Hence three extrusion dies will be needed. Each die has 441 holes of 3 mm diameter. It is suggested that these dies will be fitted to the back and front rears of the car as shown in Fig. (5- 23).
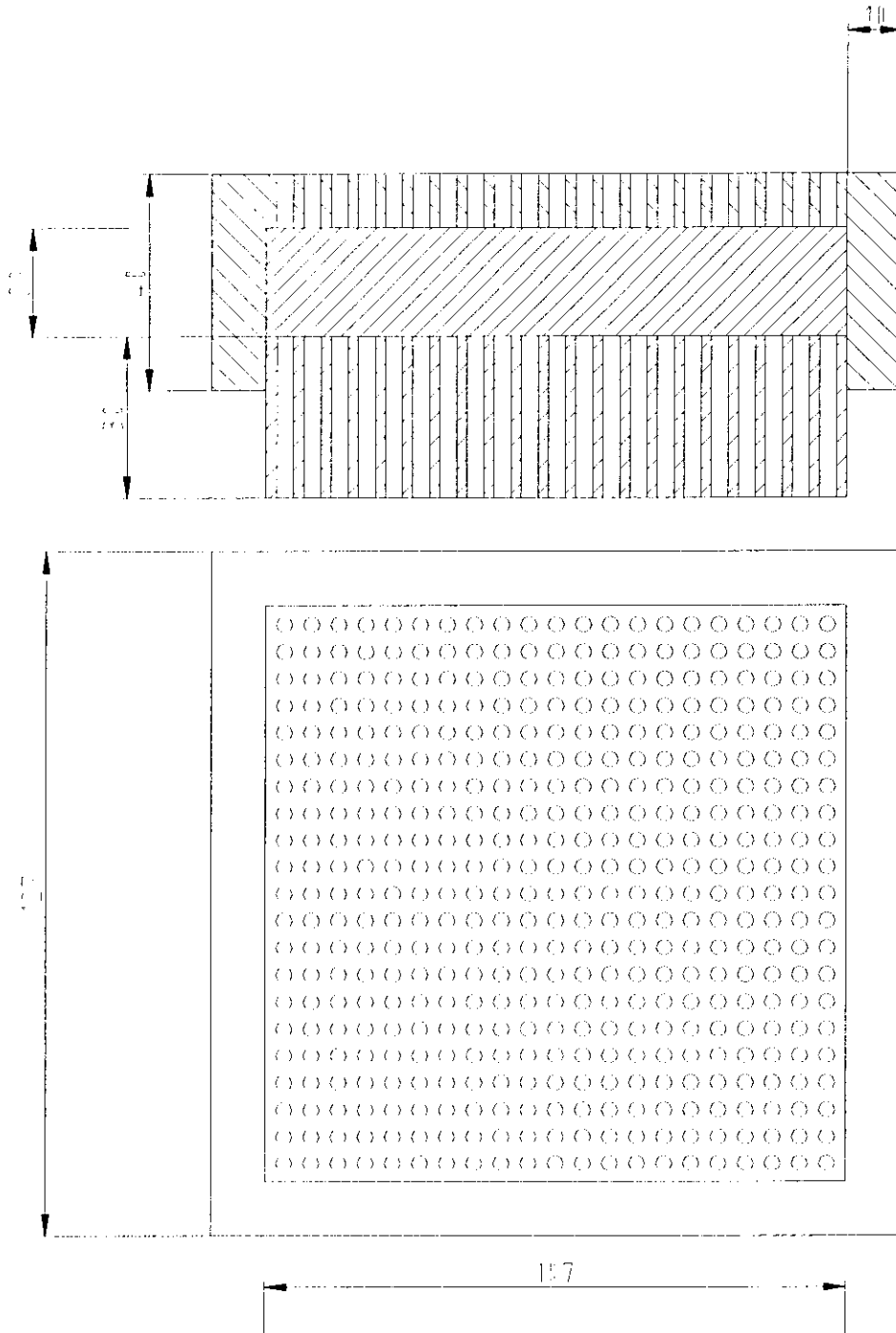
Fig. (5-23): Proposed design of actual extrusion die using Tin- Lead alloy at quasi-

static conditions

# 6. CONCLUSIONS AND SUGGESTIONS FOR FUTURE WORK

## 6.1 Conclusions

It was found that

1- The use of superplastic Tin- Lead alloy in the quasi-static loading condition is very successful to simulate the behavior of engineering materials when subjected to dynamic loading.

2- The utilization of the concept of plastic work consumed in deformation represented by extrusion and tube inversion is a successful method to be used against any collision problems in general and automobile accidents in particular to protect the car and occupants.

3- Superplastic Tin- Lead alloy is more sensitive at the lower values of strain rates and becomes less sensitive at the higher values. This is a typical behavior of a superplastic material

4- For the tube inversion system, if the collision force is high, it is better to utilize multi system in parallel, whereas if the object is to absorb the energy of collision rather than force, it is advisable to invest in the axial displacement.

4- During the rate sensitive region, the effectiveness of the system based on extrusion was 2.3 times that in the region below that region whereas the effectiveness was 6.07 times in the case of the tube inversion method, in the same strain rate region.

## 6.2 Suggestions for Future Work

The following points are worthwhile investigating:

1- Other systems following the same procedure and the same material, e.g. hollow cylinders of different ratios of internal to external diameters may be tested and the mode of deformation can be studied.

2- Other superplastic materials, e.g. Zinc- Aluminum alloy may be used instead of Tin- Lead, following the same procedure in this thesis.

3- Ordinary engineering materials, e.g. steel, copper, aluminum and their alloys may be used to replace the superplastic Tin- Lead material, and investigated following the same procedure.

4- The investigated absorbing energy systems in this theses may be tested in small scale experiments to test the validity of each system.

# 7. REFERENCES

Abdullatif, A. A., and Zaid, A. I. O.1984. The use of super plastic tin – lead alloy as a model material to simulate the dynamic lateral compression of rate sensitive metallic cylinders. *Third International Conference on Mechanical Properties of Materials at High Rates of Strain*. Oxford. PP: 1-8

Aku, S. Slater, R., and Johnson, W. 1967. The use of plasticine to simulate the dynamic compression of prismatic blocks of hot metal. *Int. J. Mech. Sci.* 9: 495- 502.

Al–Naib, T. Y. M., and Duncan, J. L. 1970. Superplastic metal forming. *Int, J. Mech. Sci.* 12 (June): 463-477.

Al-Naib, T. Y. M., and Zaid, A. I. O. 1984. Blanking of superplastic tin- lead alloy. *Al-Rafidin Journal* 13(6): 1-6

Andrews, K. R. F. England, G. L., and Ghani, E. 1983. Classification of the axial collapse of cylindrical tubes under quasi-static loading. *Int. J. Mech. Sci.* 25 (9-10): 687-696.

Bai, B. Yang, H. S. Chen, N. P., and Mukherjee, A. K. 2001. Mechanical anisotropy and stress-strain rate characteristics in superplastic deformation of titanium alloys. *Materials Science and Technology.* 17 (March): 269-277.

Baltov, A., and Vodenitcharov, S. 1976. Dynamic response of prestrained plastic continua. *Int. J. Mech. Sci.* 19: 125-128

Barra, K. Johnson, W., and slater, R. 1965. Quasi-static compressive stress- strain at various temperatures for super- pure aluminum. *Int. J. Mech. Sci.* 7: 203- 210.

Belk, J. A. 1975. A quantitative model of the blow-forming of spherical surfaces in super plastic sheet metal. *Int. J. Mech. Sci.* 17: 505-511.

Bhatt,  V., and Koechling, J. 1974. Three-dimensional frictional rigid-body impact. *J. of Applied Mechanics* 62 (December): 893-898.

Brown,  J.  C.,  and  Tidbury, G. H. 1983. An investigation of the collapse of thin-walled rectangular beams in biaxial bending. *Int. J. Mech. Sci.* 25 (9-10): 733-746.

Biswas,  S.,  and  Travis,  F.  W.  1971. Deformation patterns of annular rings of varying geometry  subjected  to  static  and  dynamic  axial  compression. *Int. J. of Machine Tool Design and Research* 2: 235- 249.

Charreyron,  P.  O.,  and  Flemings,  M. C. 1985. Rheology of semi-solid dendritic sn-pb alloys  at  low  strain  rates: application to forming process. *Int. J. Mech. Sci.* 28 (11-12): 781-791.

Chiem,  C.  Y.,  and  Leroy,  M.  1976.  Plastic  behavior of copper and aluminum single crystals deformed by pulsed magnetic fields. *Int. J. Mech. Sci.* 19: 125-128.

Chitkara,  N.  R.,  and  Hardy,  G.  M.  1977.  Rolling  of i-section beams using lead as a model material: some experimental results. *Int. J. Mech. Sci.* 19 (10): 575-594.

Clemas,  G. Al – Hassani, S., and Johnson, W. 1975. The bulging of a superplastic sheet from a square die. *Int. J. Mech. Sci.* 17: 711-718.

Clynes,  S.,  and  Campbell,  J.  1974.  The  behavior  of  copper  and lead- tin eutictic in torsion  at high strain rates. *Int. Conf. on Mechanical Properties at High Rates of Strain.* Inst. of  Phys. Series No. 21: 62-71.

Cornfield,  G.,  and  Johnson,  R.  1970.  The  forming of superplastic sheet metal. *Int. J. Mech. Sci.* 12: 479-490.

Csak,  B.  1976.  Inelastic  dynamic  behavior of structures under seismic loading. *Int. J. Mech. Sci.* 19: 125-128.

Desayi, P., and Kulkarni, A. B. 1978. Effect of membrane action on the plastic collapse load of circular orthotropic slabs with fixed edges. *Int. J. Mech. Sci.* 20: 97-108.

Drazetic, P. Level, P. Cornette, D. Mongenie, P., and Ravalard, Y. 1995. One-dimensional modeling of contact impact problem in guided transport vehicle crash. *Int. J. Impact Engng.* 16 (3): 467-478.

Duszek, M., and Sawczuk, A. 1970. Load-deflection relations for rigid-plastic cylindrical shells beyond the incipient collapse load. *Int. J. Mech. Sci.* 12: 839-848.

Fan, W. Kashyap, B. P., and Chaturvedi, M. C. 2001. Effect of layered microstructure and its evolution on superplastic behavior of AA 8090 Al-Li alloy. *Materials Science and Technology* 17 (April): 439-445.

Fan, W. Kashyap, B. P., and Chaturvedi, M. C. 2001. Effects of strain rate and test temperature on flow behavior and microstructural evolution in AA 8090 Al-Li alloy. *Materials Science and Technology* 17 (April): 431-438.

Furukawa, M. Horita, Z. Nemoto, M., and Langdon, T. G. 2000. Achieving superplasticity at high strain rates using equal channel angular pressing. *Materials Science and Technology* 16 (November - December): 1330-1333.

Gandhi, U. N., and Hu, J. 1996. Data based models for automobile side impact analysis and design evaluation. *Int. J. Impact Engng* 18 (5): 517-537.

Geng, L. Imai, T. Mao, J. F. Takagi, M., and Yao, C. K. 2001. Microstructure and high strain rate superplasticity of *in situ* composite synthesized from aluminum and nano-$ZrO_2$ particles by powder metallurgy. *Materials Science and Technology* 17 (February): 187-194.

Ghosh, A., and Duncan, J. L. 1970. Torsion tests on superplastic- tin-lead alloy. *Int. J. Mech. Sci.* 12: 499-511.

Godfrey, T. M. T. Wisbey, A. Brown, A. Brydson, R., and Hammond, C. 2000. Superplasticity and production of mechanically milled Ti-6Al- 4V-0.5B. *Materials Science and Technology* 16 (November - December): 1302-1308.

Grimes, R. Dashwood, R. J. Harrison, A. W., and Flower, H. M. 2000. Development of a high strain rate superplastic Al-Mg-Zr alloy. *Materials Science and Technology* 16 (November - December): 1334-1339.

Gupta, N. K., and Abbas, H. 2000. Lateral collapse of composite cylindrical tubes between flat platens. *International Journal of Impact Engineering* (24): 329-346.

Gupta, N. K., and Easwara Prasad, G. L. 1999. Quasi-static and dynamic axial compression of glass/ polyester composite hemi-spherical shells. *International Journal of Impact Engineering* (22): 757-774.

Gupta, N. K., and Velmurugan, R. 1997. Consideration of internal folding and non-symmetric fold formation in axi- symmetric axial collapse of round tubes. *Int. J. Solids Structures* 34 (20): 2611-2630.

Higashi, K. 2000. High strain rate superplasticity in japan. *Materials Science and Technology* 16 (November - December): 1320-1329.

Holt, D. L. 1970. An analysis of the bulging of a superplastic sheet by lateral pressure. *Int., J. Mech. Sci.* 12: 491-497.

Hosford, F. W., and Caddell, R. M. 1993. *Metal Forming, Mechanics and Metallurgy*, second edition, Prentice- Hall, Inc. London, U. K.

Huang, Y. Strangwood, M., and Blackwell, P. L 2000. Superplastic behavior of inconel 718 sheet. *Materials Science and Technology* 16 (November - December): 1309-1313.

Little, G. H. 1977. Rapid analysis of plate collapse by live-energy minimization. *Int., J. Mech. Sci.* 19 (12): 725-744.

Malatynski, M., and Klepaczko, J. 1980. Experimental investigation of plastic properties of lead over a wide range of strain rates. *Int. J. Mech. Sci.* 22: 173-183.

Male, A. T. 1966. Variations in friction co- effectiveness of metals during compression deformation. *J. Institute of Metals.* 94 : 121- 125.

Mamalis, A. G. 1976. A report on the euromech 81 international colloquium on the impact loading of tubes. *Int. J. of Mech. Sci.* 19: 129- 132.

Mamalis, A. G. Johnson, W., and Viegelahn, G. L. 1984. The crumpling of steel thin-walled tubes and frusta under axial compression at elevated strain-rates: some experimental results. *Int. J. Mech. Sci.* 26 (7): 537-547.

Mamalis, A. G. Manolakos, D. E. Saigal, S. Viegelahn, G., and Johnson, W. 1986. Extensible plastic collapse of thin-wall frusta as energy absorbers. *Int. J. Mech. Sci.* 28 (4): 219-229.

Mamalis, A. G. Manolakos, D. E. Viegelahn, G. L. Vaxevanidis, N. M., and Johnson, W. 1986. On the inextensional axial collapse of thin pvc conical shells. *Int. J. Mech. Sci.* 28 (5): 323-335.

Martin, C. F. Josserond, C. Blandin, J. J. Salvo, L. Cloetens, P., and Boller, E. 2000. X-ray microtomography study of cavity coalescence during superplastic deformation of An Al- Mg alloy. *Materials Science and Technology* 16 (November - December): 1299-1301.

Matemilola, S. A., and Stronge, W. J. 1997. Impact response of composite cylinders. *Int. J. Solids Structures* 34 (20): 2611-2630.

Matolcsy, M. 1976. Relation between the plastic deformation and crack propagation under cyclic loading. *Int. J. Mech. Sci.* 19: 125-128.

McFadden, S. X. Sergueeva, A. V. Mishra, R. S., and Mukherjee, A. K. 2000. High strain rate super plasticity in micro crystalline and nano crystalline materials. *Materials Science and Technology* 16 (November - December): 1340-1344.

Mcivor, I. K. Wineman, A. S., and Wang, H. C. 1977. Plastic collapse of general frames. *Int. J. Solids Structures* 13: 197-210.

Meng, Q. Al – Hassani, S. T. S., and Soden, P. D. 1983. Axial crushing of square tubes. *Int. J. Mech. Sci.* 25 (9-10): 747-773.

Miles, J. C. 1976. The determination of collapse load and energy absorbing properties of thin walled beam structures using matrix methods of analysis. *Int. J. Mech. Sci.* 18: 399-405.

Molnar, C. S. 1976. Plastic deformations and energy consumption by dynamic impact loads. *Int. J. Mech. Sci.* 19: 125-128.

Nader, R., 1973. *Unsafe at any Speed*, second edition. Bantam Books, London.

Naziri, H., and Pearce, R. 1970. The influence of copper additions on the superplastic forming behavior of the Zn-Al eutectoid. *Int. J. Mech. Sci.* 12: 521-513.

Neale, K. W., and Chater, E. 1980. Limit strain predictions for strain-rate sensitive anisotropic sheets. *Int. J. Mech. Sci.* 22: 563-574.

Ploch, J., and Wierzbicki, T. 1976. Impulsive loading theorem for finitely deformed plastic bodies. *Int. J. Mech. Sci.* 19: 125-128.

Reddy, T. Y. Reid, S. R. CarneyIII, J. F., and Veillette, J. R. 1987. Crushing analysis of braced metal rings using the equivalent structure technique. *Int. J. Mech. Sci.* 29 (9): 655-668.

Reid, S. R. Drew, S. L. K., and CarneyIII, J. F. 1983. Energy absorbing capacities of braced metal tubes. *Int. J. Mech. Sci.* 25 (9-10): 649-667.

Reid, S. R., and Reddy, T. Y. 1986. Axial crushing of foam-filled tapered sheet metal tubes. *Int. J. Mech. Sci.* 28 (10): 643-656.

Reid, S. R. Reddy, T. Y., and Gray, M. D. 1986. Static and dynamic axial crushing of foam-filled sheet metal tubes. *Int. J. Mech. Sci.* 28 (5): 295-322.

Silva – Gomes, J. F. Al – Hassani, S. T. S., and Johnson, W. 1978. The plastic extension of a chain of rings due to an axial impact load. *Int. J. Mech. Sci.* 20: 529-538.

Sturgess, C. E. N., and Jones, M. G. 1971. Estimation of dynamic forces in high-speed compression using a free-flight impact forging device. *Int. J. Mech. Sci.* 13: 309-322.

Styles, C. M. 2000. Superplastic forming behavior of complex shapes and post-forming mechanical properties of aluminum based sicp reinforced metal matrix composites. *Materials Science and Technology* 16 (July - August): 759-764.

Tawkyard, J. B., and Johnson, W. 1967. An analysis of the changes in geometry of short hollow cylinder during axial compression. *Int. J. of Mech. Sci.* 9 : 163- 182.

Taya, M., and Mura, T. 1974. Dynamic plastic behavior of structures under impact loading investigated by the extended hamilton's principle. *Int. J. Solids Structures* 10 (2): 197-209.

Todd, R. I. 2000. Critical review of mechanism of superplastic deformation in fine grained metallic materials. *Materials Science and Technology* 16 (November - December): 1287-1294.

Tomita, Y., and Sowerby, R. 1979. An approximate analysis for studying the plane strain deformation of strain rate sensitive materials. *Int. J. Mech. Sci.* 21: 505-516.

Volvo Car Corporation, 1992, Safety Down to the Smallest Detail. USA.

Wang, B. Yu, T. X., and Reid, S. R. 1974. Out-of-plane impact at the tip of a right-angled bent cantilever beam. *J. of Applied Mechanics* 62 (December): 887-892.

Wierzbick, T. Bhat, S. U. 'Abramowicz, W., and Brodkin, D. 1992. Alexander revisited—a two folding elements model of progressive crushing of tubes. *Int. J. Solids Structures* 29 (24): 2611-2630.

Woo, C. W. Asundi, A., and Deng, W. 1995. On rate-dependent plasticity—linear viscoelastic constitutive equations. *Int. J. Solids Structures* 32 (12): 1793-1803.

Wu, L., and Carney III, J. F. 1998. Experimental analyses of collapse behaviors of braced elliptical tubes under lateral compression. *Int. J. Mech. Sci.* 40 (8): 761-777.

Wu, L., and Carney III, J. F. 1997. Initial collapse of braced elliptical tubes under lateral compression. *Int. J. Mech. Sci.* 39 (9): 1023-1036.

Wulf, G. L. 1979. High strain rate compression of titanium and some titanium alloys. *Int. J. Mech. Sci.* 21: 713-718.

Xiang, Y. B. Chen, D. J., and Wu, S. C. 2001. Numerical analysis of effect of material and processing parameters on thickness distribution during superplastic die bulging of cavity sensitive materials. *Materials Science and Technology* 17 (February): 182-186.

Yu, T. X., and Chen, F. L. 2000. Failure of plastic structures under intense dynamic loading: modes, criteria and thresholds. *International Journal of Mechanical Sciences* (42): 1537-1554.

Zaid, A. I. O., and Belal, J. J. 2003. Investigation into cavity closure using flat ended and modified dies. Accepted for presentation, *Int. Symposium on Advanced Materials*. Pakistan.

# APPENDIX (A)

# COMPARISON BETWEEN EXPERIMENTAL RESULTS AND

# THEORETICAL ANALYSIS

In this section, comparison is made between the theoretical analysis discussed in the previous chapter and the obtained experimental results.

Consider superplastic Tin- Lead alloy is to be used in the system, then substituting the appropriate values for a, b, Y and R, as obtained before, in equation (4.23), the extrusion pressure (P) can then be determined at each strain rate, from which the total theoretical work at each strain rate was determined as follows

$$Extrusion\ ratio\ (R) = \frac{A_o}{A_f} = \frac{(26)^2}{21(3)^2} = 3.58 \qquad (4.15)$$

$$\frac{P}{Y} = a + b \ln R = 0.8 + 1.5 \ln(3.58) = 2.71 \qquad (4.23)$$

Values of the yield stress and the calculated values of extrusion pressure are shown in the table below

Table (6-1): Values of extrusion pressure for different values of strain rates

| Strain rate /s | $3 \times 10^{-4}$ | $5 \times 10^{-3}$ | 0.1 |
|---|---|---|---|
| Y(Mpa) | 48 | 74 | 104 |
| P(Mpa) | 130.1 | 200.5 | 281.8 |

Affected volume = $\pi (13 \times 10^{-3})^2 (0.01) = 5.3 \times 10^{-6} \text{ m}^3$

Theoretical consumed work =

**564808**

=Extrusion pressure x Cross sectional area of the billet x Distance

These results together with the experimental results for the work consumed are shown in Table (6-2)

Table (6-2): Values of theoretical and experimental work for different values of strain rates

| Strain rate /s | $3\times10^{-4}$ | $5\times10^{-3}$ | 0.1 |
|---|---|---|---|
| Theoretical Work(J) | 689.5 | 1062.7 | 1493.5 |
| Experimental Work(J) | 835 | 1376 | 1944 |

The difference between the experimental and theoretical results is attributed to the work consumed in both friction and redundant work. It can be seen from Table (6-3) that their percentages lies between 21.1 to 30.2% of the theoretical work, which falls within the range reported in the literature for metal forming processes in general and extrusion processes in particular.

Friction and redundant work = Experimental Work - Theoretical Work

Table (6-3): Values and percentages of friction and redundant work for different values of strain

| Strain rate /s | $3\times10^{-4}$ | $5\times10^{-3}$ | 0.1 |
|---|---|---|---|
| friction and redundant work(J) | 145.5 | 313.3 | 450.5 |
| %Friction and redundant work | 21.1 | 29.5 | 30.2 |

Let a car of 1000 kg weight driving at a speed of 80km / hr be stopped

Initial kinetic energy = (0.5) (1000kg) (80 km/hr)$^2$ (1000m/km)$^2$ (hr/3600s)$^2$

$$= 246.9 \text{ KJ}$$

1-Using an extrusion die set at a strain rate of 0.1/s, the energy absorbed is 1944 J

then we need (2.469 x 10$^5$ / 1944) = 127 die set required.

These die sets are divided to 6 identical square sets, each is equivalent to 21 die sets

$A_o$ =21 x $\pi$ x (13)$^2$ = 11150 mm$^2$

Number of holes = 21 x 21 = 441

$L_o$ = sqrt ( 11150 ) = 106 mm

2-Using an extrusion die set at a strain rate of 1000/s (dynamic condition), the energy

absorbed for 10 cm deflection can be calculated as follows

$$Y = 1.589 \times 10^8 \dot{\varepsilon}^{0.1466} = 1.589 \times 10^8 (1000)^{0.1466} = 437.4 MPa$$

P = 2.71 x 437.4 = 1185.4 MPa

Theoretical consumed work = 1185.4 x 10$^6$ x $\pi$ x ( 13x10$^{-3}$ )$^2$ x ( 0.1 ) = 62.9 KJ

Friction and redundant work is approximately 30% of the theoretical work =

$$0.3 \text{ x } 62.9 = 18.9 \text{ KJ}$$

and the total work = 62.9 + 18.9 = 81.8 KJ

Then we need (246.9 / 81.8) = 3 die set required

These die sets are divided to 3 identical sets, each is equivalent to 1 die sets

$A_o$ = $\pi$ x (13)$^2$ = 531 mm$^2$

Number of holes = 21

# APPENDIX (B)

# SIMULATION OF THE BEHAVIOR OF STEEL USING

# SUPERPLASTIC TIN- LEAD ALLOY AS A MODEL MATERIAL

In this section, simulation of the behavior of steel using superplastic tin- lead alloy as a model material was performed

Substituting the appropriate values for a, b, Y and R in equation (4.23), the extrusion pressure (P) can be determined at each strain rate, from which the total theoretical work at each strain rate was determined as follows

$$Extrusion\ ratio\ (R) = \frac{A_o}{A_f} = \frac{(26)^2}{21(3)^2} = 3.58 \qquad (4.15)$$

$$\frac{P}{Y} = a + b \ln R = 0.8 + 1.5 \ln(3.58) = 2.71 \qquad (4.23)$$

Considering mild steel in the annealed condition to be used. Its average flow stress in the quasi-static range of strain rate is 280 Mpa (Kalpakjian, 1997). Consider the rate sensitivity of 2 in order to allow for the effect of strain rate in the impact process (1000 /s), (Zaid, 1996). Hence the average dynamic flow stress will be 600 Mpa. Substituting this value in equation (4.23)

P = 2.71 x 600 = 1626 Mpa

Let the extrusion distance be 10 cm, then

Affected volume = $\pi$ ( $13 \times 10^{-3}$ )$^2$ ( 0.1 ) = 5.3 x $10^{-5}$ m$^3$

Theoretical consumed work =

=Extrusion pressure x Cross sectional area of the billet x Distance

= 1626 x $10^6$ x 5.3 x $10^{-5}$ = 86.2 KJ

Friction and redundant work is approximately 30% of the theoretical work =

0.3 x 86.2 = 25.9 KJ

and the total work = 86.2 + 25.9 = 112.1 KJ

Let a car of 1000 kg weight driving at a speed of 80km / hr be stopped

Initial kinetic energy = $(0.5) (1000kg) (80 \text{ km/hr})^2 (1000\text{m/km})^2 (\text{hr/3600s})^2$

$$= 246.9 \text{ KJ}$$

then we need $(246.9 / 112.1) = 3$ die set required.

These die sets are divided to 3 identical sets, each is equivalent to 1 die sets

$A_o = \pi \times (13)^2 = 531 \text{ mm}^2$

Number of holes = 21

# اداء مادة الرصاص- القصدير فائقة اللدونه كأنظمه لامتصاص الطاقه

اعداد

رياض محمد عبد اللطيف ابو ملوح

المشرف

أ.د.سعد محمد الدبالي

المشرف المشارك

أ.د. عدنان ابراهيم زيد الكيلاني

ملخص

لقد تم سابقا استخدام انظمه مختلفه و مواد عديده لحماية ركاب السيارات خـلال وقـوع الحـوادث.ان اغلـب الابحـاث

المنشوره في هذا المجال تتجه نحو استخدام عناصر مصنوعه من مواد هندسيه عاديه يتم تعريضها لظـروف تحميـل شبه

ثابته. و من المعروف ان تصرف المواد تحت ظروف التحميل الديناميكيه يختلف عن تصرفها تحت ظروف التحميـل شبه

الثابته.

في هذه الرساله تم استخدام سـبيكه فائقة اللدونـه مكونـه مـن معدني القصدير و الرصـاص – والتـي تتصـف

بحساسيتها لعدل الانفعال ضمن المدى شبه الساكن و الواقع في معُدل انفعـال مـن ١٠⁻² /ث الى ١/ ث -لتمثـل تصـرف

المواد الهندسيه العاديه في مستويات معدلات الانفعال المتوسطه و العاليه . المواد الهندسـيه العاديـه هـي حسـاسـه لعـدل

الانفعال ضمن المدى من ١ الى ١٠⁴ / ث والذي يتعذر الوصول اليه باستخدام ماكينات الفحص المتوفـره في المختـبرات و

يحتاج لتصميم ماكنات و معدات خاصه.

لقد تم اختبار اسلوبين مختلفين. الأول يستخدم الشغل المستنفذ في عملية التشكيل اللدن عن طريق عملية البثق الى نسبة بثق عاليه و ذلك من خلال القيام بعملية بثق لعينه اسطوانيه من قطر ٢٦ مم الى ٢١ اسطوانه بقطر ٣ مم لكل منها. أما الأسلوب الثاني فيستغل الشغل اللدن المستنفذ خلال عملية قلب لأسطوانه مجوفه. لقد تم تجربة كلا الأسلوبين باستخدام سبيكة القصدير– الرصاص فائقة اللدونه و ذلك عند ثلاث معدلات انفعال مختلفه. أحدها يقع ضمن منطقة الحساسيه لمعدل الانفعال للسرعه والثاني أقل منه أما الثالث فأعلى منه.

تم التوصل الى النتيجة التاليه و هي أن استخدام سبيكة القصدير– الرصاص فائقة اللدونه ضمن ظروف التحميل شبه الساكنه كان ناجحا جدا في تمثيل أداء المواد الهندسيه العاديه عند تعرضها لحمل ديناميكي.

وجد أيضا أن استغلال مفهوم الشغل اللدن المستنفذ في عملية التشكيل والمتمثل بعمليتي البثق وقلب الأسطوانه المفرغه يمثل وسيله ناجحه يمكن استخدامها في الحمايه من الاضرار التي قد تنجم عن أي مشكلة اصطدام بشكل عام و اصطدام السيارات بشكل خاص.

أخيرا لقد وجد أنه خلال فترة الحساسيه لسرعة الأستطاله فان فعالية النظام المبني على عملية البثق كانت أضعاف الفعاليه خلال الفتره الأدنى بينما كانت الفعاليه أضعاف في أسلوب قلب الأسطوانه.